

**An Experimental Investigation Into The Process
of Reattachment On An Aerofoil Undergoing A
Constant Negative Pitch Motion.**

By

David Geoffrey Francis Herring.

Ph.D Thesis

**Department of Aerospace Engineering
Glasgow University**

(c) David Herring April 1993

ProQuest Number: 13818757

All rights reserved

INFORMATION TO ALL USERS

The quality of this reproduction is dependent upon the quality of the copy submitted.

In the unlikely event that the author did not send a complete manuscript and there are missing pages, these will be noted. Also, if material had to be removed, a note will indicate the deletion.



ProQuest 13818757

Published by ProQuest LLC (2018). Copyright of the Dissertation is held by the Author.

All rights reserved.

This work is protected against unauthorized copying under Title 17, United States Code
Microform Edition © ProQuest LLC.

ProQuest LLC.
789 East Eisenhower Parkway
P.O. Box 1346
Ann Arbor, MI 48106 – 1346

Thesis
9787
copy 1



Acknowledgments

I owe an immense debt of gratitude to my supervisor and mentor, Dr. R.A.McD. Galbraith, without whose firm guidance this thesis would never have materialized in anything resembling its present form. Dr. Galbraith's research into unsteady aerodynamics has provided, and will hopefully continue to provide, a powerful data set on which a furthering of our understanding in unsteady aerodynamics can be realized. I am indebted to all members of staff at the university of Glasgow's Aerospace department, under the leadership of Dr. Galbraith. I should like to acknowledge the help of my predecessors in this research, Gordon Leishman and Lup Seto, for establishing the data acquisition system used, and also my contemporaries, Andrew Niven, Mark Gracey and Roger Angell, for their discussions on this work. The help of all the technical staff involved in this project is gratefully acknowledged, in particular Elizabeth Leitch for providing cohesiveness within the research group and Robert Gilmore for listening to and providing reasoned argument. I would also like to thank Marco Vezza for providing a thorough proof reading of this thesis.

Outside Glasgow University, special thanks must be given to Mr. T. Beddoes of West-land Helicopters Ltd. Had it not been for the time he gave to discussing his dynamic stall prediction code chapter five of the thesis could never have been accomplished. Lastly I would like to thank Mr. A. Jones of Royal Aerospace Establishment for acting as my external supervisor throughout this work.

The encouragement of my wife and the support of family and friends during the write up of the dissertation is gratefully acknowledge. Thank you.

The work was carried out with Department of Trade and Industry funding via M.o.D. agreement number 2048/033. Whereas much of the credit, then, lies elsewhere, the responsibility for this thesis and its shortcomings cannot be delegated, but rests with me alone.

David Herring.

April 1993

Abstract

Experimental dynamic stall research has been ongoing at Glasgow University over the past ten years. The data this has furnished have led to the development of empirical predictive codes that form part of the total aerodynamic helicopter rotor blade model. This dissertation has added another complete set of data for a completely new aerofoil, indicative of an aerofoil found on the inboard section of a helicopters rotor.

Additionally, through visual data analysis of the ramp down motion type across the entire dynamic stall database, it has been possible to identify the predominant features of the reattachment process. The analysis was performed on three aerofoils all having a geometric similarity with the NACA 23012 section. The tests were performed at a Reynolds number and Mach number of 1.5 million and 0.11 respectively. The tests cover pitch rates from 0.0 to 400.0 degrees per second, over the range of incidences going from +35 degrees to -5 degrees.

The predominant features of the reattachment process have been identified and commented upon. Having qualified these features, they have then been mathematically modelled by extending the Beddoes empirical dynamic stall model. The inclusion of a time delay associated with the presence of the wake is shown to dramatically improve the Beddoes model in the prediction of aerodynamic loads during the reattachment process.

Contents

Heading	Page
Acknowledgments	2
Abstract	3
Contents	4
Chapter 1: Introductory	10
1.1 Static stall	12
1.2 Dynamic stall	14
1.3 Research at Glasgow University	16
1.4 Modelling of dynamic stall	18
1.5 Outline of dissertation	22
Chapter 2: Design of an experimental section	24
2.1 Design criteria	24
2.2 Design procedure	26
2.3 Aerofoil program	28
2.4 Structure of aerofoil	29
2.4.1 Aerofoil spar	32
2.5 Conclusions	33
Chapter 3: Experimental procedure	35
3.1 Handley Page wind tunnel	35
3.2 Pitch control mechanism and measurement	36
3.3 Dynamic pressure	36
3.4 Pressure transducers	38
3.5 Data acquisition system	41
3.6 System calibration	41
3.6.1 Angle of attack	42
3.6.2 Dynamic pressure	43
3.6.3 Pressure transducers	43
3.7 Test procedure	45
3.7.1 Flow visualisation experiments	47
3.7.2 Static	48
3.7.3 Unsteady static	49
3.7.4 Sinusoidal	49
3.7.5 Ramp	50
3.7.6 VAWT	51
3.7.8 Ramp wave	51

3.7.9 Random incidence variation	53
3.8 Data reduction	53
3.9 Conclusions	55
Chapter 4: Overview of results for the NACA 23012B	56
4.1 Visual data analysis	56
4.2 Experimental errors	58
4.2.1 Dynamic pressure	59
4.2.2 Wind tunnel	61
4.2.3 Model motion	62
4.2.4 Pressure transducers	62
4.3 Oil flow visualisation	65
4.4 Static tests	68
4.5 Oscillatory tests	69
4.6 Ramp, up tests	72
4.7 Impulsive loadings	72
4.8 Conclusions	74
Chapter 5: Coding the Beddoes dynamic stall model	77
5.1 Introduction	78
5.2 Main features of dynamic stall	78
5.3 Linear dynamic flow model	80
5.4 Dynamic stall	80
5.5 Types of Aerofoil	81
5.6 The point of flow separation	82
5.7 Trailing edge separation	82
5.8 Impulsive loading	84
5.9 Time dependant pressure response	85
5.10 Time dependant boundary layer	85
5.11 Extension to the non-linear regime	86
5.12 Computer Implementation of the beddoes model	88
Chapter 6: Analysis of Reattachment	89
6.1 Introduction	90
6.2 Test facility	91
6.3 Experimental results	93
6.3.1 Introduction	93
6.3.2 Method of Analysis	93
6.3.3 Leading edge reattachment	95
6.3.4 Speed of reattachment	97
6.3.5 Reattachment time delays	97
6.3.6 Boundary-layer response	99
6.4 Modelling	100
6.5 Conclusions	102

Chapter 7: Conclusions	104
7.1 Recommendations for future research	104
Bibliography	106
Appendix A: Memo on update of Data Analysis facility for Dynamic Stall Data at Glasgow University	119
Appendix B: Letter confirming Shock Stall testing had been successfully completed at RAE Farnborough	121
Appendix C- Letter discussing the impulsive load tests	122
Appendix D: Complete set of tables for experimental tests performed on the NACA 23012	124

List of Figures

Figure No.	Title	Page No.
1.1	Helicopter flow field phenomena	10
1.2.	Computed Rotor Incidence Variation In Forward Flight	11
1.3	Basic three static stall types	13
1.4	Correlation of low speed stalling characteristics	14
1.5	The events of dynamic stall	15
1.6.	Deep Dynamic stall on the NACA 23012B	16
1.7.	Dynamic overshoot of static stall	16
1.8.	“Family” of NACA23012 aerofoils.	19
2.1	NACA 23012B aerofoil profile	25
2.2	Nose blending methods	27
2.3	tree diagram of aerofoil program	28
2.4	Thickness and camber line plot for NACA 23012B	29
2.5	Construction of test model	31
2.6	Pressure transducer locations	32
2.7	Panel edge pressure coefficient distribution	34
3.1	Plan view of the Handley page wind tunnel	37
3.2	Cross section through wind tunnel working section	37
3.3	Dynamic stall test rig	38
3.4	Alternative method of mounting pressure transducers	40
3.5	Schematic layout of data acquisition system	42
3.6	Handley page wind tunnel flow angularity	43
3.7	Pressure transducer calibrations graph	44
3.8	Comparison of data quality	45
3.9	Dynamic stall log	46
3.10	Definitions of tested motion types	52
3.11	Run number identification	54
4.1	Individual sweeps plotted as vectors	57
4.2	Surface pressure histories	58
4.3	Pressure contour plot	59
4.4	Variation in dynamic pressure during static tests	60
4.5	Variation in dynamic pressure during oscillatory tests	61
4.6	Variation in dynamic pressure during oscillatory tests	61
4.7	Variation in dynamic pressure during ramp tests	62
4.8	Comparison of oscillatory motion type	63
4.9	Comparison of ramp motion types	63
4.10	Erroneous transducer output checking	64
4.11	Oil flow visualisation photographs	66

4.12	Flow separation curve	67
4.13	Effect of trip wire on leading edge bubble	68
4.14	Static characteristics for increasing Reynolds number	69
4.15	Pressure tangent coefficient variation with Reynolds number	70
4.16	Moment coefficient about 1/4 chord variation with Reynolds number	70
4.17	Typical sinusoidal test data for the NACA23012B aerofoil	71
4.18	Impulsive loading measurement of C_n	72
4.19	Masking of impulsive loads by dynamic stall effects	73
4.20	Secondary peak in impulsive loadings	74
4.21	Impulsive loading under fastest ramp	75
4.22	Illustration of T.E suction peak	75
6.1	Family of aerofoils	90
6.2	Dynamic Stall Test Rig	92
6.3	Standard presentation of dynamic stall data	94
6.4	Trailing Edge Separation Movement For Static Tests.	95
6.5	Typical Chordwise Pressure Distribution.	95
6.6	Angle of Reattachment @ 2.5% chord Versus Reduced Pitch Rate.	96
6.7	Reattachment point variation with increasing pitch rate	97
6.8	Reattachment point at 2.5,50 and 97% chord over the range of reduced pitch rates.	98
6.9	Non-dimensional time for full reattachment to occur once initiated at 2.5% chord	99
6.10	Trailing Edge Separation Movement For Static Tests.	100
6.11	C_n versus Incidence for a range of pitch rates.	101
6.12	Correlation of C_n from predictive method and test data.	102
6.12	Correlation of C_n from predictive method with wake modelling inclusion and test data.	102

List of Tables

Table No.	Title	Page No.
1.1	Dynamic stall parameters	17
1.2	Published thesis's on dynamic stall at Glasgow University	18
1.3	Dynamic stall database at Glasgow University	20
2.1	NACA 23012B aerofoil coordinates	25
2.2	Characteristics of four experimental sections	27
2.3	Aerofoil constants considered of interest	30
2.4	Pressure transducer locations	32
2.5	Spar designs	33
2.6	Comparison of the design criteria with achieved results	33
3.1	Typical wind tunnel settings	35
3.2	Manufactures specification for pressure transducers	39
3.3	Flow visualisation tests	48
3.4	Summary of oscillations with mean angle of 10 degrees	49
3.5	Summary of oscillations with fixed amplitude of 8 degrees	50
3.6	Summary of oscillations with varying Reynolds number	50
3.7	Summary of ramp tests performed	51
3.8	Impulsive loading tests	51
3.9	VAWT function tests	51
3.10	typical run information header block	53
6.1	Summary of dynamic stall database of the NACA23012 family	91

Chapter 1

Introductory

Dynamic stall is the name given to the aerodynamic phenomena associated with an aerofoil undergoing incidence variation which passes through the static stall incidence. One of the first investigations of the phase was by KRAMA (1952) who observed that the boundary layer remained attached at much higher incidences when an aerofoil was pitched at a sufficiently high rate of incidence change. The net effect of this he noted was increased lift. The phenomena at that time was not known as dynamic stall.

Most fixed wing aerodynamics used in aeroplane design need not consider dynamic stall, as firstly, the range of incidence encountered are below static stall and secondly, the rate of any incidence change is slow (< 23 degrees/second.). (One possible exception to this is gust loading). However, the branch of aerodynamics that deals with the helicopter environment is intrinsically linked to understanding the dynamic stall phenomena. This is because helicopters primarily use cyclic pitch to overcome the differ-

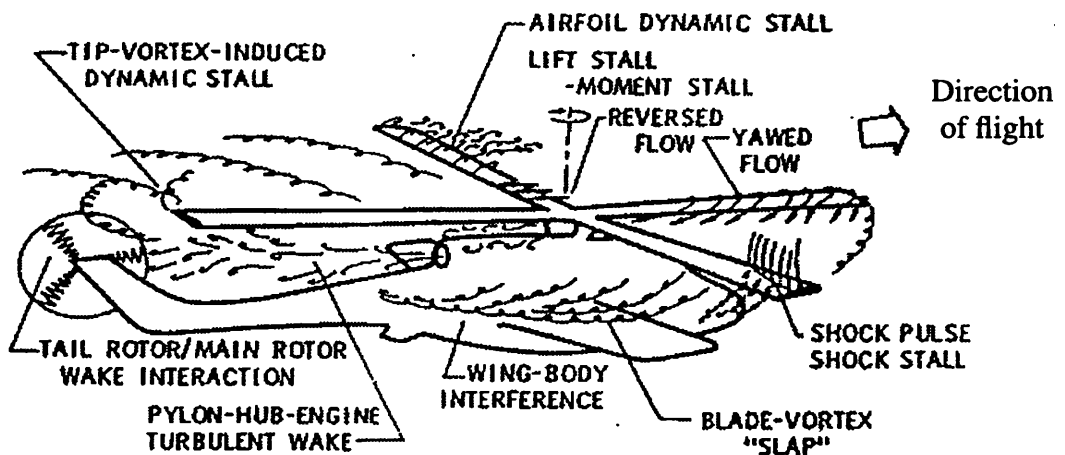


Figure 1.1 - Helicopter flow field phenomena (Ward and Young, 1972)

ence in velocities observed between the retreating blade and advancing blade on a helicopter rotor during forward flight. The faster this forward flight, so the more cyclic pitch is required to prevent helicopter roll. This eventually can lead to dynamic stall occurring on the retreating rotor blade, as depicted in figure 1.1.

At the current maximum obtainable speeds in a helicopter, (slightly less than 250m.p.h, achieved by a Westland Helicopters Ltd. customized helicopter using a BERP “paddle blade” rotor), dynamic stall effects became one limiting factor as the harsh transient dynamic overloads of dynamic stall cause excessive vibration in the helicopter rotor. Softening these dynamic loads through better blade design is seen as one of the ways of increasing the flight envelope for modern helicopters. Helicopter flight has been achieved for some time without knowledge, and currently without full understanding, of the dynamic stall process. Even as recently as 1967 (Harris and Pruyn) noted the forward speed flight boundary, using cyclic pitch, to be greater than that predicted by static stall. Thus indicating the favourable presence of dynamic stall effects.

A typical incidence variation around the rotor in forward flight is given below.

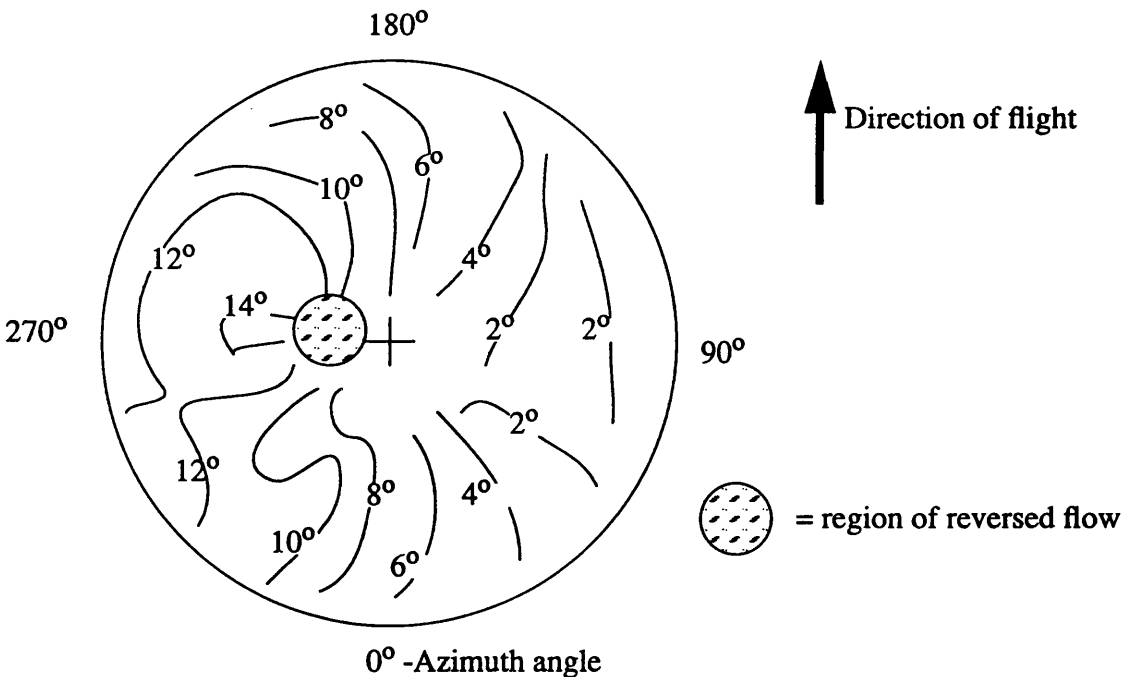


Figure 1.2 - Computed Rotor Incidence Variation In Forward Flight (Crimi, 1975)

1.1 Static Stall

Static stall data have been obtained for both two dimensional (End plated models used in wind tunnel testing), and three dimensional flows for a large number of aerofoils. Much of these data have been published in volumes such as Abbot and Doenhoff's "Theory of wind sections". The static stall data is traditionally three plots of C_l , C_d and C_m (1/4 chord) against angle of incidence over the approximate range -2 to 20 degrees. Parameters that effect these curves are primarily:

- Aerofoil Shape
- Reynolds No
- Aerofoils smoothness in leading edge region
- Turbulence of oncoming airflow
- Mach No

One detailed research investigation into how these parameters affect static stall was performed by the National Advisory Committee for Aeronautics (NACA) in 1929. From this work three distinct types of stall were identified:.

1. Leading Edge Stall

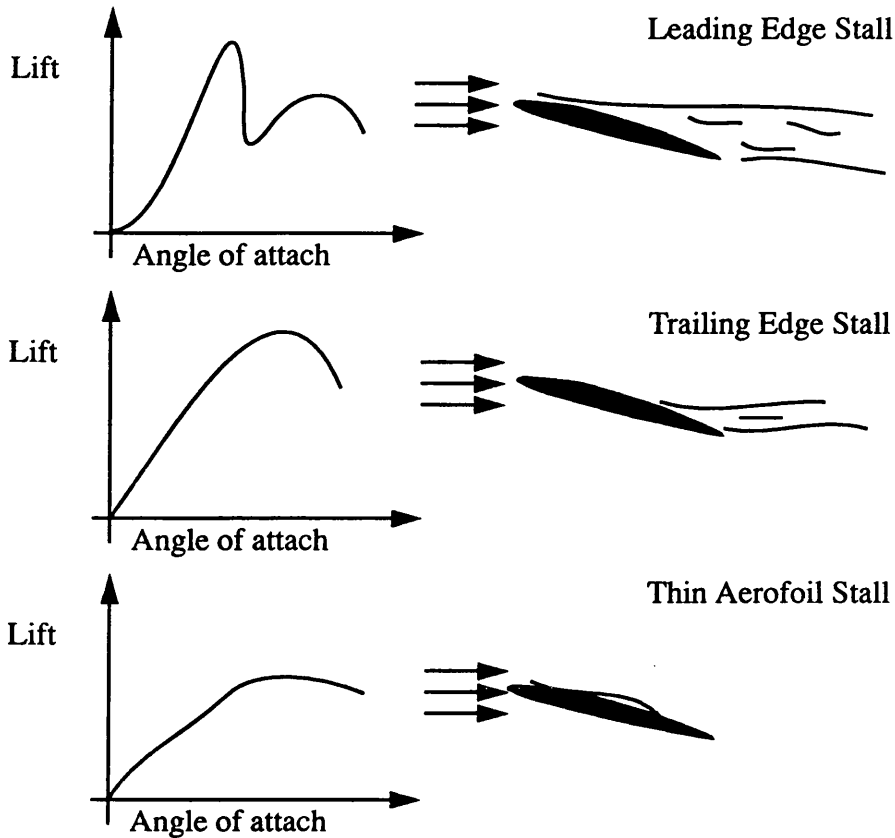
Sometimes known as short bubble stall, this is characterized by an abrupt loss in lift. The cause of this is related to the formation of a laminar separation bubble that precludes a turbulent reattachment. This bubble is typically of <1% chord in length and occurs immediately after the leading edge suction peak. As incidence is increased, so the adverse pressure gradient at the turbulent reattachment point increases, until it can no longer reattach. In affect, the bubble has burst.

An alternative mechanism (Van den Berg, 1980) in which leading edge stall may occur is through a turbulent separation just after the turbulent reattachment.

2. Trailing Edge Stall.

This is a much more gradual stall, with the turbulent separation point progressively moving forward towards the leading edge of the aerofoil as incidence is increased. This stall is typical of thick aerofoil behaviour and high Reynolds numbers.

Figure 1.3 - Basic three static stall types (Crimi and Reeves, 1972)



3. Thin Aerofoil Stall

This stall is also termed long bubble stall. It typically occurs on thin aerofoils ($<10\%$ thick), and at low Reynolds ($<10^6$). The laminar separation point remains fixed, however as incidence increases the turbulent reattachment following the bubble moves progressively towards the trailing edge of the model

A given aerofoil's stall may be prove to be a mixture of these stall types, as is thought to be the case of the NACA 23012 section (Leishman, 1984). (The derivation of these aerofoil sections and their relevance to this thesis is explained in section 1.4). From the results provided by the NASA, GAULT (1957) formed the following correlation (figure 1.4) between aerofoil nose geometry, Reynolds number and stall type. The values for the NACA 23012,23012A and 23012B and 23012C aerofoils have been noted on the graph

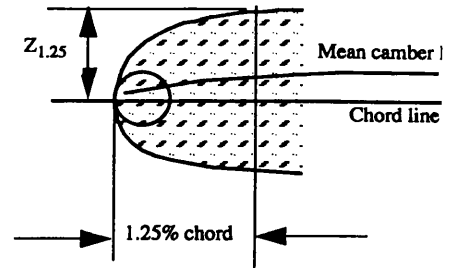
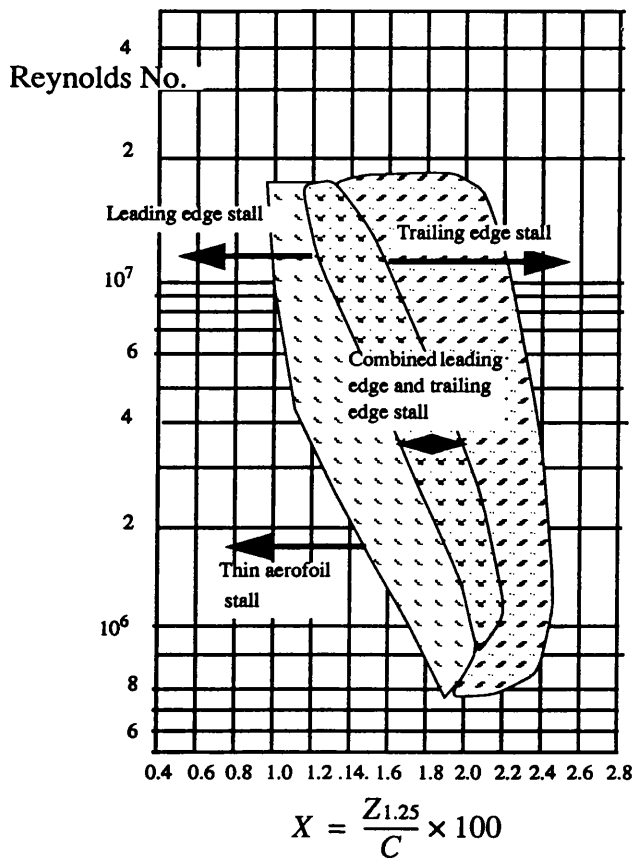


Figure 1.4 - Correlation of low speed stalling characteristics with leading edge geometry and Reynolds number (Gault, 1957)

Aerofoil	X	Stall prediction
NACA 23012	2.67	Trailing edge
NACA 23012A	2.72	Trailing edge
NACA 23012B	3.33	Trailing edge
NACA 23012C	1.93	Leading edge

1.2 Dynamic Stall

The physical process of events characterizing dynamic stall are well noted (McCroskey et al, 1975) and are illustrated in figure 1.5. This experimental work which led to the 1970's classification of dynamic stall owes much to the work of HAM (1968), Fisher and McCroskey (1972). They pioneered the time history pressure measurement around an aerofoil undergoing cyclic pitch change in a two dimensional velocity field.

An early result from these tests are the classification of "deep dynamic stall". This occurs when the amplitude, maximum incidence and reduced frequency, (a non-dimensional measurement of the frequency of model motion that expressed distance travelled in half chord lengths by the free stream velocity, Eqn 1.1), are all sufficiently

Reduced frequency:

$$k = \frac{\omega V}{2C}$$

Eqn - 1.1

high, that the resulting aerodynamic loadings become independent of the aerofoils

The events of dynamic stall on the NACA 0012 aerofoil

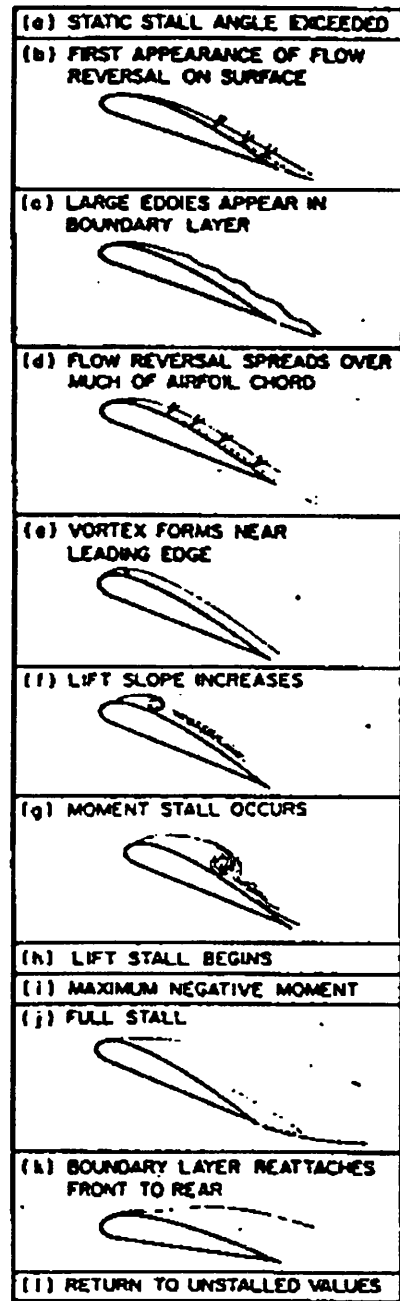
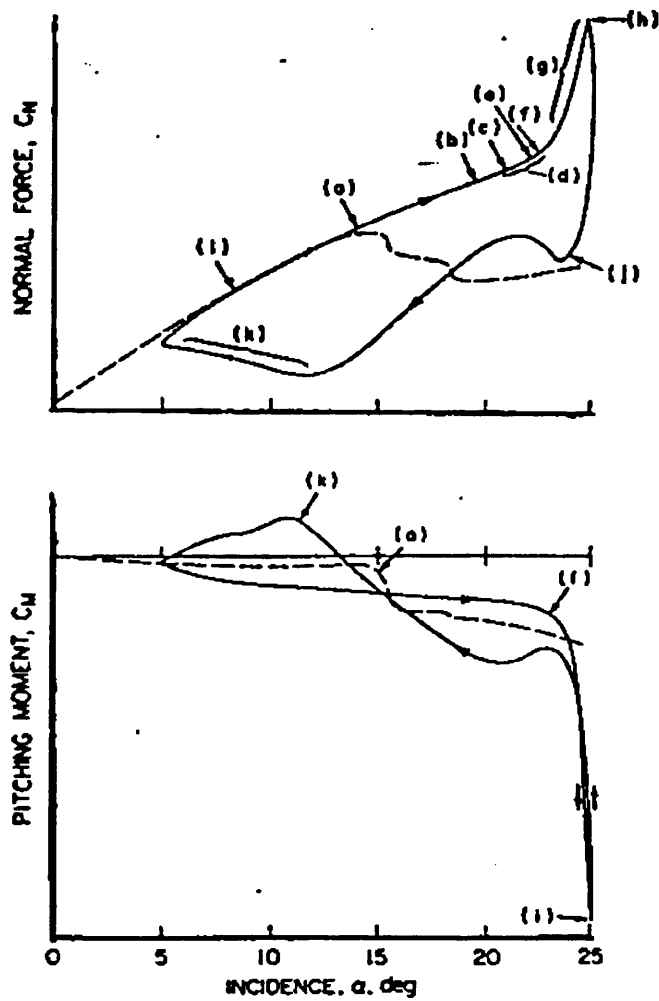


Figure 1.5- The events of dynamic stall on the NACA 0012 aerofoil (Carr et al, 1977)

geometry or the Reynolds number. This deep dynamic stall is denoted by a vortex building up over the leading edge of the aerofoil, its subsequent passage over the aerofoil and eventual shedding from the trailing edge. This vortex is commonly termed the dynamic stall vortex and is singularly the largest factor in determining the resultant aerodynamic loads on aerofoil undergoing deep dynamic stall. A typical dynamic stall on the NACA23012B is given below.

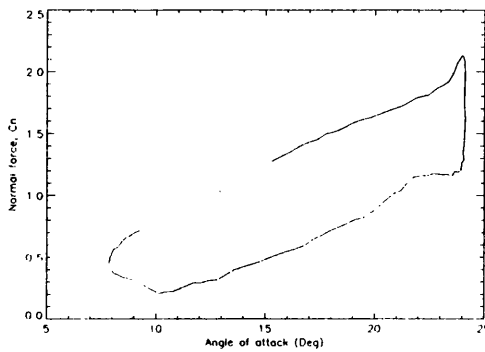


Figure 1.6 - Deep Dynamic stall on the NACA 23012B with a motion of $16.0 + 8.0 \times \sin(\omega t)$ at an oscillation frequency of 3Hz

At lesser maximum angles, although still exceeding the static stall incidence, the deep dynamic stall process does not occur. Instead the stalling process appears to have been completely avoided (see figure 1.7), with a net gain to the integrated total lift over

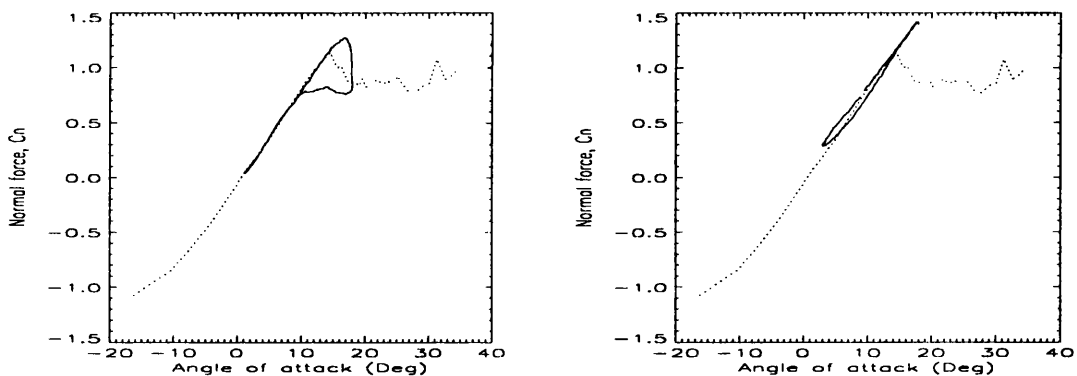


Figure 1.7 - Dynamic overshoot of static stall illustrating how with increased motion frequency the static stall can be completely avoided

the motion. As the maximum angle of the oscillation is increased, so we start to see a loss in the expected lift generated. From analysis of pressure distributions this can be attributed to a trailing edge separation occurring, without loss of the leading edge suction peak ever occurring. No vortices are generated in this process, which has been

termed light dynamic stall. The factors affecting light dynamic stall are still subject to investigation since this is the area of most interest to the helicopter aerodynamicist. The premise being to maximize the use of the dynamic stall loadings without deep dynamic stall ever occurring. Possible factors effecting these are given in table 1.1.

Table 1.1 - Dynamic stall parameters, (McCroskey et al., 1980)

Stall Parameter	Effect
Aerofoil geometry	Large in some cases
Mach number	Small below $M < 0.2$ Large above $M > 0.2$
Reynolds Number	Small at low Mach number Unknown at high Mach number
Reduced frequency	Large
Mean angle, amplitude	Large
Type of motion	Virtually unknown
Three dimensional effects	Virtually unknown
Tunnel interference effects	Virtually unknown

Lastly, we must mention the dynamic case where reduced frequencies are so small that the aerodynamics are dominated by the aerofoils static characteristics. No dynamic stall process is invoked. This typically occurs for reduced frequencies < 0.10 .

1.3 Research At Glasgow University.

Experimental Research into dynamic stall has been ongoing at the department of Aerospace Engineering, at Glasgow University since 1980 under the leadership of Dr. R McD Galbraith. An impressive dynamic stall test facility has been built up around the departments Handley Page Wind Tunnel that allows recording of pressure time histories over an aerofoils chord whilst undergoing an arbitrary motion. Additionally, to facilitate the understanding of aerofoil geometry on the light dynamic stall process, expertise has been built up in the design and manufacture of fibre glass aerofoils to precise geometries. This research effort has accredited several Ph.D studies into dynamic stall, as show in table 1.2

Table 1.2 - Published thesis's on dynamic stall at Glasgow University

Author	Thesis title	Year
G. Leishman	Contributions to the experimental investigation of aerofoil dynamic stall	1984
L.Seto	An experimental investigation of the low speed dynamic stall and reattachment of the NACA 23012 aerofoil under constant pitch motion	1988
R. K. Angell	An experimental investigation into the dynamic suitability of thick section aerofoils for the blades of large scale vertical axis wind turbines	1990
A. J. Niven	An experimental investigation into the influence of trailing edge separation on an aerofoil's dynamic stall performance	1991
M. W. Gracey	The design and low Mach number wind tunnel performance of a modified NACA 23012 aerofoil, with an investigation of dynamic stall onset	1991

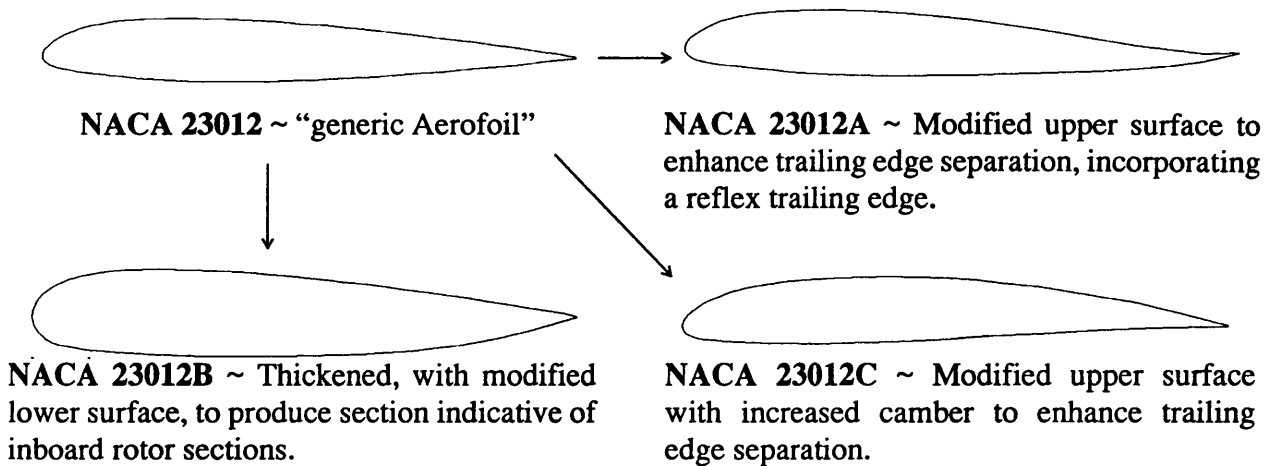
As stated earlier, there is still a lack of understanding of the role played by the aerofoil geometry in the dynamic stall vortex initiation. McCroskey (1978) noted the following four possible boundary inception mechanisms

- **Bursting of the laminar separation bubble**
- **Breakdown of the turbulent flow immediately downstream of the laminar separation bubble**
- **A thin tongue of reversed flow within the turbulent boundary layer. This reversed flow would rapidly creep forward from the trailing edge, without causing flow separation, until it reaches the laminar separation bubble. Then it would cause the bubble to burst.**
- **The start of transonic flow at the leading edge. This only applies to Mach numbers greater than 0.2.**

One aim of the research being carried out at Glasgow University is to classify the effect of aerofoil geometry on the dynamic stall process by testing a number of aerofoils with a specific family connection. This family connection is that all the aerofoils have been derived from the NACA 23012, as shown by figure 1.8.

Another feature of the test facility at Glasgow University is its ability to generate

Figure 1.8 - “Family” of NACA23012 Aerofoils Tested Under Dynamic Stall Condition.



arbitrary motion tests. Early investigations have shown the ability of constant pitch rate motions (ramp up) to be beneficial to the understanding of dynamic stall. In particular they have been used to investigate both the vortex initiation mechanism (Niven, 1991) and initial separation (Gracey, 1991). However, to the author’s knowledge there is no published work on the use of ramp down motion tests. This thesis has concentrated on particular ramp down data in order to gain a fuller understanding of the reattachment process.

The current data base of experimental dynamic stall data collected at Glasgow University offers a unique chance to analyse both the effects of aerofoil geometry and motion type on the dynamic stall process at low Reynolds numbers. This database currently contains over 20 million pressure readings collected over 10 models for a range of motion types. It is depicted by table 1.3

1.4 Modelling of dynamic stall

The methods for prediction of aerodynamic loads during dynamic stall have been categorized (McCroskey, 1981 also Galbraith, 1985) into the following four types:

- **Navier Stokes equation.**

Solution to the Navier Stokes equation is fundamental to all fluid dynamic problems. However it’s solution is elusive for the very viscous flow field surrounding an aerofoil during dynamic stall. The complexity of the time varying turbulent boundary layer

Table 1.3 - Dynamic stall database at Glasgow University

Dynamic Stall database at Glasgow University								
Model Number	Static	Sine	Ramp Up	Ramp Down	Unsteady Static	VAWT	Other	Total
NACA23012	48	549	87	37	0	0	0	721
NACA23012A	1	86	28	0	0	0	0	115
NACA23012B	56	279	123	45	90	29	51	673
NACA23012C	23	229	77	32	54	0	0	415
NACA0015	52	324	84	32	71	84	26	673
NACA0018	52	324	84	32	71	84	26	673
NACA0021	52	324	84	32	71	84	26	673
NACA0024	52	324	84	32	71	84	26	673
NACA0030	52	324	84	32	71	84	26	673
NACA0015	10	62	6	0	0	38	0	116
Total	398	2769	741	242	499	487	181	
Grand Total =								5317

makes it difficult to achieve a stable solution. Additionally the computational power required to solve this with a mesh of sufficient granularity around an aerofoil to capture the dynamic stall effects, would be large

- **Discrete potential vortex method**

A potential flow, (no viscosity), is assumed over a region of flow which incorporates the boundary layer and wake. Discrete vortices are fed into this flow field to drive the correct computational agreement with experimental data. These empirical data are used to determine the vortex introduction mechanism. This mechanism can then be applied to other models.

Newer discrete vortex methods have removed the need for empirical data to govern the vortex introduction method, and hence can be more predictive in determining dynamic stall airloads.

- **Zonal approach**

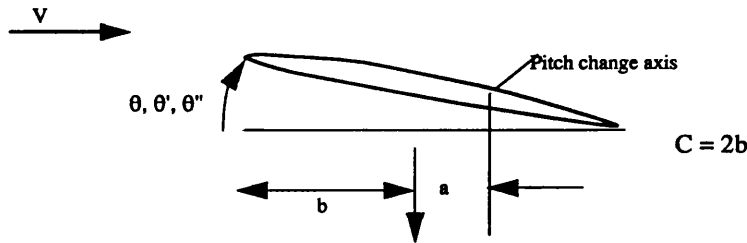
The basic premise of these models is to separate the flow field into viscous and inviscid regions which are artificially coupled by an iterative scheme.

- **Empirical models**

From the collected experimental data a set of correlations are formed with a number of chosen parameters that are considered to influence the dynamic stall. These parameters are typically the aerofoils static characteristics along with parameters that describe the models motion. There have been many approaches to this solution since it is the easiest to drive (assuming you have access to a database of experimental dynamic stall data). These methods rely on the availability of a high quality experimental dynamic stall database, such as the one available at Glasgow University. In the work carried out in this thesis two of these experimental methods have been coded. Firstly the work of Gormont (1973) was reproduced. This early dynamic stall model solved Theodorsen's Equation for a thin aerofoil oscillating in pitch and heaving about a mean incidence of zero degrees. (Eqn 1.1), with the assumptions of incompressible, inviscid flow being made.

$$Lift = \rho b^2 \left(V \pi \theta' + \pi h'' - \pi b a \theta'' \right) + 2 \pi \rho V b C \left(V \theta' + h' + b \left(\frac{1}{2} - a \right) \theta' \right)$$

Eqn - 1.1



This gives good account of the behaviour below static stall having incorporated no dynamic stall effects. These are added empirically by monitoring a reference angle of attack that 'lags' the actual incidence by a function dependent on the rate of pitch change. It is this reference angle that allows the static lift curve slope to extend beyond static stall values. However it does not allow the lift curve slope to increase in value, nor is any account made changes in dynamic stall between different aerofoil geometries. A working model of this code is available at Glasgow University coded in Fortran 77.

The second empirical model to be considered was that originated by Tom Beddoes of Westland Helicopters Ltd. This code has been published in various papers (Beddoes, 1984 etc.), and is currently used by Westland Helicopters Ltd as part of their overall rotor load predictive code.

The Beddoes model concluded from experimental data that there is a common non-dimensional time delay for the main dynamic stall events (figure 1.5). The non-dimensional time delay is expressed in chord lengths of flow travel, equation 1.2. The

$$\text{Non dimensional time} \quad NDT = \tau = T x \frac{V}{C} \quad \text{Eqn 1.2}$$

total lift produced is separated into the circulatory and impulsive loadings, these are calculated by superposition of indicial responses to step changes in incidence. Thus the model can theoretically predict the aerodynamics for any motion type. This model is discussed in detail in chapter five, where it is used to predict the reattachment loadings during the ramp down motion tests. One of the major advantages of this model is how it attempts to model the physical observed events of the dynamic stall. Thus it is easy, given experimental evidence, to incorporate any new physical feature of the flow into the model. An example of this is given in chapter five, where the model initially models reattachment very poorly due to the presence of the large wake behind the aerofoil dominating the flow until it has been convected sufficiently far downstream. A simple method to model this behaviour is introduced into the Beddoes model, which remarkably improves the correlation.

1.5 Outline of Dissertation

The experimental aerofoil used throughout this dissertation is described in chapter two. It's design, manufacture and instrumentation are discussed.

The experiments performed in the Handley Page wind tunnel are discussed in chapter three. The computational and mechanical apparatus that make up the Glasgow University dynamic stall test rig is briefly reviewed (see Leishman 1981 for more details on this facility). Additionally changes made to the calibration of the system, and changes to the algorithm for data capture are presented.

Chapter four presents a summary of the experimental data. This is included for

completeness, with no specific analysis being performed on the data other than presentation format. A detailed comparison with the other experimental aerofoil sections is left for future work.

The Beddoes dynamic stall model is outlined in Chapter five. The basic equations and assumptions that make up this semi-empirical model are outlined.

Chapter six considers the process of reattachment in detail. From detailed analysis of the ramp down data, a correlation between the presence of the wake and the initiations of aerodynamic loads is formed. This is incorporated into the Beddoes dynamic stall model and correlations are performed.

Lastly, a conclusions chapter outlines the findings made on the reattachment process and recommends areas where future research is required.

A complete set of available references on dynamic stall is given in appendix A. Where appropriate these have been referenced throughout this thesis using the Harvard system.

Chapter 2

Design of an Experimental Aerofoil Section.

This chapter succinctly describes the design method used to create the NACA 23012B, an experimental aerofoil section (Fig. 2.1). Prior to the design of this experimental section two other experimental sections had been derived using an inverse panel method (Leishman and Galbraith, 1981). This approach was not employed in the design of the NACA 23023B for the following reasons:

- **The modification to the NACA 23012 had to be large to achieve the required 16% thickness and the method is known to be unstable with large modifications.**
- **There was no particular required design pressure gradient to feed into the method.**
- **The validity of a potential flow method to design an aerofoil for an unsteady viscous environment is dubious.**
- **The design method only allows for one angle of attack, the aerofoil will obviously be operating over a range of angles.**

Instead a set of required criteria was created for this new aerofoil, that would firstly maximize its potential to enhance the dynamic stall data base at Glasgow University, thereby benefitting future research and secondly be representative of an aerofoil section used on the inner section of an helicopter rotor. This second requirement was requested by RAE Farnborough. To achieve this similarity they donated the coordinate for the RAE 9651 section to be used in the design process.

2.1 Design Criteria:

Six design criteria were decided upon. These can be listed as:-

- 1 • **16% thick.**

Indicative of the thickness currently found on the root section of a rotor blade for

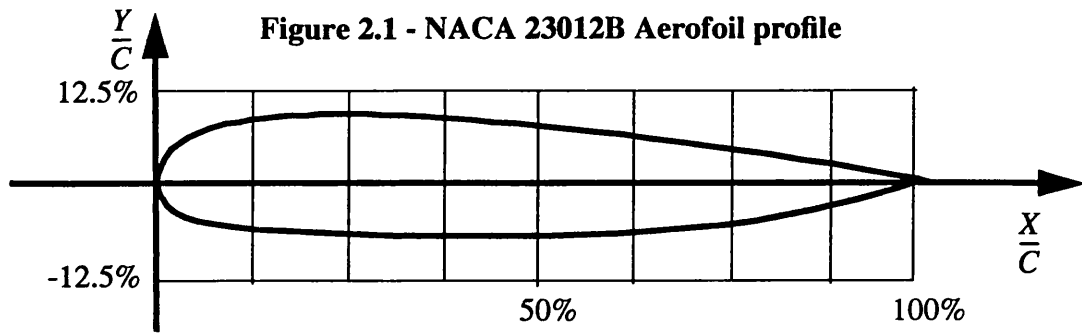


Table 2.1 - NACA23012B Aerofoil coordinates

Upper Surface		Lower Surface	
Station	Ordinate	Station	Ordinate
0.000	0.000	0.000	0.000
0.110	0.943	0.035	-0.597
0.833	2.795	0.299	-1.697
1.800	4.043	1.221	-3.132
4.138	5.637	2.341	-4.089
5.371	6.220	3.728	-4.784
9.164	7.461	5.403	-5.333
12.135	8.052	7.455	-5.755
13.822	8.282	9.941	-6.111
17.151	8.568	12.811	-6.400
23.186	8.731	16.044	-6.651
25.174	8.724	19.622	-6.874
29.942	8.618	23.495	-7.059
32.324	8.524	27.634	-7.215
37.880	8.213	32.998	-7.324
40.656	8.016	36.540	-7.385
46.998	7.481	41.210	-7.406
50.168	7.175	45.989	-7.360
53.732	6.803	50.807	-7.264
60.859	5.986	55.625	-7.119
64.421	5.544	60.395	-6.925
68.378	5.030	65.076	-6.661
76.290	3.935	69.620	-6.309
80.245	3.356	73.987	-5.847
84.198	2.755	78.129	-5.287
92.103	1.488	85.588	-3.915
96.055	0.819	91.700	-2.459
99.500	0.135	96.256	-1.185
100.000	0.000	100.000	0.000

obvious structural reasons.

2 • Similar upper surface geometry to the NACA 23012.

To give more value to the experimental results when compared to the previously tested sections at Glasgow.i.e retaining the family connection.

3 • Low speed C_{m0} of about 0.04.

The ideal for the whole rotor is to have zero pitching moment about the 1/4 chord to reduce control loads. Obviously this is unattainable for all flight conditions. However, the large dynamic effects on the tip section which lead to high negative pitching moments which can be offset by having positive pitching moment on the inner rotor section.

4 • Unstalled near zero lift incidence at a Mach number of 0.6.

A design consideration for an actual rotor blade.

5 • C_l at stall similar to NACA 23012.

See criteria 2 above, retain family connection.

6 • Minimize leading edge modifications.

See criteria 2 above, retain family connection.

2.2 Design procedure

Four aerofoils were initially designed, each was then marked against the above criteria for the final selection. All four sections have an upper surface derived from the NACA 23012. The lower surface of three of the aerofoils was derived from the RAE 9651 section. The fourth having a lower surface, as well as upper, derived from a NACA 23012.

To achieve 16% thick sections in each case, the NACA 23012 top surface was rotated about the trailing edge until 16% thickness was achieved. A blending operation was then performed in the leading edge region, to match the upper and lower sections. This “Nose Blending” was performed in three manners (figure 2.2). The aerofoils resulting from an extension of the lower surface were discarded as they tended to alter the upper section considerably, thus diminishing the family connection.

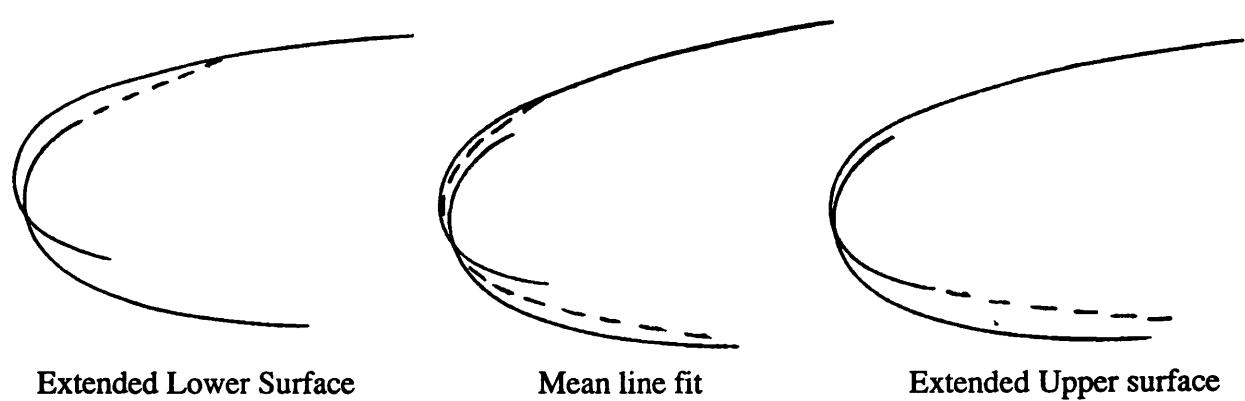
The same also applies, to a lesser extent, with the mean line fit. Only one of the four aerofoils given here employ this approach, the remaining three all have nose sections derived from the NACA 23012 top surface being extended.

The data for each section has been normalized such that the leading edge is represented by (0.0, 0.0), and the trailing edge by (1.0, 0.0). This process was necessary as the nose blending tended to move the chord line off the x-axis. Table 2.2 gives the initial top surface rotation and final resultant rotations after the co-ordinates have been normalized.

Table 2.2 - Characteristics of four experimental sections

No	Top Surface	Top Surf Rota.	Lower Surface	Nose Matching Technique	Resulting Aerofoil
1	NACA 23012	0.68°	RAE 9651	Extended Top Surface	TS = NACA 23012 rotated 1.4°, from 17.5 to 98.5% LS = RAE 9651 rotated 1.0°, from 5 to 100%
2	NACA 23012	1.70°	Normalized RAE 9651	Extended Top Surface	TS = NACA 23012 rotated 0.8°, from 10.0 to 98.5% LS = RAE 9651 rotated 1.0°, from 4 to 100%
3	NACA 23012	1.70°	Normalized RAE 9651	Mean Line Fit	TS = NACA 23012 rotated 1.4°, from 10.0 to 98.5% LS = RAE 9651 rotated -0.1°, from 0 to 100%
4	NACA 23012	3.15°	NACA 23012	Extended Top Surface	US = NACA 23012 rotated 1.4°, from 20.0 to 98.5% LS = NACA 23012 rotated -1.6°, from 5 to 100%

Figure 2.2 - Nose blending methods



It was found that be normalizing the RAE 9651 data prior to matching with the NACA 23012, a lesser leading edge modification was required. Since the Family Connection is not related to the RAE 9651, both the straight and normalized RAE 9651 data were used.

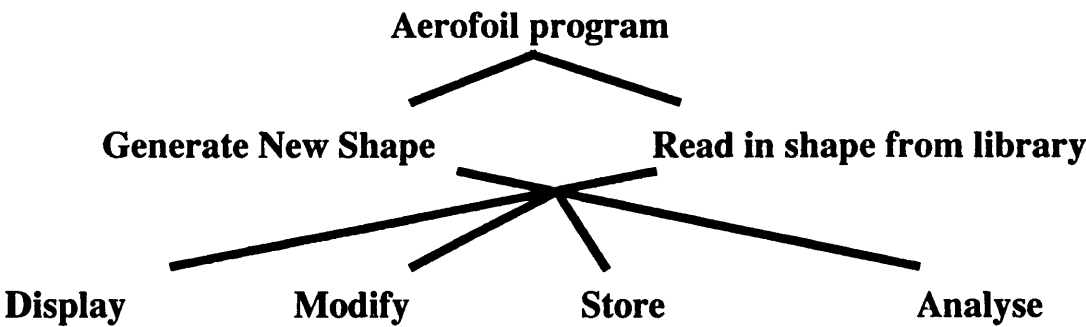
In the design process up to 500 points were used to define each aerofoil. This number was reduced to 71 points once the shape was finalised. The main reason for doing this being the need to provide data for a panel algorithm to predict the aerofoils static characteristics. By comparison of each of the four designs against the design criteria, design number 2 (as indicated on the above table) was selected as the aerofoil to be tested (see conclusions for comparisons). This experimental aerofoil has been named “NACA 23012B”, see figure 2.1.

2.3 Aerofoil program

As a result of the work carried out in the above design procedure, a package of Fortran 77 routines was written to perform the task of maintaining a library of aerofoil data and to supply a set of routines for doing geometric manipulation of this data. This program is still in existence at Glasgow University to aid future geometric design.

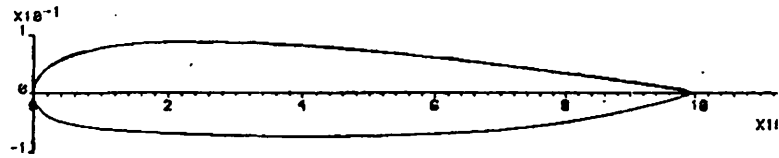
The tree diagram below illustrates the basic elements of this program.A typical

Figure 2.3 - Tree diagram of Aerofoil Program

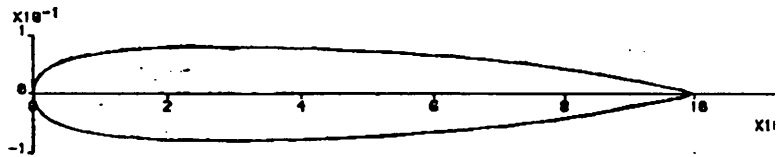


example of the type of graphical output are given in figure 2.4, where the mean camber line and thickness distribution is given for the NACA 23012B section. Interestingly, this figure shows how an aerofoil may achieve a reflex camber line without having a reflex trailing edge, due to dominant thickness distribution over the trailing edge of the aero-

Aerofoil profile

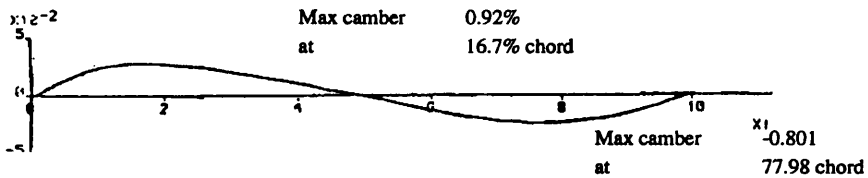


Thickness distribution



Max thickness 15.98
at 27.9% chord

Mean camber line, amplified by a factor of 3.



Max camber 0.92%
at 16.7% chord

Max camber $x1 = -0.801$
at 77.98 chord

Figure 2.4 - Thickness and camber line plot for the NACA 23012B aerofoil

foil.

The aerofoil program was given the ability to generate aerofoils that have known formulae (i.e NACA sections - Abbot and Von Doenhoff, 1968). Also a database was kept of sections denoted by a set of co-ordinates (i.e NACA 23012B section). Modify routines enable the user to normalize the current working set of points, rotate a portion of the points, combine two sets of points performing an add/delete or change individual points. The analysis routines were primarily used to return a set of geometric statistics about the given shape, and by use of a potential flow panel method (Leishman and Galbraith, 1981) predict a set of aerodynamic constants for the given shape. Table 2.3 lists these geometric and aerodynamic constants.

2.4 Structure of Aerofoil

Table 2.3 - Aerofoil Constants considered of Interest	
Geometric	Aerodynamic
Max Thickness, and it's x/c location	Cl, Cm at 0° incidence
Max Camber, and it's x/c location	Zero lift angle
Leading Edge radius	Cl vs angle gradient
Trailing edge angle	Cm ₀ angle
Trailing edge thickness	
Area enclose	
Ixx and Iyy about 1/4 chord	

A standard method of aerofoil construction for dynamic stall testing was used. This is summarized here, but is discussed in greater detail by Niven, 1981.

Initially a set of female templates for the upper and lower surfaces were hand manufactured out of 10mm thick mild steel. The chord length for the model was set to 0.55m, as used on previous models. This is a compromise between achieving high Reynolds Numbers during testing and minimizing the tunnel blockage effects (see chapter four).

These templates were used as a guide to build the upper and lower surface moulds out of wax. This was performed by a rack mounted router that was hand drawn over the wax. The cut was 2mm oversize to allow for final machining.

Initially the pod section was laid up using a 3mm thick layer of gel surface coat followed by epoxy resin impregnated with slate powder and chopped glass fibre stands. Three layers of 280g glass fibre woven matting were added on top of this to provide rigidity. These were layered at 45 deg to achieve maximum torsion rigidity. Finally a layer of plywood was attached using epoxy resin. This provided the mounting surface for the pressure transducers. Since the pod is positioned at mid-span to house the pressure transducers, it is the most important part of the model in terms of reflecting the required design shape.

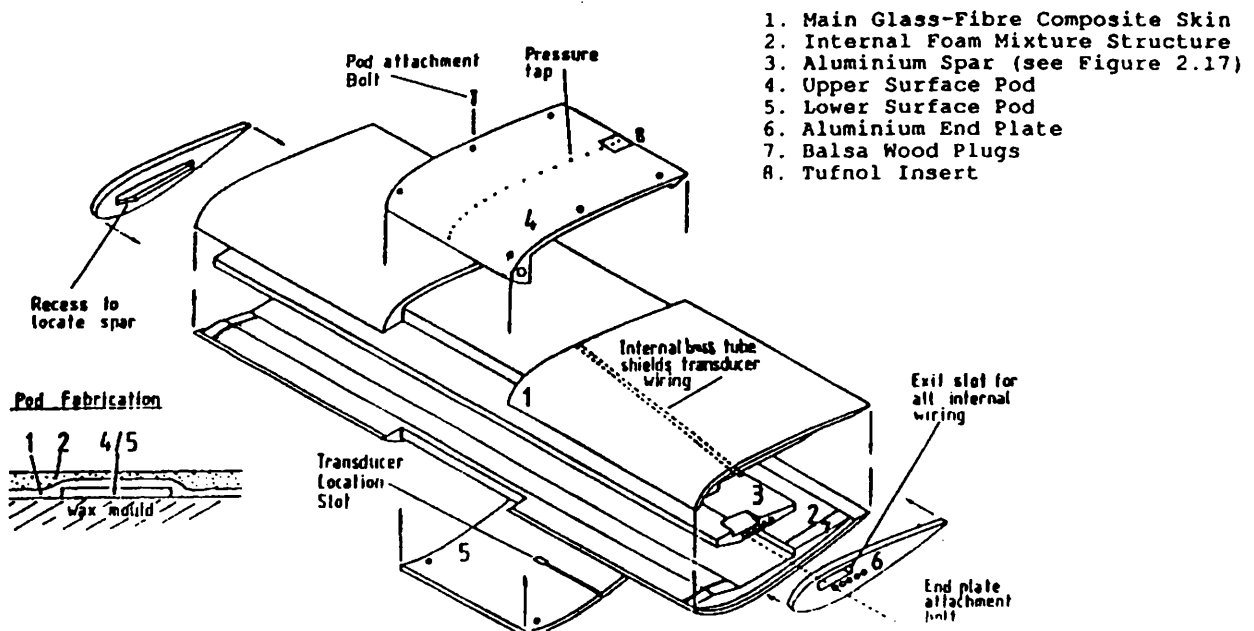


Figure 2.5 - Construction of test model (Niven, 1981)

5mm diameter were laid from one edge of the pod to the pivot point location to carry the transducer wires through the model structure, figure 2.5

Finally the entire model, with pod attached, was machined using a metal router to the required design shape. The final finish being made smooth using fine grade wet and dry emery paper. It's accuracy was tested against the female templates by checking the clearance with feeler gauges. The overall accuracy was assessed to be within 5/1000 of an inch.

The model was then drilled and fitted with fine copper tubes flush with the surface that went directly into the pod section. Perspex pressure transducer housings were attached to the ends of these tubes, before finally the thirty pressure transducers were added to the model (see chapter three for details of pressure transducer). The locations of these thirty pressure transducers were based upon:

- **Need to minimize integration errors when calculating C_n and C_t coefficients for all encountered pressure distributions. (The dynamic stall obviously having a large effect on this).**
- **Need to match locations with previously tested models to allow direct comparisons.**

The resulting locations are shown in figure 2.6 and table 2.4.

Figure 2.6 - Pressure transducer locations for NACA 23012B

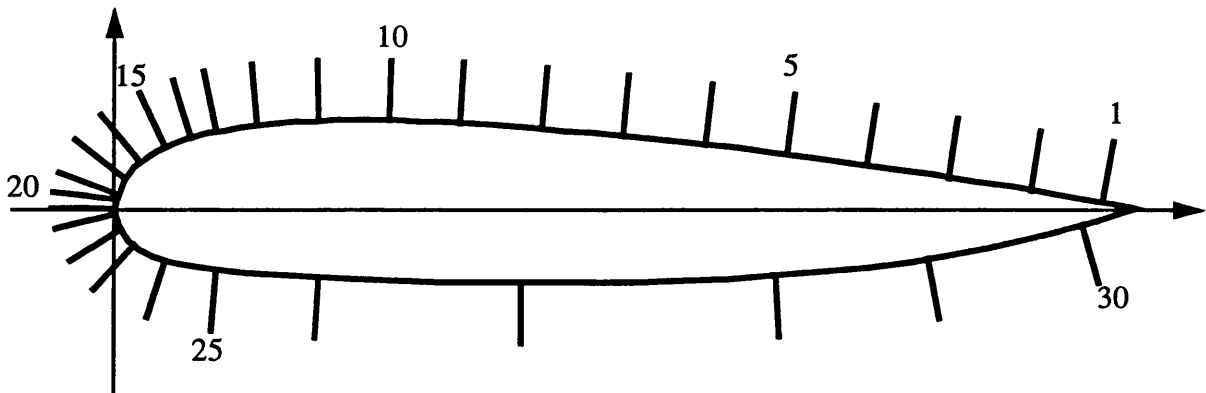


Table 2.4 - Pressure transducer locations

Thirty Pressure Transducer Locations									
X(1)/C	0.970	X(2)/C	0.900	X(3)/C	0.820	X(4)/C	0.740	X(5)/C	0.660
X(6)/C	0.580	X(7)/C	0.500	X(8)/C	0.420	X(9)/C	0.340	X(10)/C	0.270
X(11)/C	0.200	X(12)/C	0.140	X(13)/C	0.100	X(14)/C	0.075	X(15)/C	0.050
X(16)/C	0.025	X(17)/C	0.010	X(18)/C	0.003	X(19)/C	0.001	X(20)/C	0.000
X(21)/C	0.001	X(22)/C	0.900	X(23)/C	0.020	X(24)/C	0.050	X(25)/C	0.100
X(26)/C	0.200	X(27)/C	0.500	X(28)/C	0.650	X(29)/C	0.800	X(30)/C	0.950






2.4.1 Aerofoil spar

Much effort had been employed in previous models in designing and manufacturing a spar that would minimize the weight of the model, yet still provide enough torsional stiffness. All the calculations are based on the assumption that the spar takes all the loading. In reality this weight consideration is of little importance (apart from the ergonomics of two people being able to physically load the model in the wind tunnel), so a much simplified spar design was employed. This is summarized by table 2.5.

2.5 Conclusions

A set of programs has been written to aid future work on aerofoil design, these

Table 2.5 - Spar designs

Aerofoil	Researcher	Spar shape	Weight (Kg)	Tor. Stiff. GJ (Nm ² x 10 ⁻⁵)	Bend. Stiff. EI (Nm ² x 10 ⁻⁴)
NACA 23012	G. Leishman & L. Seto		36.8	4.81	1.2
NACA 23012A	A. Niven		19.5	3.10	1.8
NACA 23012B	D. Herring		37.6	19.9	1.3
NACA 23012C	M. Gracey		19.6	2.16	1.25
NACA 0015	R. Angell		45.2	24.0	1.34

are currently available through Glasgow university as the “Aerofoil program”. A new experimental section has been designed using these routines. In relation to the six design criteria, the NACA 23012B section achieved the following:

Table 2.6 - Comparison of the design criteria with achieved results

Criteria	Attainment
16% Thickness	Yes
Similar upper surface to NACA 23012	Yes, see table 2.2
Low speed C_{m_0} of 0.04	Yes, as predicted by a panel method (Galbraith, 1981), see figure 2.7.
Unstalled at Mach 0.6	Yes, test carried out computationally at RAE Farnborough by Alan Jones. See appendix B for letter of communication.
C_l at stall similar to NACA 23012	No accurate way to measure this, see chapter 4 for actual measurements
Minimize leading edge modifications	Yes, by extending NACA 23012 section over nose section.

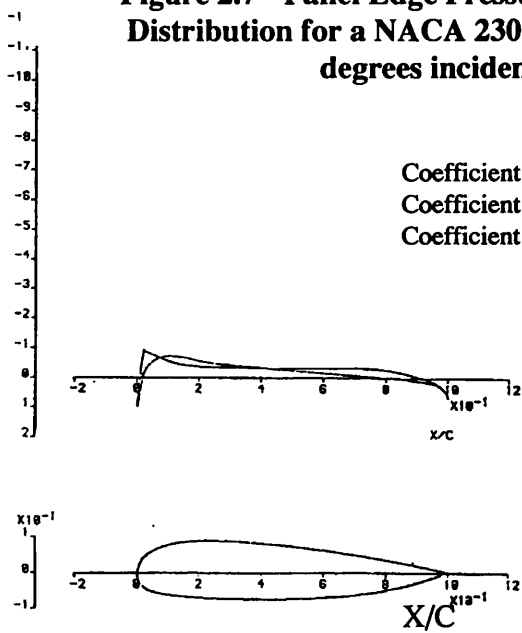
Additionally, the spar design process has been rationalized.

The current lack of a dynamic stall design code should be noted for future work

Cp

Figure 2.7 - Panel Edge Pressure Coefficient Cp
Distribution for a NACA 23012B section at 0.0
degrees incidence.

Coefficient of Lift	-0.0706
Coefficient of Drag	-0.0004
Coefficient of Moment, 1/4chord	0.0371



Chapter 3

Experimental procedure

This chapter describes the equipment that makes up the dynamic stall test rig at Glasgow University. This facility has been built up over a number of years and owes much to the research work of Leishman (1984), Seto, (1988), Niven (1991), and Gracey (1991)

The main components of this facility are:

3.1 Handley Page wind tunnel

This is a low speed, closed return type wind tunnel with an octagonal working section of 1.61 by 2.13m. The air velocity can be varied between 0-60 ms^{-1} , however at the velocities above the 40 ms^{-1} the tunnel's propeller would be considerably stressed, and additionally the air temperature would rise in the tunnel such that thermal equilibrium would not be determined without leaving the tunnel running under stress for an unacceptable length of time. Most of the tests carried out were performed at 40 ms^{-1} . This is highlighted in table 3.1 which shows typical relationships between tunnel air speeds and Reynolds / Mach numbers.

Table 3.1 - Typical wind tunnel settings

Velocity (ms^{-1})	Reynolds Number ($\times 10^{-6}$)	Mach Number	Dynamic Pressure (Pa)
21.1	0.8	0.064	260
29.0	1.1	0.088	560
39.6	1.5	0.12	930
59.4	2.0	0.18	1700

A plan view and cross section of the wind tunnels working section are illustrated in figures 3.1 and 3.2

3.2 Pitch control mechanism and measurement

The angular pitch of the model was controlled by a linear hydraulic actuator, UNIDYNE 907/1 which has a normal dynamic thrust of 6.0 kN when operated from a supply pressure of 7.0MN/m². The actuator was mounted horizontally beneath the wind tunnels working section, being connected to the tunnel support structure by a pivot hinge and to the model at the aluminum spar end plate. A MOOG 76 series 450 servo valve was used via a UNIDYNE servo controller unit. Feedback for this unit was provided by a precision linear angular displacement transducer. This angular displacement transducer was based upon a wire-wound potentiometer that was connected to the models rotational axis via tufnell gears in the ratio 5:1. The output from this transducer provided three purposes:

- **Feedback to hydraulic actuator controller**
- **Connection to data acquisition unit for recording instantaneous angle of attack**
- **Connection to a Schmitt trigger on the data acquisition unit, to initialize data sampling when an angle threshold had been reached.**

The command signal to the actuator was provided by a commodore PET computer. An 8-bit digital-to-analogue convertor was attached to an output port of the PET. A set of BASIC routines with embedded raw 65012 machine code was used to generate digital wave forms of the required motion type. The frequency of the output wave form was controlled using the 1Mhz internal instruction clock in the PET computer.

3.3 Dynamic Pressure

This was measured using a FURNESS FC012 micromanometer as the difference between the static pressure in the tunnels settling chamber and the static pressure in the working section. The static pressure was measured 1.2 m upstream of the model's leading edge in the working section, through apertures 4mm in diameter on each side wall. A similar arrangement was used in the settling chamber.

Figure 3.1- Plan view of Handley Page wind tunnel

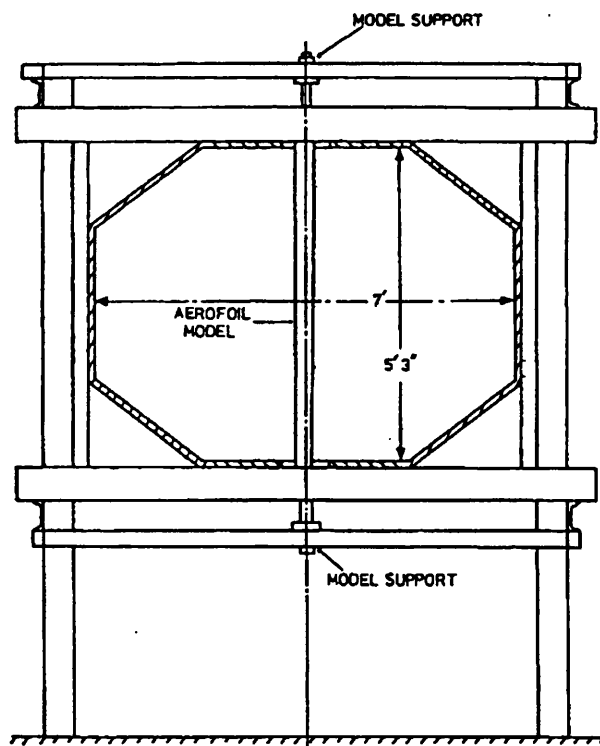
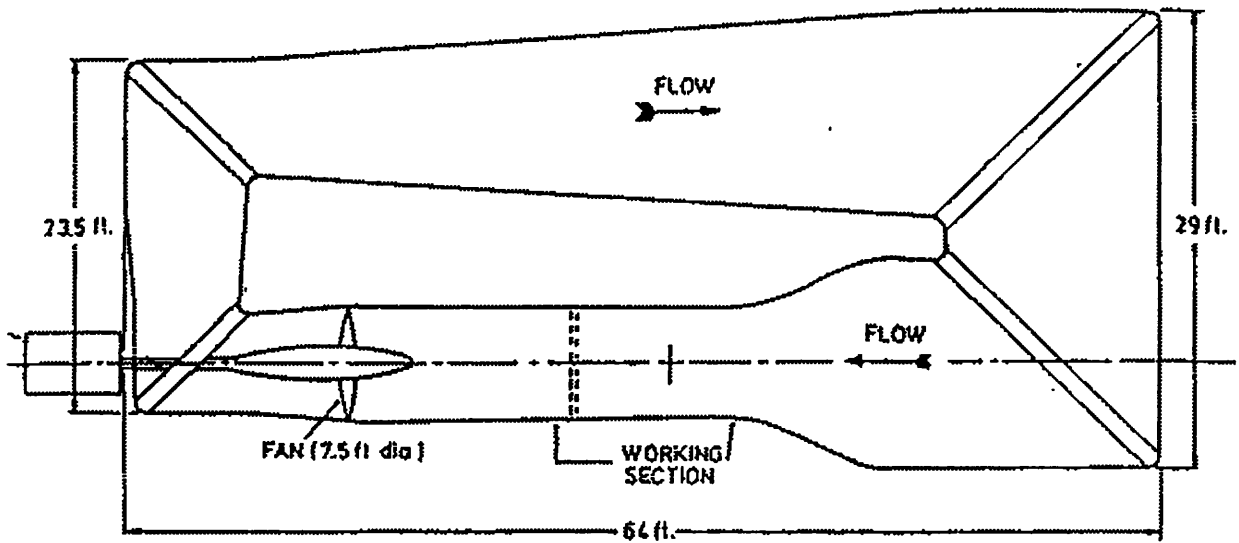


Figure 3.2- Cross section through wind tunnel working section

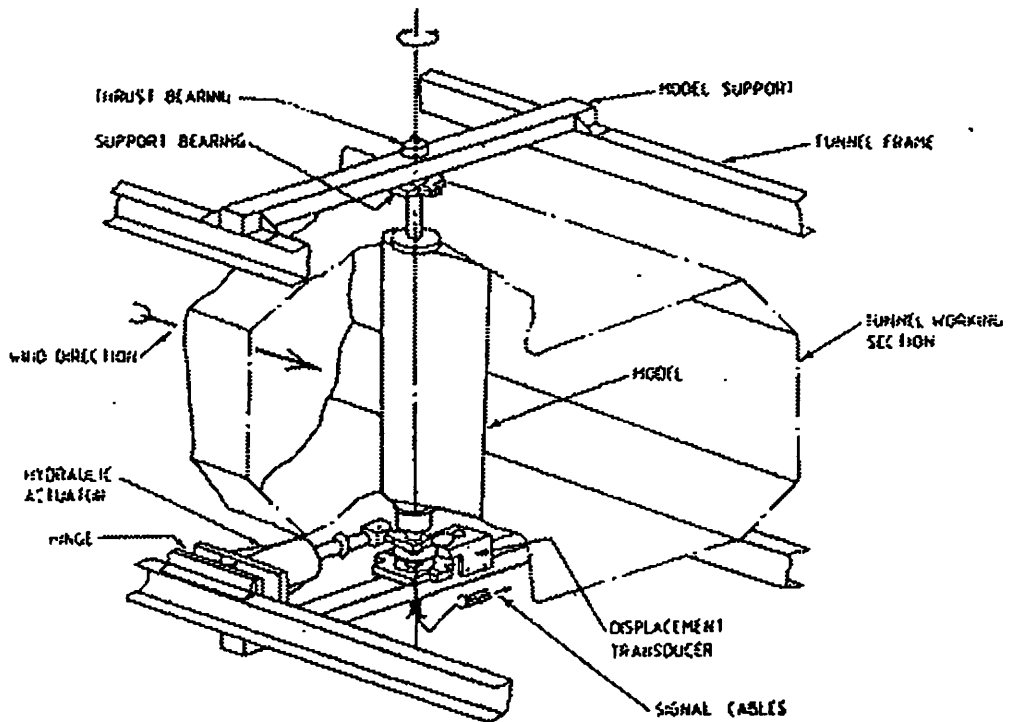


Figure 3.3 - Dynamic stall test rig (Leishman, 1981)

Alternatively, the FURNESS micromanometer could be switched to use a pitot-static probe positioned in the working section at mid tunnel height on the lower surface of the aerofoil side of the tunnel. This measurement could be used to assess the effects of blockage as the model was rotated to large angles of attack, whilst the difference in static pressure represents an averaged dynamic pressure across the entire working section. (See chapter four - Experimental errors sections for a discussion on this).

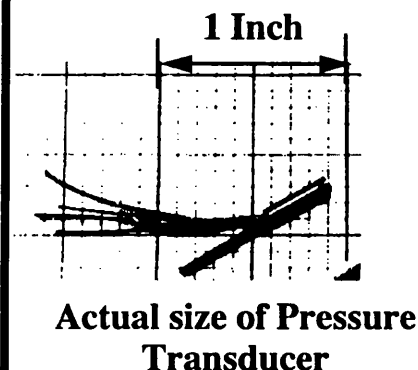
The FURNESS FC0122 micromanometer provide a digital display output, which allowed manual setting of tunnel speeds. Additionally it provided an analogue signal which was connected to the data acquisition computer for data logging.

3.4 Pressure Transducers

The pressure transducers used were a mixture of ENTRAN EPIL-080B-5S ultra-miniature pressure transducers and KULITE XCS-093-5-G pressure transducers, both types performing equally well. The main difference between these pressure transducers being the KULITE XCS-093-5-G type had a reference pressure of atmospheric pressure,

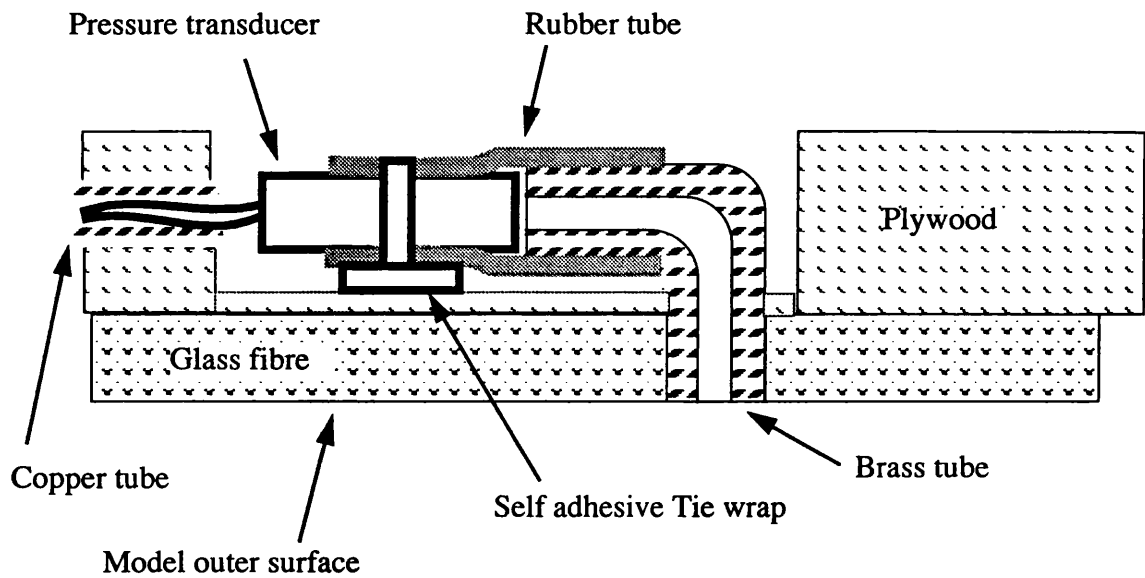
whilst the ENTRAN were of sealed reference pressure type. Both designs use an excitation voltage of 15V, which is fed to a wheatstone bridge arrangement of resistors mounted on a silicon diaphragm. A temperature compensation unit is attached to each transducer to minimise drift, this is particularly important for working in closed section tunnels where temperature can vary considerably (20-35deg). The basic manufacturer's quoted properties and size are given in the table below.

Table 3.2 - Manufacturers Specification for Entran Ultra-miniature Pressure transducer

[illegible]

One improvement to the system was in the method of mounting the pressure

Figure 3.4 - Alternative method of mounting pressure transducers

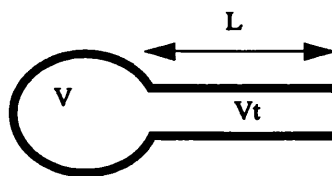


transducers. Previously all transducers were mounted in specially constructed perspex blocks using a silicon wax sealant. This proved unreliable in terms of seal and lead to a large percentage of damaged transducers due to silicon wax entering the transducer housing. The new method was simplified to directly attaching the transducer to the brass tube via a rubber sleeve. This rubber sleeve was of sufficient elasticity to suffer no observed deflection at pressure differences in excess of the maximum experienced under experiment, (see chapter 4 - experimental errors).

The resonant frequency of this pressure chamber was calculated to be $> 10\text{Mhz}$ (Eqn 3.1) (Fluid Mechanics - Robert A. Granger). This is far above the models motional excitation frequencies (12.5 Hz). Additionally, the pressure waves associated with dynamic stall are far below this resonant frequency.

The resonant frequency of a fixed chamber with similar volume to the tubing volume.

Natural frequency:
$$\omega = \left(\sqrt{r \left(\frac{P}{\rho} \right)} \right) / \left(L \left(\sqrt{\frac{1}{2} + \frac{V}{V_t}} \right) \right) \quad \text{Eqn - 3.1}$$



V_t = tubing volume

V = Chamber volume

P = average pressure

r = ratio of specific heats

ρ = density of air

3.5 Data acquisition system

A DEC MINC-11 microcomputer was the central component for data acquisition. It was fitted with an LSI-11/32 16bit microprocessor. Data storage during a sequence of runs was provided by an RX02 dual floppy disc system, a THORN EMI DATATECH D6100/48 Winchester disc drive and a THORN EMI DATATECH 9800 magnetic tape unit. A VT105 terminal was attached to the system for graphical output, with hard copies being output on an ANADEx dot matrix printer.

The DEC MINC-11 microcomputer had the following additional laboratory modules to enable it to perform data acquisition:

- **An analog to digital convertor module, with a 16-channel multiplexer incorporated. The 12-bit successive approximation convertor had a conversion time of approximately 30 micro-seconds, but multiplexer settling time, channel selection and data transfer increased the time required for reading to 44 micro seconds.**
- **A multiplexer module of 16 single-ended channels. This increased the data recorded channels to 32.**
- **A real time clock module, with two Schmitt triggers. This was used as a time-base generator to accurately set the sampling frequency. One of the Schmitt triggers was used to initialize data sampling by feeding off the angular displacement transducer.**
- **A digital to analog convertor module which housed four independent 12-bit digital to analog convertors. This was used to provide a signal to the actuator controller to set the angle of attack during static tests.**

The low voltage outputs from the pressure transducers were amplified in a rack of differential amplifiers and passed to a sample and hold unit which prevented time skew problems when sampling data at the higher frequencies. The angle of attack reading was similarly recorded using a sample and hold circuit, whilst the dynamic pressure was read at the same time as the sample and hold circuits were triggered. Additionally, to prevent data clipping, the signal outputs from the thirty pressure transducers were passed through a comparator, if outside -5 to +5V a LED on the appropriate channel would display. The user could then adjust the amplifier gain for that channel, recalibrate (see System Calibration), and repeat the run.

3.6 System Calibration

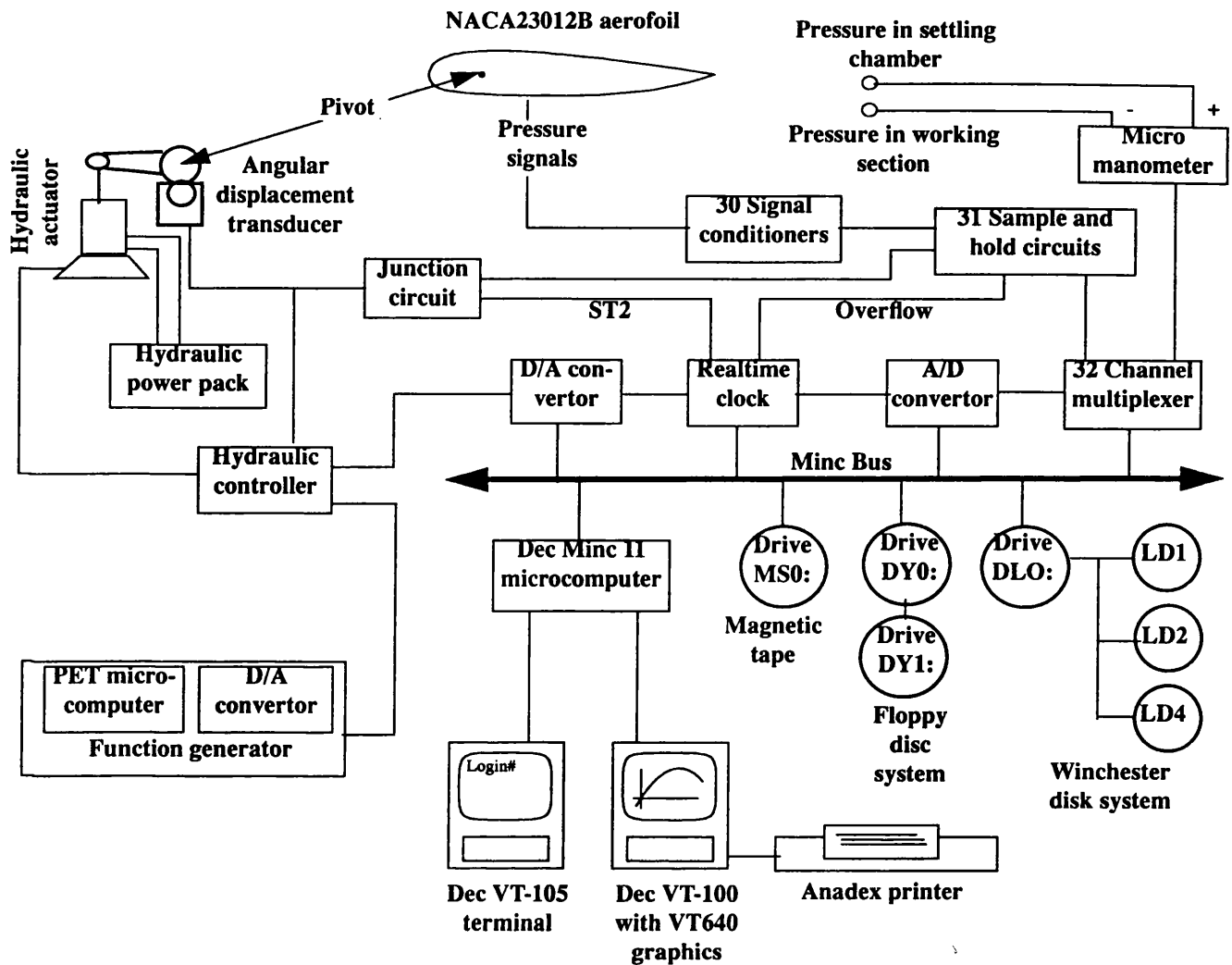


Figure3.5 - Schematic layout of data acquisition system, (Leishman, 1981)

Before any testing was performed, each of the three principle measurements were calibrated with the model in the tunnel.

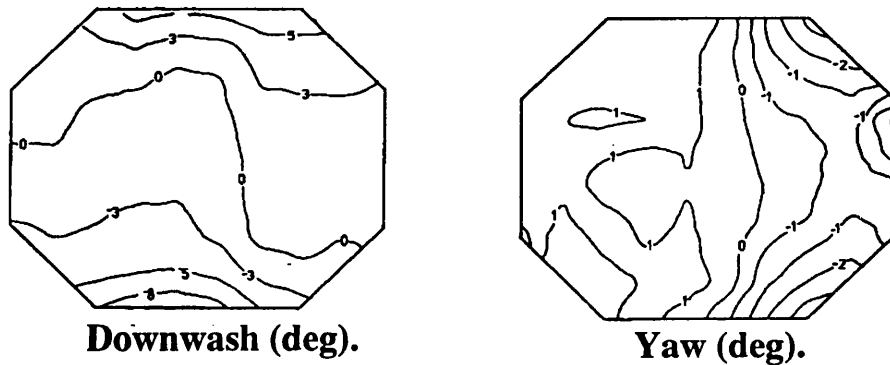
3.6.1 Angle of attack

Initially the model was manually rotated in the tunnel over the working range (-20 to 50 degrees), whilst continuously monitoring the output from the potentiometer. This ensured that over the angular operating range the transducer's limits were not exceeded, thus preventing dangerous feedback signals being sent to the hydraulic actuator. A FORTRAN 77 program was then employed to step the model through 32 discrete angle changes, pausing at each change for the user to input the tunnel measured angle.

The tunnel measure angle was read from a calibration strip attached to the tunnel floor over the arc described by the model's trailing edge. This calibration strip was geometrically aligned to the tunnels center line. The computer program was thus able to output an Angle Vs. Voltage relationship. This was basically a linear relationship, but in keeping with previously tested models a polynomial fit was applied.

The actual angle of attack experienced by the model in any wind tunnel will be affected by the tunnels accuracy in producing 2-D flow. A previous experiment has measured the yaw, downwash and turbulence experienced in the Handley Page wind tunnel. These are summarised in figure 3.6.

Figure 3.6 - Handley Page wind tunnel flow angularity measurements



Despite these tunnel irregularities, the absolute incidence measurement at the tunnel centre line was considered to be within < 1 deg accuracy by comparison of the static data for the previously tested NACA 23012 aerofoil with data obtained from other wind tunnels (Abbot and Von Doenhoff, "Theory of wing sections"). However, more importantly for the nature of this work, relative incidence changes of the model could be measured to < 0.01 degree accuracy.

3.6.2 Dynamic pressure

The Furness micromanometer was factory calibrated at regular intervals. It's accuracy was stated as < 0.01 Pa

3.6.3 Pressure Transducers

Previous models had relied upon the manufacturers data for each pressure transducer (mV/PSI) combined with the gain of each individual amplifier in the data acquisition system to provide a single coefficient for mapping voltage readings to pressures.

$$Pressure = \frac{\Delta Voltage \times Calibration}{AmplifierGain} \quad \text{Eqn - 3.1}$$

This process was improved upon by directly calibrating each pressure transducer right through the system by sequentially applying pressure and suction firstly over the model pressure transducer's orifice. Using a small electric pump, pressures were applied in the expected test range -2.0 to 0.5 P.S.I. (This is based upon a wind tunnel dynamic pressure of approximately 1000 Pa with a C_p variation at the transducer location of -15 to +1). Simultaneously 128 recordings of the transducers output were made by the data acquisition system, along with the output from a reference pressure transducer that was built into the pump. These calibrations dramatically improved the overall quality of the data, as demonstrated by the improved smoothness of pressure distribution plots, figure 3.8. A typical calibration graph for a pressure transducer is given in figure 3.7.

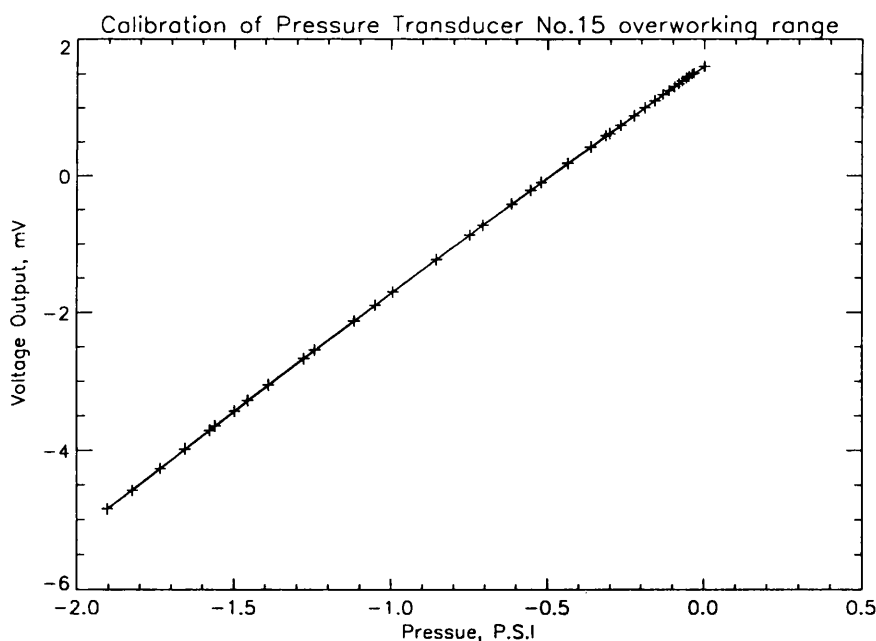
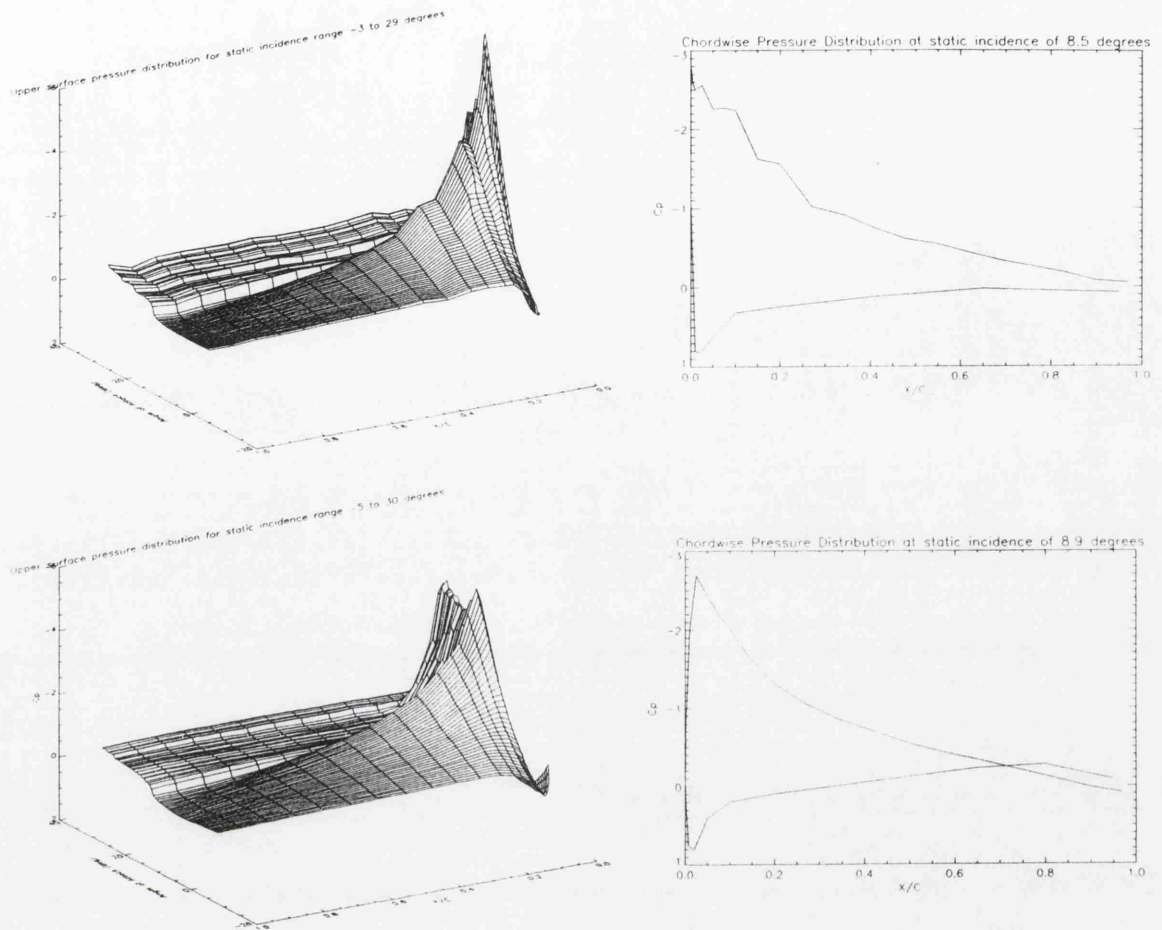


Figure 3.7 - Pressure transducer calibration graph

Figure 3.8 - Comparison of quality of pressure data between two models to illustrate the improvement achieved through calibrations of the pressure transducers through the entire systems



3.7 Test procedure

Before any tests were performed a review was carried out on the test procedure used on previous models. This basically involved running the tunnel at high speed for approximately 30 minutes followed by leaving it running at low speed for 30 minutes. This was to ensure thermal stability in the tunnel and allow the pressure transducers within the model to thermally soak. Next, the tunnel was shut down, (zero air speed), and a zero offset recording was made for all the pressure transducers and stored for later data reduction (see section 3.8 data reduction). Immediately after this the tunnel was started up and set to run at the required velocity. Whilst the tunnel was starting up (a process that takes around 3 minutes to achieve 40 ms^{-1}), data acquisition software was

started on the MINC computer. This prompted the user for several inputs for this particular test, (run number, temperature, motion type, frequency/ amplitude/mean angle, starting angle etc.). When the tunnel had reached the required speed, the motion control computer was started, again prompting the user for the motion type inputs, then generating the signal to start the required model motion. Once this had been achieved, the user initiated the start of data acquisition on the MINC computer. Once completed the tunnel was shut down and the process restarted for the next data run. Each test performed was assigned a run number which was manually recorded in the "Dynamic Stall Data Log". A typical page entry is shown in figure 3.9.

DEPT OF AERONAUTICS & FLUID MECHANICS							UNIVERSITY OF GLASGOW		
DYNAMIC STALL LOG							DATE 19th Nov 87		
434									
RUN N°	TYPE	$\frac{1}{2} \rho V^2$	$Re \times 10^{-3}$	M	α (°)	α_0	Tested $\frac{1}{2} \rho V^2$ (N/m²)	Sampling (Hz)	REMARKS
4/050/1	CALIBRATION STALL	2000	1.5	0.12	0		27.0	100	The data may need to be adjusted with
4/051/1	"				2		27.8	"	a new set of distributions, as a
4/052/1	"				4		28.0	"	better method is in the making!
4/053/1	"				6		28.2	"	
4/054/1	"				8		28.3	"	Took Transition to record
4/055/1	"				10		28.4	"	15 data files
4/056/1	"				12		28.5	"	
4/057/1	"				13		28.6	"	
4/058/1	"				14		28.8	"	
4/059/1	"				15		28.9	"	
4/060/1	"				16		28.8	"	
4/061/1	"				18		28.9	"	
4/062/1	"				20		29.1	"	
4/063/1	"				24		29.2	"	

Figure 3.9 - Dynamic stall log

This process meant that a typical series of 200+ tests could take several months to record, meanwhile tying up the Handley Page wind tunnel, which is an expensive resource to run. To enhance this process the FORTRAN data acquisition programs used were overhauled. They were modified to perform a batch of test runs, reading the input

data from batch files with minimal user input. Additionally, the prompting of inputs required to generate the control motion software was incorporated into this software. Thus, for example, the model could remain in sinusoidal motion at a fixed mean angle and amplitude, whilst the frequency was stepped through the test range pausing at each frequency just long enough to allow data acquisition. Tests continued in this automated manner until the temperature had risen by 2 deg in the wind tunnel. Only then was the tunnel shut down, and the zero offsets recorded. This change enabled a model's testing time to come down from 3 months to 2 weeks, for a comparable set of runs, with no loss in data accuracy.

If the data acquisition system had been fully coupled to the motion generator, then this process could have been reduced to days. Additionally, since over the whole range of tests the zero offset change was negligible, it would have been acceptable to extend the allowed temperature change (2 deg) to a greater value between tunnel shut-downs.

3.7.1 Flow visualisation Experiments

Initially a set of flow visualisation experiments were performed on the NACA 23012B to assess the static separation characteristics of the aerofoil and also observe any tunnel three dimensional effects. All these tests were performed at a Reynolds number of 1.5×10^6 , with the pressure orifices sealed using "magic" tape.

Flow visualization was performed by first covering the entire upper surface of the model with a mixture of saturn "dayglow" powder, iodine oil and paraffin. This mixture was stippled onto the surface, and the required angle of attack set with the tunnel shut down. The tunnel was then started up at a velocity equivalent to Reynolds number 1.5×10^6 (approximately 40 m/s, with slight variations depending upon the air temperature). The tunnels observation windows had been sealed to allow no light in, additionally the fluorescent tubes in the tunnel had been changed to ultra-violet tubes. The flow pattern was allowed to develop fully before the result was recorded using black and white photographs taken through a yellow filter using a 35mm camera. In high incident cases, gravitational effects on the oil start to distort the aerodynamically achieved flow pattern, thus at incidences above the stall the result was recorded prior to these effects

predominating. A typical time for the flow pattern to be clearly visible would be 3 minutes after the wind tunnel had reached the required velocity.

An additional set of tests were carried over a limited angle range to access the effect of using a trip wire on the model. The trip was varied in location around the leading edge region, and also varied in thickness from 0.2 mm thick wire to 2 mm thick wire.

Table 3.3 - Flow visualisation tests

Flow visualisation test tests at 1.5 million Reynolds Number.,				
Upper Surface Photographed Angles of Attack				
-10.0	-8.3	-8.0	-5.8	-3.5
-2.6	-1.6	0.6	2.3	2.7
4.8	6.5	9.9	11.2	11.7
13.3	13.8	14.9	16.0	16.8
17.0	17.8	18.0	20.4	21.8
23.9	25.9	27.7	29.6	31.8
34.1	36.6	39.9		
Upper surface with trip wire - Angles of attack				
-2.0	2.3	3.0	7.4	11.7
12.6				
Lower surface - Angle of attack				
-9.2	-4.9	0.9	5.5	10.1
14.4	19.4	24.2		

3.7.2 Static

A large number of static tests were performed on the model, with variations in the Reynolds number and the measured arc range. Unlike conventional wind tunnel static experiments, these were performed in an automated manner. The data acquisition software would step the model through 64 discrete incident changes, typically going from -2 deg to 30 deg in 0.5 deg steps. At each incidence 100 samples of the pressure transducers were taken over a 1 second period and averaged. This averaged result was recorded. Since there was no time restriction on the software during static tests, a computed C_n Vs. angle graph was displayed by integrating these C_p pressure distributions and outputting to an attached graphics terminal.

Once the 64 increasing angle steps had been completed, the software reversed the stepping direction and measured a further 64 angles of attack, with the model stepping down in -0.5 degree increments. Thus a static data run recorded 128 sweeps of data, measuring both the separation and reattachment processes. A complete listing of the test runs performed, including static tests are given in appendix D.

3.7.3 Unsteady static

These were carried out at a fixed angle of attack to measure the “unsteady” component in the static data. Basically 256 samples of the pressure transducers output were recorded at the highest possible frequency (550Hz). This was repeated for a range of incidences at Reynolds numbers of 1.0×10^6 , 1.5×10^6 and 2.0×10^6 .

3.7.4 Sinusoidal

These tests represented the bulk of the experimental data, since they most closely describe the incidence change experienced by a helicopter rotor during forward flight. The parameters that could be varied were mean angle, amplitude and reduced frequency. The range of tests performed is illustrated by the tables 3.4 to 3.6. For each test 128 sweeps of data were recorded over a complete oscillation, and 10 complete oscillations were recorded. At the highest reduced frequencies it was not possible to record 128 sweeps at 550 Hz (max sampling frequency) within the time frame of one oscillation. In these cases the 128 number of sweeps was reduced to the number that could be recorded at 550Hz within the oscillation time period. Each of the 10 recorded oscillations was started at the same “trigger” angle of attack, by use of the Schmitt trigger.

Table 3.4 - Summary of Oscillations with mean angle of 10 degrees

Mean Angle	10 degrees							
Amplitude	4		6		8		10	
Reduced frequency	0.010	0.025	0.050	0.075	0.100	0.125	0.150	0.175
Reynolds number	1.5×10^6							

Table 3.5 - Summary of oscillations with fixed amplitude 8 degrees

Mean Angle	10	11	12	13	14	15	16	17	18	19	20	25
Amplitude	8											
Reduced frequency	0.010		0.050		0.100		0.125		0.150		0.175	
Reynolds number	1.5x10 ⁶											

Table 3.6 - Summary of tests with varying Reynolds number

Mean Angle	2	4	6	8	10	12	14	16
Amplitude	10							
Reduced frequency								
Reynolds number	0.8x10 ⁶		1.0x10 ⁶		1.5x10 ⁶		2.0x10 ⁶	

3.7.5 Ramp

The use of constant pitch rate tests has been previously applied to understanding dynamic stall, (Carat, 1971), and this facility has proved very beneficial by previous researchers at Glasgow University in investigating the separation process (Niven, 1991). To continue this trend and apply it to the process of reattachment a complete set of tests were carried out for ramp up and ramp downs (decreasing incidence). Once again the range of tests is shown in the following tables.

Note that the non-dimensional reduced pitch rate is used instead of the pitch rate, and is defined in a similar manner to the reduced frequency used on the oscillatory tests,e.g.:

$$\text{Reduced pitch rate: } r = \frac{\theta'c}{2V} \quad \text{Eqn - 3.}$$

Table 3.7 - Summary of ramp tests performed

Start angle	-5 (Ramp up)	35 (Ramp down)
Arc	40 degrees	
Reduced pitch rate, r	0.00 to 0.05 in steps < 0.002	

Table 3.7 - Summary of ramp tests performed

Reynolds number	0.8×10^6	1.0×10^6	1.5×10^6	2.0×10^6
-----------------	-------------------	-------------------	-------------------	-------------------

Table 3.8 - Impulsive loading tests - (Fast ramps at low speeds)

Start angle	0							
Arc	4		8		12		20	
Reduced pitch rate	0.00 to 0.08 in steps < 0.002							
Reynolds numberx(10 ⁶)	0.4	0.6	0.8	1.0	1.2	1.4	1.6	1.8

Each ramp test consisted of the model at zero incidence whilst the tunnel reached the required velocity. Then the model was automatically moved to the starting angle by the motion control software and ramped at the required pitch rate over the required arc. During this ramp motion 256 sweeps of data were recorded, the data recording period going beyond the duration of the motion to record the transient aerodynamic effects. This process was performed for five separate ramps over the same arc. Data initialization was once again set via the Schmitt trigger to be consistent between the five sets of results

3.7.6 VAWT

The incidence function encountered by a Vertical Axis Wind Turbine is illustrated in figure 3.10. This motion type was programmed into the motion generating software and a range of tests performed to cover it. The point of interest being that since the incidence function is not symmetrical, then would not a non-symmetrical aerofoil achieve the best output on a VAWT? A separate study by Roger Angell (1992) looks into this type of data.

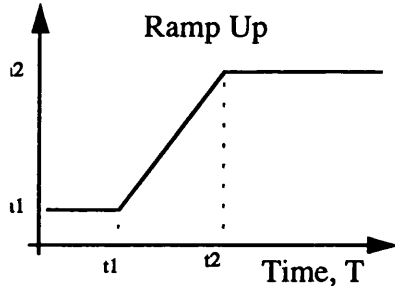
Table 3.9 - VAWT function tests

Tip speed ratio, B	0.75	2.33	2.8	3.25	3.5	4.0	5.0	6.0
Reduced frequency	0.02		0.04		0.06		0.08	
Reynolds number	1.5x10 ⁶				2.0x10 ⁶			

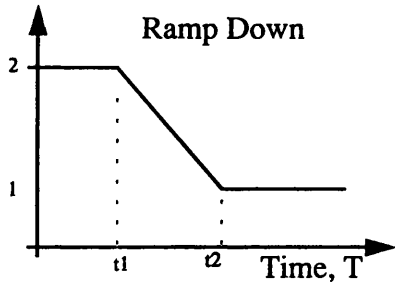
3.7.7 Ramp wave

This motion type is a derived discontinuous function illustrated in figure 3.10.

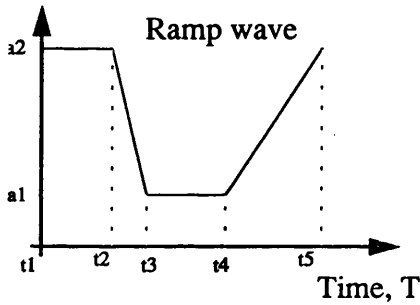
Figure 3.10 - Definitions of tested motion types



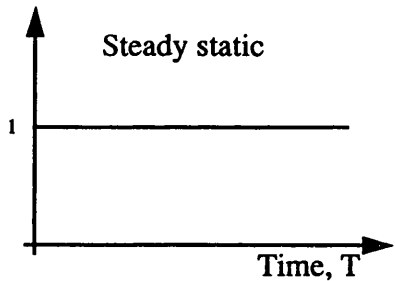
For $T < t_1$, $\alpha = a_1$
 for $t_1 \leq T \leq t_2$, $\alpha = a_1 + (T-t_1) \times (a_2-a_1) / (t_2-t_1)$
 for $t_2 < T$, $\alpha = a_2$



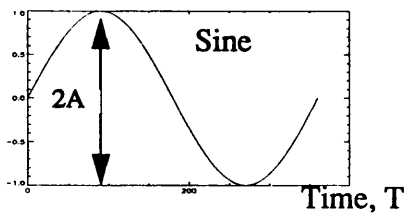
For $T < t_1$, $\alpha = a_2$
 for $t_1 \leq T \leq t_2$, $\alpha = a_1 + (T-t_1) \times (a_1-a_2) / (t_2-t_1)$
 for $t_2 < T$, $\alpha = a_1$



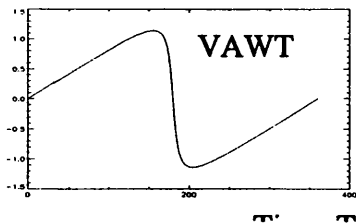
For $t_1 < T \leq t_2$, $\alpha = a_2$
 for $t_2 < T \leq t_3$, $\alpha = a_2 + (T-t_2) \times (a_2-a_1) / (t_3-t_2)$
 for $t_3 < T \leq t_4$, $\alpha = a_1$
 for $t_4 < T \leq t_5$, $\alpha = a_1 + (T-t_4) \times (a_2-a_1) / (t_5-t_4)$



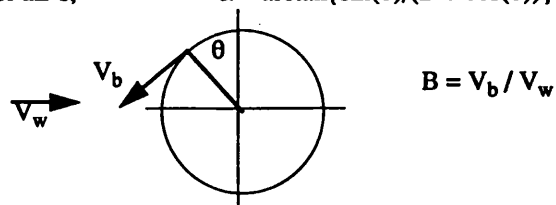
For all T , $\alpha = a_1$



For all T , $\alpha = A \sin(\omega t)$
 ω = Oscillation frequency



For all T , $\alpha = \arctan\{\sin(\theta) / (B + \cos(\theta))\}$



The purpose of testing this type of motion was for validation of any theoretical models that predict dynamic stall behaviour. These models should be able to cope with any angle of attack histories. As with the other oscillatory tests, 10 cycles of 128 data sweeps were recorded. A list of the runs performed in this manner is given in appendix D.

3.7.8 Random incidence variation

Here the model was moved randomly in incidence by a hand held dial input into the motion generator. Obviously only one cycle of 256 data sweeps could be recorded with the non-repeatable motion tests. Again their purpose is in validation of theoretical dynamic stall models.

3.8 Data reduction

The raw data files recorded for the motion type described above contained voltage values for the various transducers. These has to be converted using the calibration coefficients into angles, dynamic pressure and pressure coefficients. The coefficients to perform this were stored in the run information block of 128 real values that heads every raw data file. The basic format for a raw data file is given in table 3.10.

Table 3.10 - Typical Run information block

1 Run number	2 Day of test	3 Month of test	4 Year of test
5 Temperature (deg. C)	6 Pressure (MM Hg)	7 Motion type	8 Mean angle
9 Amplitude	10 Oscillation freq	11 No. of sweeps	12 no. data values
13 No. of Cycles	14 No. of Samples	15 No. of Blocks	16 Clock: IRATE
17 Clock: IPRSET	18 Sampling Freq	19 Unused	20 Reynolds Number
21 Mach Number	22 Reduced Frequency	23 Velocity (MS**-1)	24 No. of Blocks/Cycle
25 No. in unfilled silo	26 Aver/Unaver	27 Interpolated for	28 Cps = 0olts = 1
29 Dynamic Pressure	30 Model No.	31 Coefficient file no	32 Requested Pitch Rat
33-64 Transducer Zero offsets			
65-96 Transducer Gains			
97-128 Amplifier Gains			

The data reduction process was carried out on a VAX11/750 computer using a set of FORTRAN 77 programs. The calculations it performed were basically a simple

multiplication of the voltages against the calibration coefficients. The coefficients of pressure (C_p), were measured relative to the instantaneous dynamic pressure in the tunnel - see chapter 4 for a discussion on this. Therefore, for each sweep of data one angle, one dynamic pressure and thirty coefficient of pressure calculations were performed as follows:

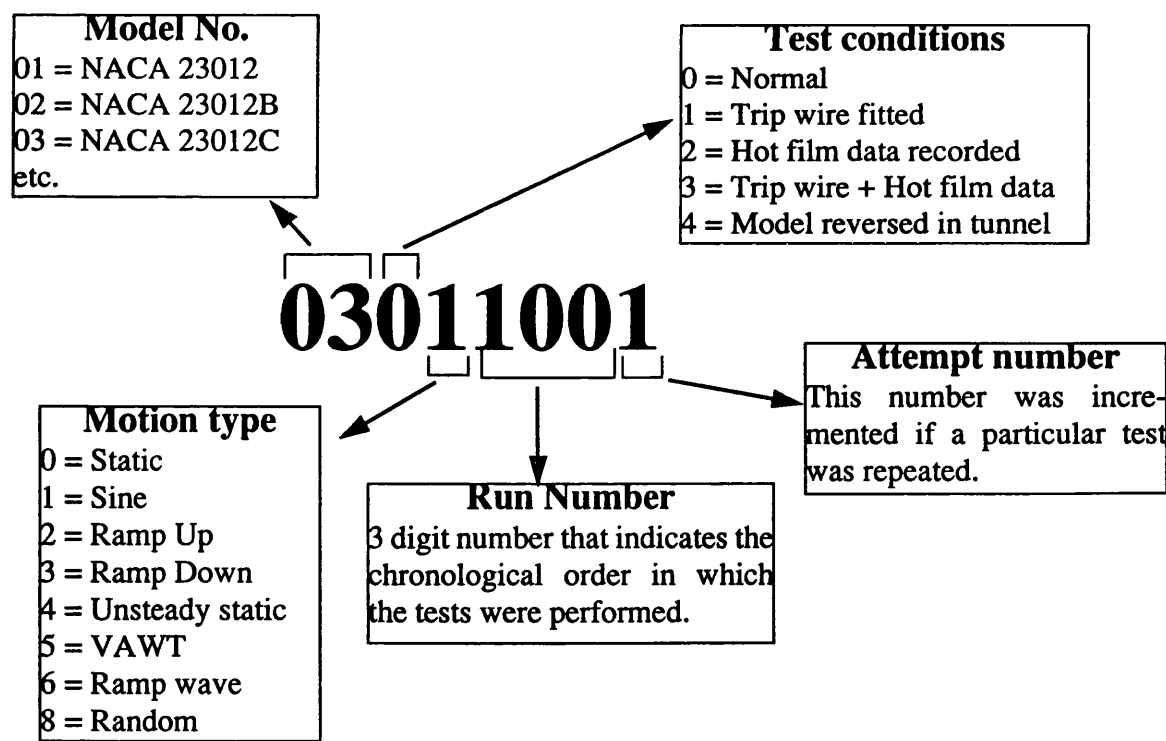
$$C_p = \frac{MeasuredPressure}{DynamicPressure}$$

Eqn - 4.1

The 10 cycles for oscillatory tests were averaged to form a simple set of data describing one complete cycle. This process enhanced the salient features of the test whilst removing any random differences between the cycles. The unaveraged data was also stored for analysis. A similar averaging process was carried out for the ramp, VAWT and ramp wave tests.

The resultant averaged data have been transferred to the dynamic stall database for analysis. Each test was assigned a unique eight digit number which encoded the salient points for that test. Figure 3.11 illustrates the breakdown of this encoding.

Figure. 3.11 - Run number identification



3.9 Conclusions

The standard test procedure has been enhanced to provide better pressure quality data.

The test procedure has been improved to allow better usage of wind tunnel time.

A full set of test data has been recorded for the NACA 23012B aerofoil and made available on the Glasgow University dynamic stall data base.

Chapter 4

Overview of Results for the NACA 23012B

A full graphical listing of the complete set of test results for the NACA 23012B has been published in four volumes (Herring and Galbraith, 1988). The data presented in these reports is in a standard format with the upper surface time history pressure distribution, alongside plots of C_n , C_t and $C_{m_{1/4}}$ against incidence and also against non-dimensional time. An example of one standard report plot is given by figure 6.3.

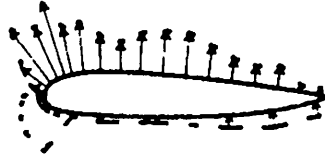
At the time of writing only the data for the NACA 23012B aerofoil was available. For a comparison of the dynamic stall characteristics of the family of NACA 23012 models see GRACEY, (1991). The ramp down data is not considered in this chapter, it being covered in chapter five.

4.1 Visual data analysis

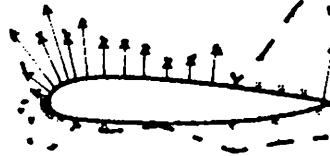
“..Thought is impossible without an image.” Aristotle, 325 B.C

Although the standard report plot summarises the data, they cannot solely provide the means to do experimental analysis on the data. This frequently requires the analysis of individual pressure transducer outputs etc. Initially the analysis of the dynamic stall database was done via a suite of display programs written in Fortran 77 using the NAG and Ginograf plotting libraries. Output was either to a “dumb” VT240 graphics terminal, or hardcopy on a Versatec plotter. This work resulted in a wealth of plotting routines to output the data in imaginative formats that assisted the research. Appendix A contains the proposal that outlines the nature of this work. One typical example of this work is given in figure 4.1, where pressures are shown in vector form around the aerofoil. Another example is the “DSDISPLAY3D” plot routine which plots the entire upper and lower surface pressure distribution time histories on one plot by

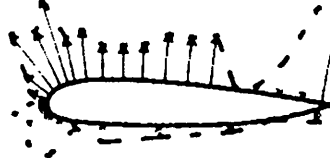
1. Sweep No. : 45
Angle = 10.8 (Deg).



2. Sweep No. : 46
Angle = 10.8 (Deg).



3. Sweep No. : 47
Angle = 10.8 (Deg).



4. Sweep No. : 48
Angle = 10.8 (Deg).

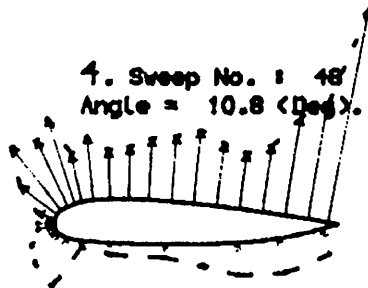


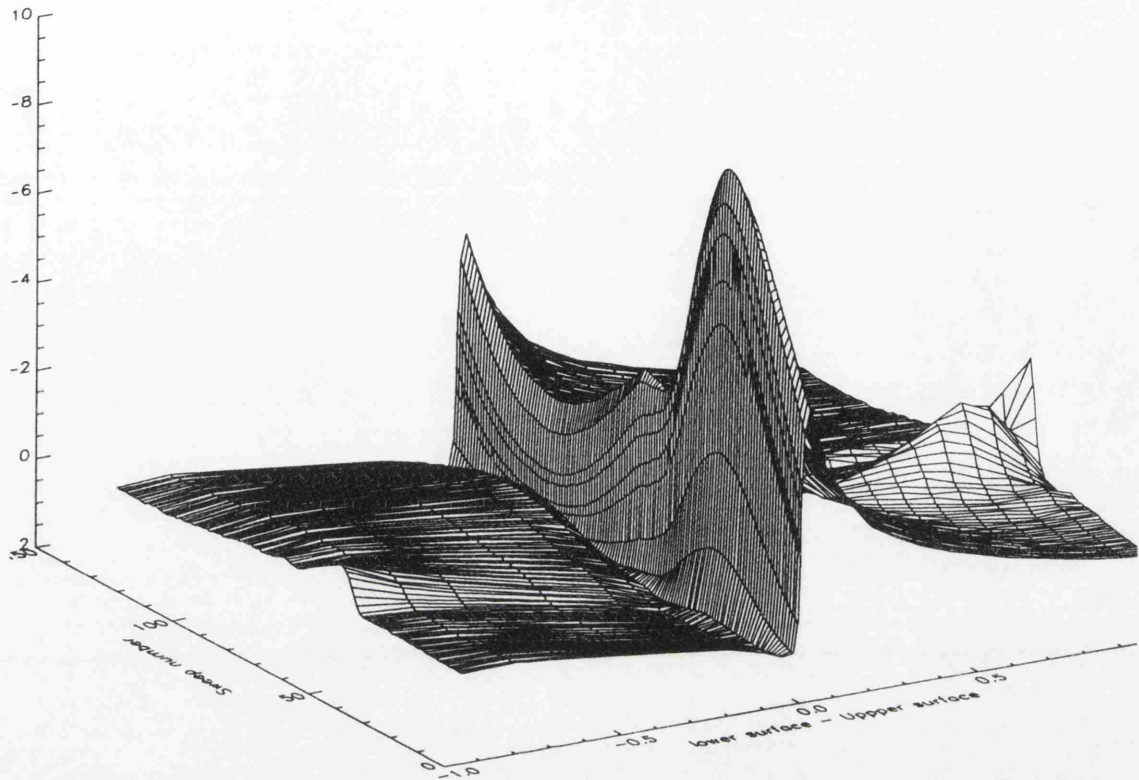
Figure 4.1 - Individual sweeps of data plotted as pressure vectors around the aerofoil

unrolling the aerofoil about the trailing edge such that the nose lies in the middle of a horizontal flat line that represents the aerofoil surface from lower surface trailing edge to upper surface trailing edge. This plot led to the first visualization of the pressure wave that traverses the lower surface in sympathy with the vortex pressure wave passing over the upper surface, (Figure 4.2).

The whole process of experimental data analysis has recently been termed “Visual Data Analysis”. Customised computer packages exist that allow the user to interact with the data. One such package used for the work contained herein is “PV-

Output from DSPL3D for NACA23012B

Figure 4.2 - Surface pressure histories



WAVE". These packages allow the researcher to quickly view the data in a variety of formats without having to produce any code. Additionally the ability to add colour and animation to the output gives better understanding and clarity to the data. Once this package had been adopted, the previous hundreds of researcher man hours in coding display routines was made redundant. All the graphs presented within are from PV-WAVE.

Figure 4.3 shows the same test run as figure 4.2 plotted as a contour plot, from this plot, timings for the passage of the vortex on the upper surface can be derived (Niven, 1992).

4.2 Experimental errors

Before presenting any data it is important to assess the quality of the data being investigated. The following sections look at the individual areas of experimental error. Overall the quality of the data recorded at Glasgow University's dynamic stall test rig is

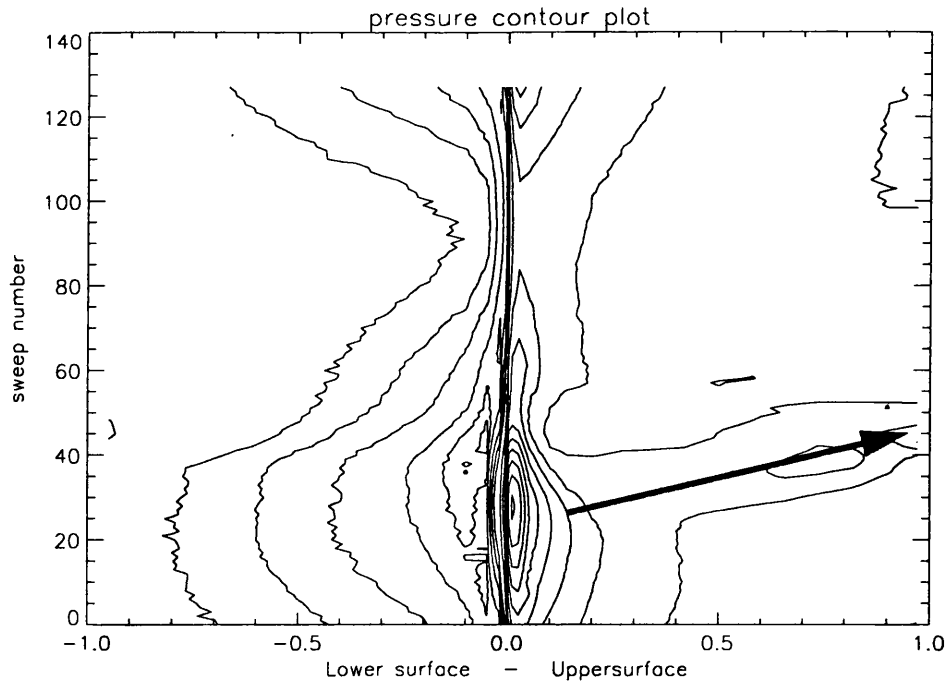


Figure 4.3 - Pressure contour plot
(Mean angle = 16.0, amplitude=10.0 Freq= 4.28)

considered of sufficient quality to allow investigation into the physical process's that make up dynamic stall. Additionally the data can be used to verify and enhance dynamic stall predictive codes. However it must always be regarded as wind tunnel test data, that is unlikely to be repeated in the three dimensional, no blockage flow, surrounding a helicopter rotor.

4.2.1 Dynamic pressure

The main area of concern for these experiments comes from the measurement of dynamic pressure and it's influence on the calculation of individual coefficients of pressure, (Eqn 4.1). The variation in dynamic pressure for a range of static tests is given in figure 4.4. This illustrates the drop off in dynamic pressure as the model's incidence is increased in discrete steps, and it's recovery as the model's incidence is decreased in incidence. There is no hysteresis in this process. The percentage reduction in dynamic pressure going from 0° to 25° incidence is the same for all three Reynolds numbers, at 15%.

Figures 4.5 and 4.6 illustrate the dynamic pressure variation for oscillatory tests,

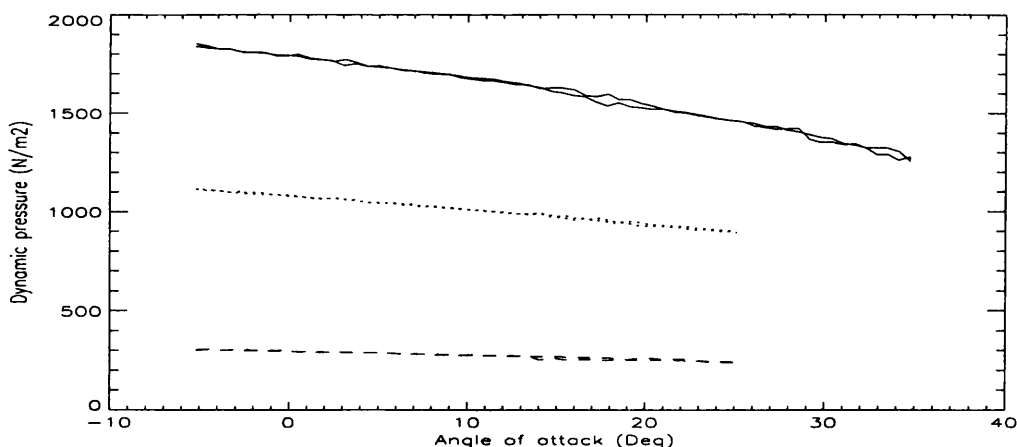


Figure 4.4 - Variation in dynamic pressure during static tests

showing firstly the variation with both increased mean angle at a fixed amplitude and frequency, and secondly the effect of increased frequency. The relationship with increased mean angle is similar to that shown by the static tests, in that there is a mean fall off of about 15% as the mean angle is increased from 0° to 25° . The effect of increasing the models frequency is to reduce the variation in dynamic pressure during the motion, as depicted by the tighter hysteresis loops for higher frequencies in figure 4.6.

The method used to measure dynamic pressure throughout these results was to measure the static pressure on both sides of the wind tunnel 1.2m upstream of the models leading edge and compare this with the static pressure measured in the settling chamber. Thus an instantaneous, averaged across the working section, dynamic pressure was used for each coefficient of pressure (C_p) calculation. Previous models had measured the dynamic pressure using a pitot static tube mounted on one side of the tunnel. Their corresponding results for figures 4.4-4.6 differ vastly in that they show up the marked asymmetry of the flow and feed this into resulting C_p calculations.

It is important to realise that the flow asymmetry is still present in these tests. Inaccuracies in the dynamic stall measurement, or more importantly the asymmetry of flow in the wind tunnel at high incidence, as measured by the pitot static probe (Leishman, 1998), will grossly distort the integral calculations for the aerodynamic constants. However, the relative differences between pressure transducer recordings on each side

Figure 4.5 - Variation in dynamic pressure with increasing mean angle on oscillatory tests

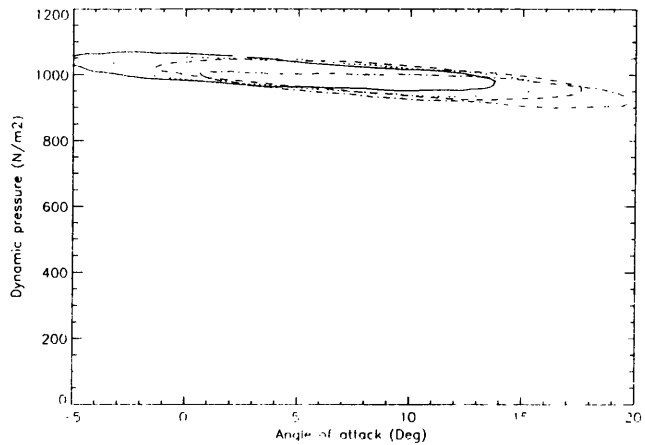
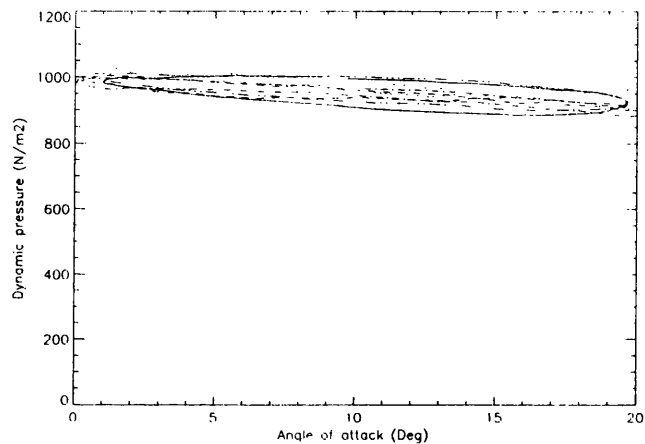


Figure 4.6 - Variation in dynamic pressure with increasing reduced frequency



of the model will be unaffected, thus timing measurements based upon individual transducer outputs are unaffected.

To investigate the influence of tunnel blockage further a series of tests are being carried out on identical models with reduced chord lengths. The results of these will be compared to the 0.55m models. This work should clarify the magnitude of this problem.

4.2.2 Wind tunnel

The oil flow visualisation pictures presented later in this chapter clearly show a three dimensional flow pattern across the wind tunnel. Figure 3.6 also illustrates the flow angularity problem of the wind tunnel. However both these problems are greatly reduced by the positioning of the pressure transducers at mid span, where the flow appears to be nominally two dimensional. This mid span measurement also diminishes problems associated with the small clearance (2mm) between the wind tunnel and the model ends to allow free motion.

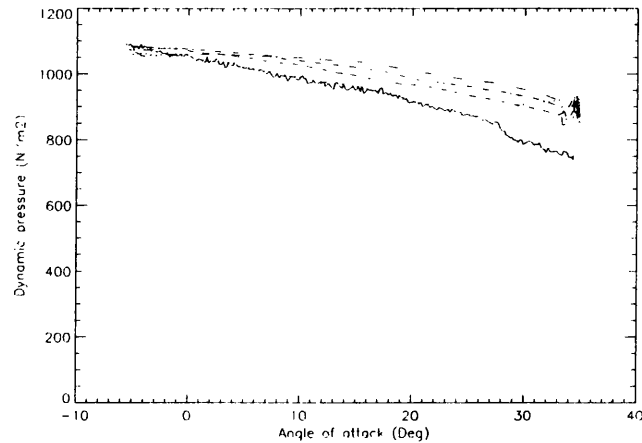


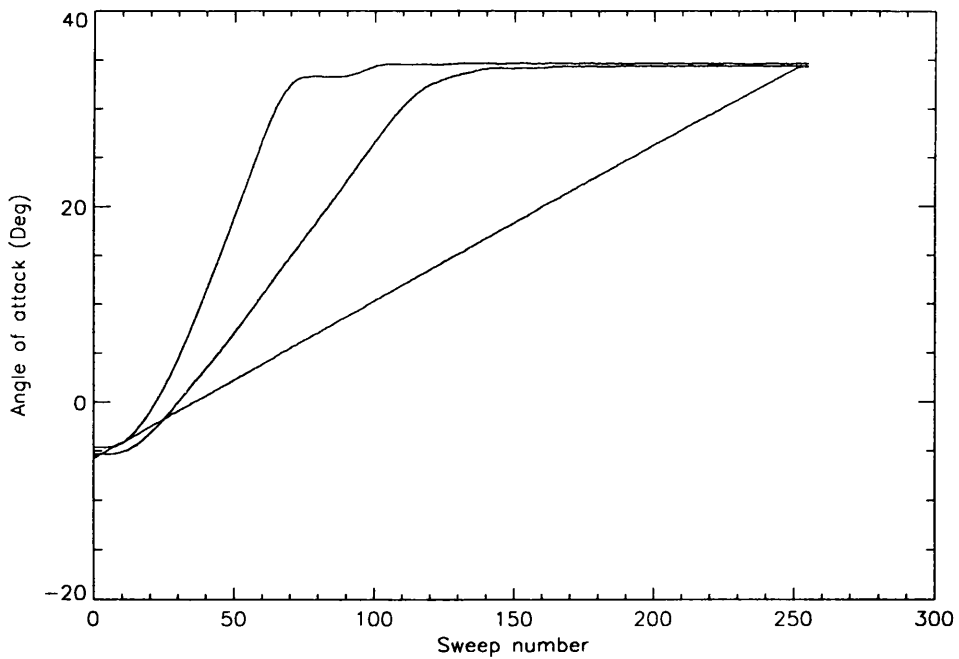
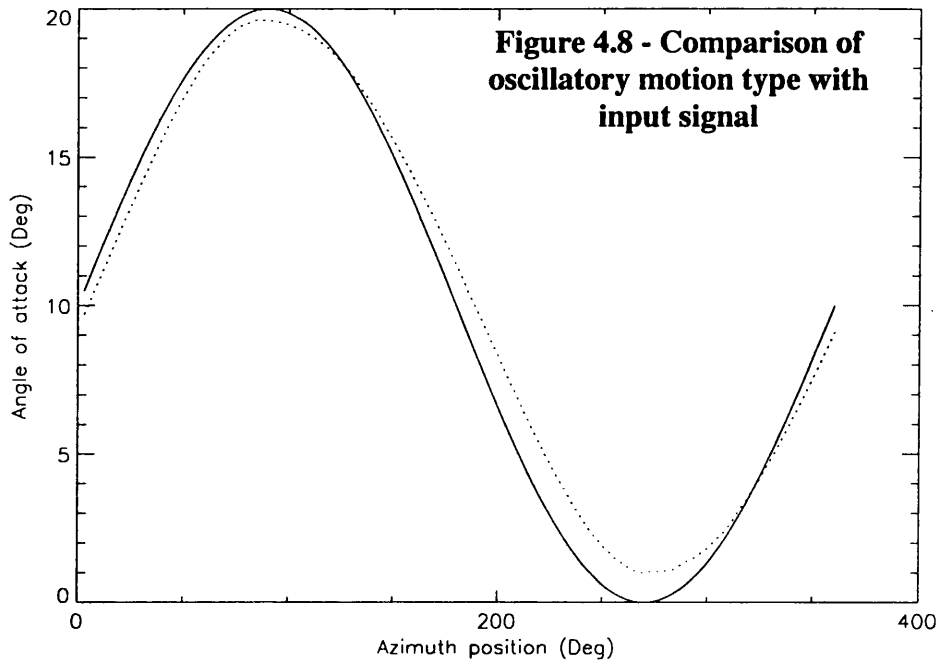
Figure 4.7 - Variation in dynamic pressure with increasing ramp rates

4.2.3 Model motion

The hydraulic actuator that governed the models motion was sufficiently powerful to easily overcome the aerodynamic forces involved. However its own dynamics meant that whatever motion was requested would never be exactly realised. Figure 4.8 shows a perfect $10 + 10\sin(\omega t)$ for a frequency of 4.23 Hz against the actual achieved model motion for this test run.

The comparison illustrates the slight imperfections introduced by the hydraulics dynamics. This is more pronounced on the ramp motion inputs, particularly as they get faster, approaching a step function. Figure 4.9 shows the models motion for a slow, medium and fast ramp rate going from -5° to 30° . These respectively show the system behaviour changing from linear, to first order and then second order as the pitch rate is increased from $< 1^\circ/\text{sec}$ to $398^\circ/\text{sec}$. For the majority of the research this is not considered a problem, as the actual motion is very accurately recorded. Thus, unless one is concerned with absolute motion types, e.g perfect sine waves, the research can be based upon the observed motion type, e.g imperfect sine waves. The only problem encountered with this in this dissertation was when considering the measurement of reattachment initialisation as a function of the ramp rate (which is not constant). How this problem was resolved is covered in chapter five.

4.2.4 Pressure transducers



The calibration of the pressure transducers output right through the system (figure 3.8) gave very accurate individual pressure readings at each location. The pressure

transducers were very fragile in nature and could easily become damaged during operation in the wind tunnel in the middle of a series of tests. To check the validity of all the pressure transducers within the dynamic stall database a FORTRAN 77 program was written that checked each transducer output for each sweep of data with the corresponding output for the two adjacent transducers. If the transducers output had a very low standard deviation (constant output), or did not lie between the two neighbouring readings, it was considered suspect. For each suspect transducer, an output similar to figure 4.10 was displayed for the user. The user then decided whether the transducers output needed to be interpolated for, and whether that test run needed to be repeated.

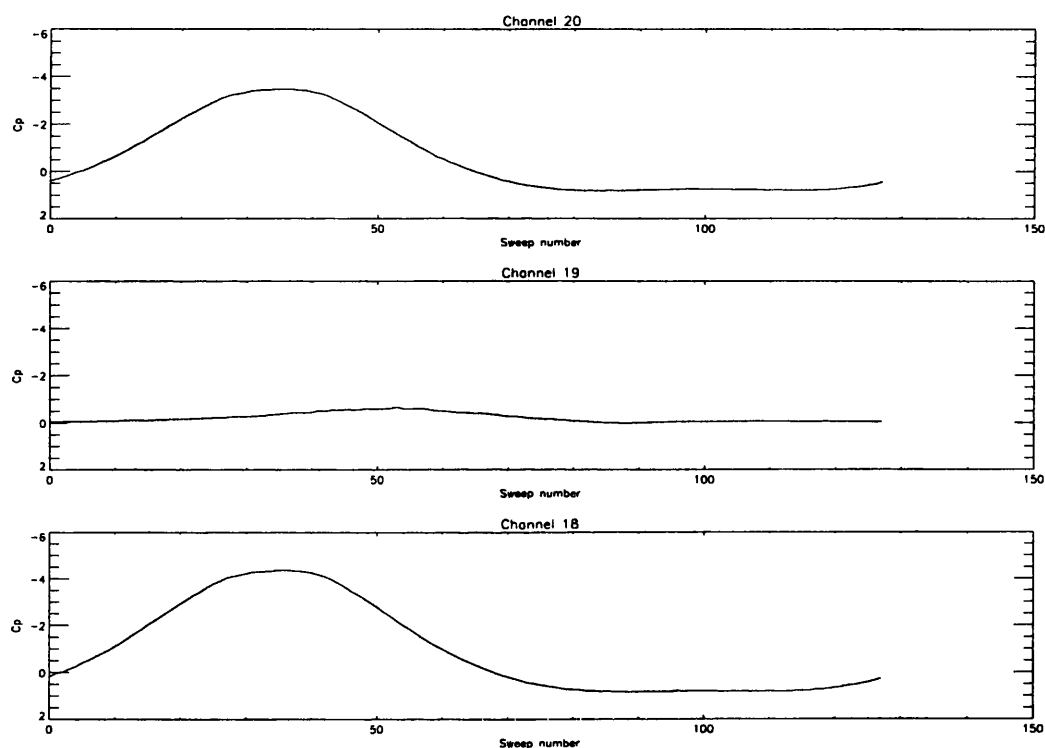


Figure 4.10 - Example of erroneous output from channel 19 that need to be interpolated for

Another error with the pressure transducers was their sensitivity to acceleration when mounted parallel to the axis of acceleration. This was not the case for the majority of transducers, which were mounted perpendicular to the chord line around the model. No acceleration effects were measured on these transducers. However due to space restrictions around the trailing edge of the model, the last two transducers in the upper

surface were mounted parallel to the chord. The acceleration forces measured on these transducers can be clearly seen in the impulsive loading tests that were carried out (Figure 4.17. These tests were short arc, very fast ramps at low tunnels speeds (therefore small aerodynamic loads) to isolate the impulsive pressure loadings due to a step change in incidence. It is recommended for future models that these transducers be mounted perpendicular to the chord, even if this means slightly longer brass tubes feeding the model surface pressure to the transducer. This will mean less favourable frequency response from these transducers, but since this is measured in Mhz and the actual model motion frequencies are Hz, it should not pose a problem.

4.2.5 Repeatability of the data

The repeatability of the measured data was found to be excellent (Angell, 1990). Both comparison of each of the ten individual cycles of data from a test and comparison of similar tests performed over a year apart have remarkable agreement. All the data being displayed in this dissertation uses averaged over either ten (oscillatory) or five (ramp) cycles. The unaveraged data is not currently available for analysis, however it is planned to put this data alongside the averaged data on the dynamic stall database for future analysis.

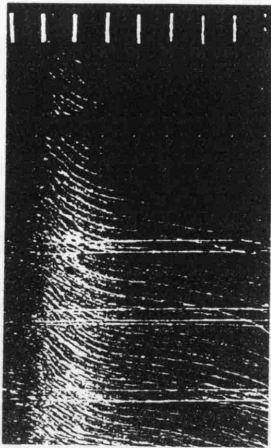
4.3 Oil flow visualisation

The purpose of carrying out a set of flow visualization tests was primarily to measure the static separation point behaviour with increasing incidence. The flow visualisation pictures also illustrate the location and size of the laminar separation bubble. Additionally they illustrate the presence of three dimensional flow within the tunnel. Figures 4.11 (a - h) are reproductions of photographs of the upper surface of the model at a range of incidences, with a Reynolds number of 1.5million.

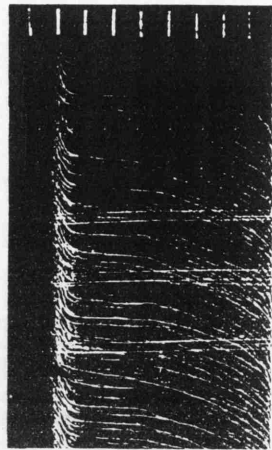
The flow separation point is measured by observing a series of photographs (e.g. figure 4.11(f) shows 20% separation) where the chord is marked at 10% intervals. From these photographs the leading edge bubble can be clearly seen as a region near the leading edge where the oil flows downwards under the influence of gravity. As the incidence is increased this region is seen to become small in size and to move towards the leading

Figure 4.11 - Oil flow visualisation photographs

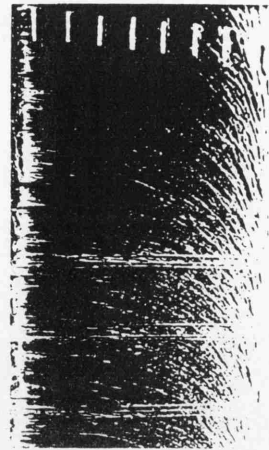
a) -2.6



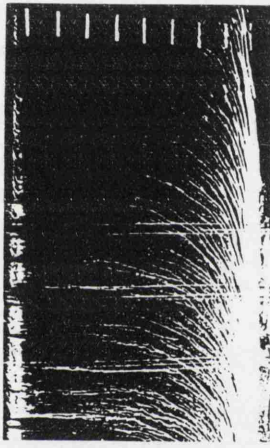
b) 0.6



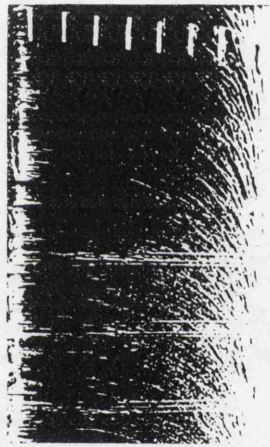
c) 11.2



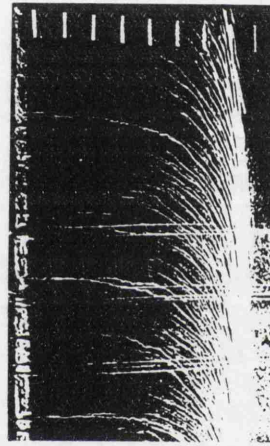
d) 11.7



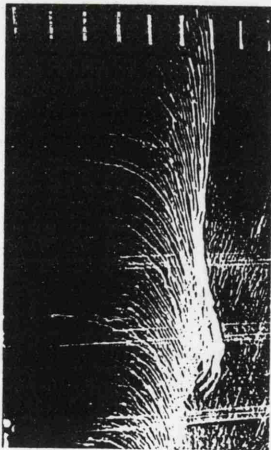
e) 13.3



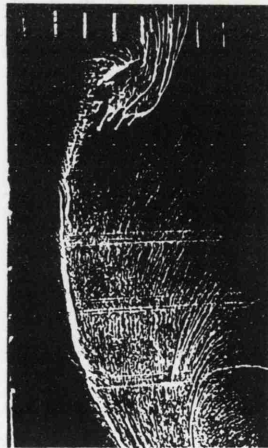
f) 16.0



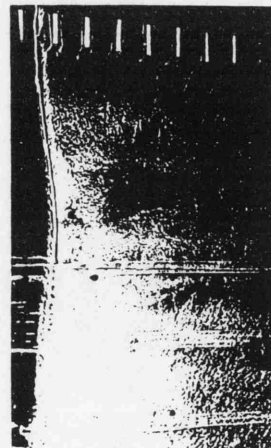
g) 17.0



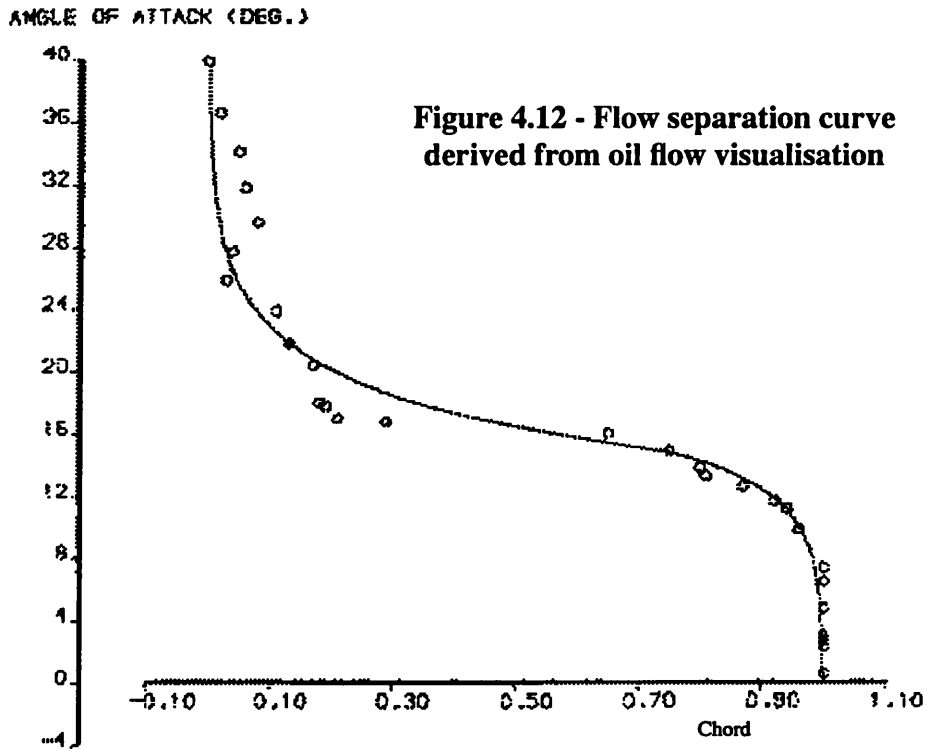
h) 21.0



i) 30.0



edge. The separation point is determined as the position where the oil starts to fall rapidly downwards, again under the influence of gravity, rather than be carried chordwise in the attached boundary layer flow. From these photographs figure 4.12 has been



derived.

A best least squares fit has been applied to the data, and this is shown on the graph. A function is required to model this separation point movement in the Beddoes model. In chapter five a function is described that follows this curve.

All the oil flow tests were performed by rotating the model to the desired incidence before the wind tunnel was started up. So in effect this separation point measurement is really a measurement of reattachment point.

The photographs clearly show an “S” pattern at higher incidences, which indicates three dimensional flow within the tunnel. (Figure 4.11 (h))

The addition of a trip wire over the lower 50% of the span (figure 4.13) clearly

shows that the laminar separation bubble has been replaced by a turbulent boundary layer over this section of the span. Note that the upper surface is unaffected by this. This same phenomena can be seen on a smaller scale in the oil flow photographs without a trip wire present, where leading edge imperfections/ contamination lead to a localised turbulent stream of flow. The very presence of the leading edge pressure tapping holes may cause this effect over the mid span instrumented section.

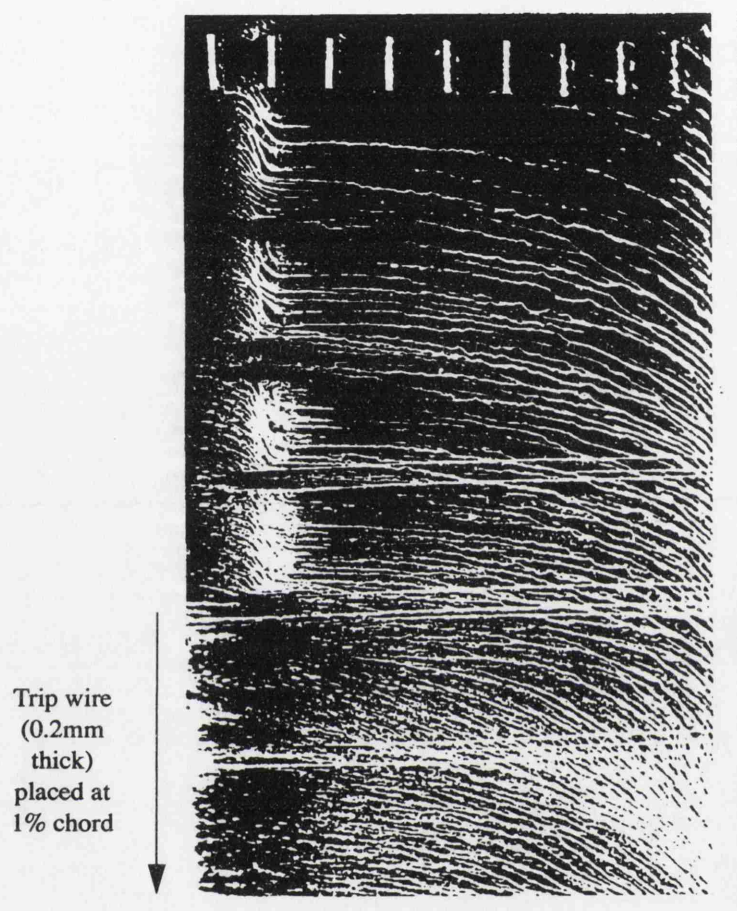


Figure 4.13 - Effect of trip wire on leading edge bubble

4.4 Static tests

The static characteristics of the NACA 23012B were measured in a number of tests at Reynolds numbers of 0.8, 1.5 and 2.0 million. A typical set of results is given in figure 4.14. The static stall angle at 1.5 million is 14.3° , this increases to 15.0° at 2.0 million and decreases to 13.9° at Reynolds number 0.8 million. The lift curve slope is fairly consistent at 0.088 per degree, being slightly less for the lower Reynolds number.

These small changes with Reynolds number can be attributed to the thickening of the boundary layer at lower Reynolds numbers, which in turn leads to a loss in lift and earlier separation.

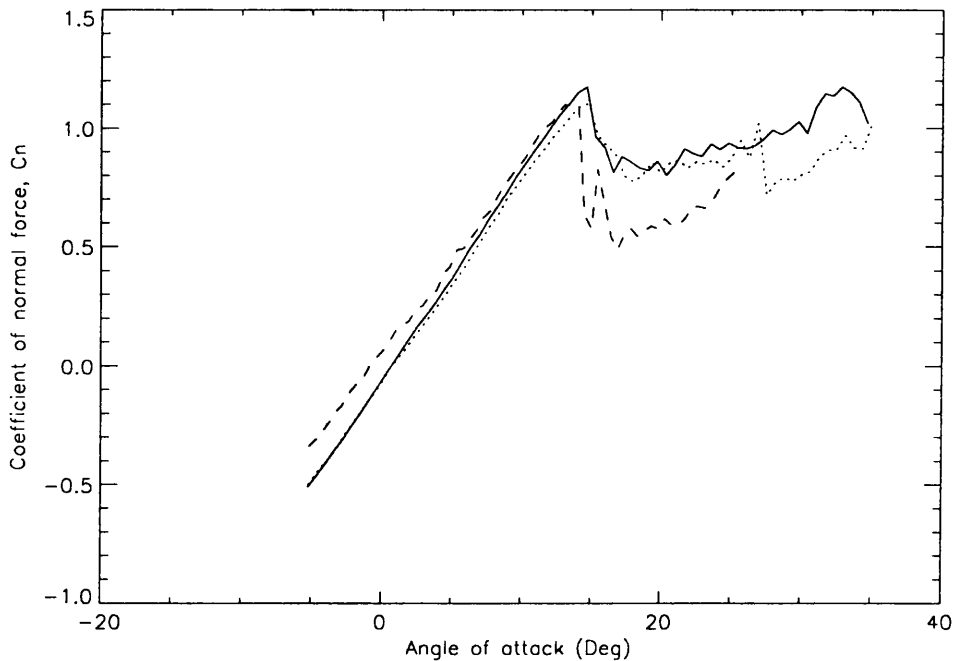


Figure 4.14 Static characteristics for the NACA 23012B with Reynolds number variation

A similar set of graphs for both C_t and C_m are given in figures 4.15 and 4.16. Note that all results are being presented as C_n , C_t rather than C_l , C_d . This is because C_n is the most accurate coefficient to integrate the pressure distribution for, since it acts over the largest length (chord). Also the coefficient of drag would be misleading to present, as it would not take into account the surface skin friction component.

By analysis of the individual pressure distributions around the aerofoil at each static incidence, a flow separation point can be determined, figure 6.9. This shows good agreement with the oil flow visualisation tests, thereby validating this method of pressure point analysis which is used extensively in chapter five.

4.5 Oscillatory tests

The oscillatory data is the most commonly measured in the investigation of dynamic stall, since this is most often the motion type being utilized, e.g helicopter

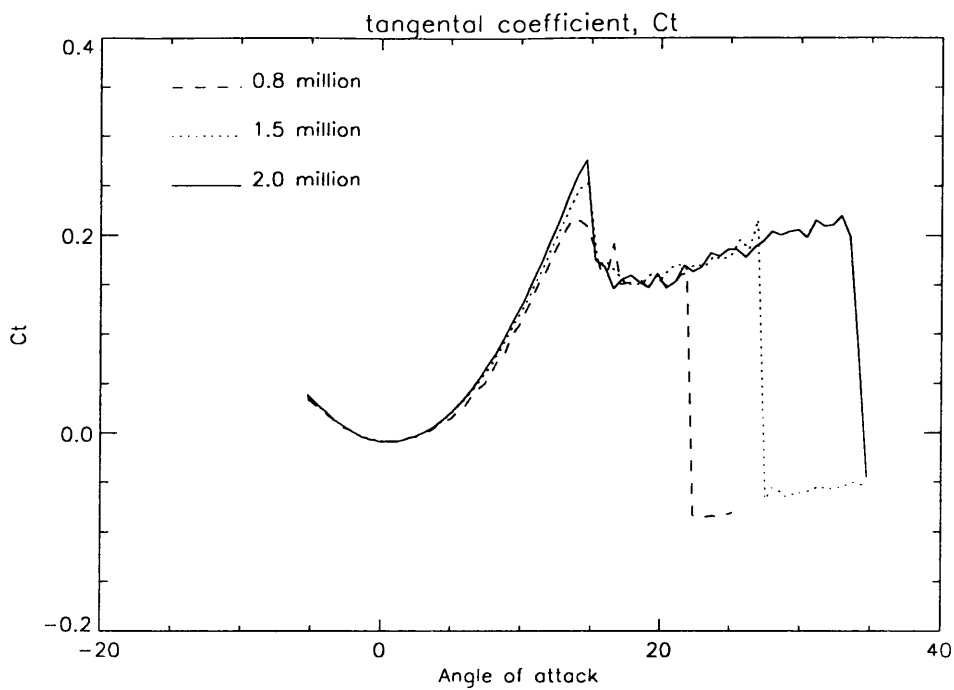


Figure 4.15 - Pressure Tangent coefficient variation with Reynolds number

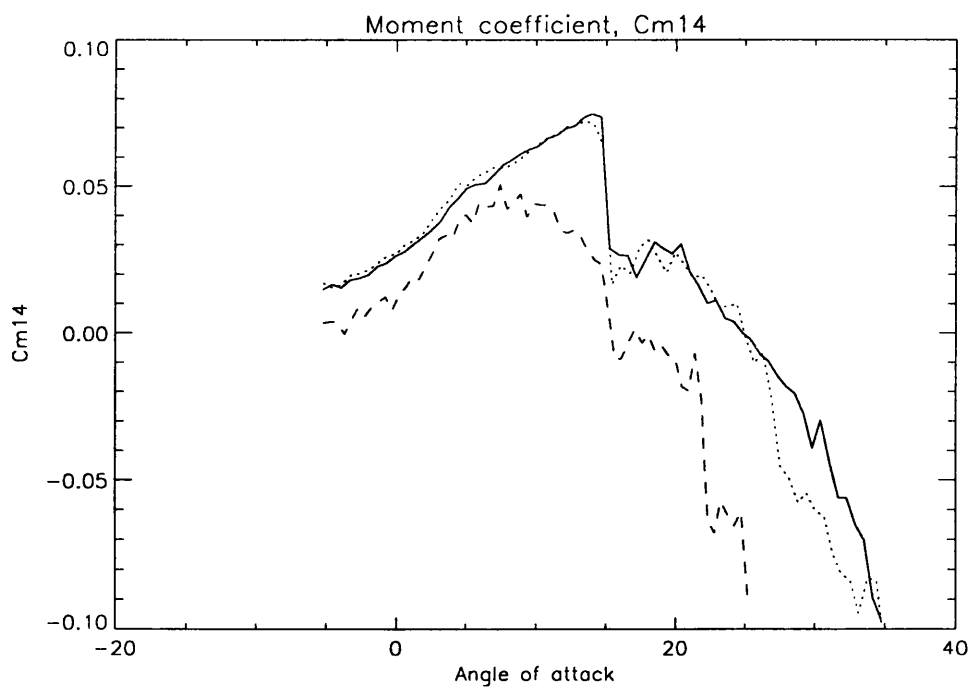


Figure 4.16 - Moment coefficient about 1/4 chord variation with Reynolds number

rotor. Previous research at Glasgow University has examined this data with regard to the timing events of the dynamic stall. This dissertation is concerned with just the reattachment part of this process, and is therefore utilizing the ramp down data. However, a full series of oscillatory tests were performed on the model to allow other researchers to exploit the data. A typical set of oscillatory results are given in figure 4.17 to indicate the type and quality of data available.

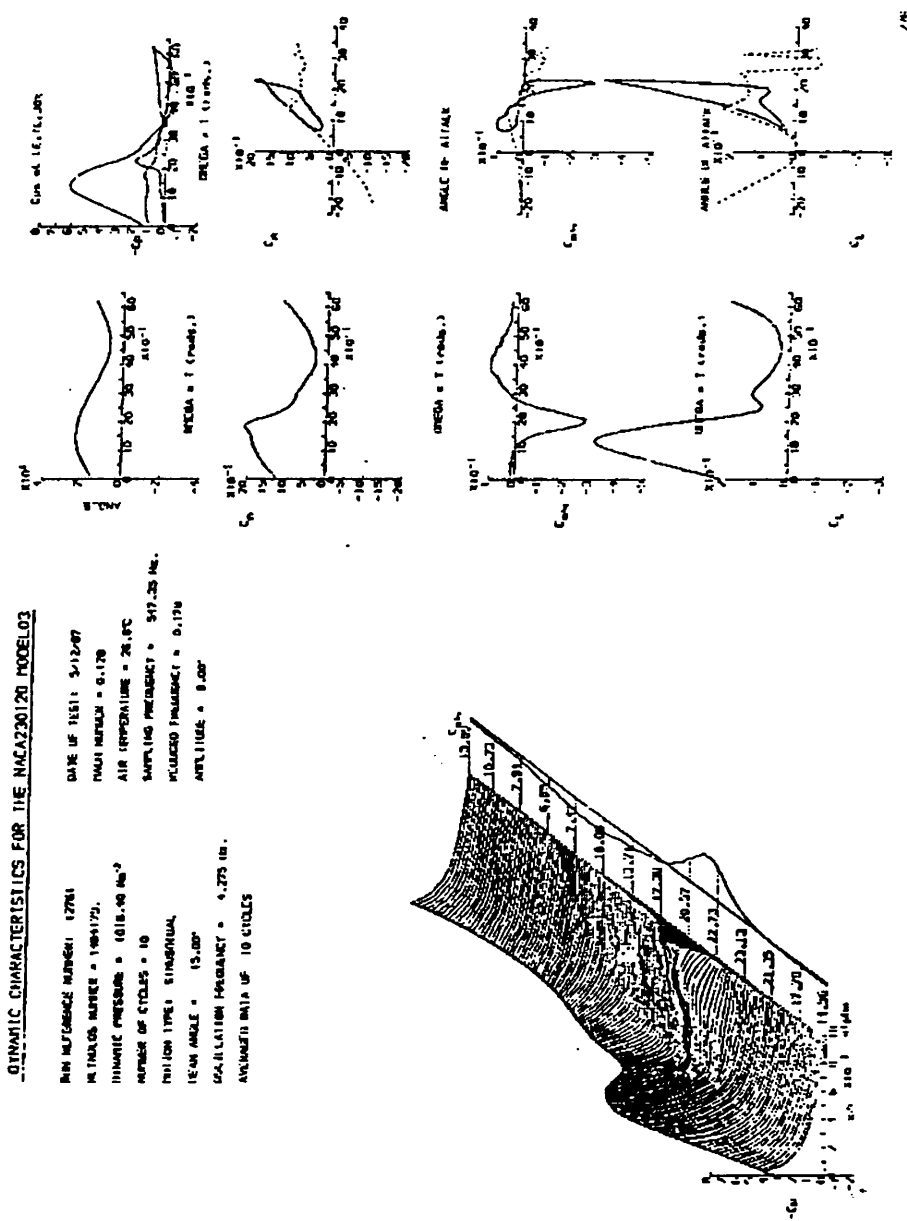


Figure 4.17 - Typical Sinusoidal test data for the NACA23012B aerofoil

4.6 Ramp Up

The ramp up data has been successfully analysed by Niven and Gracey, (1991), to predict the dynamic separation characteristics of the family of NACA 23012 sections tested at Glasgow University. One section of this data that has not been previously looked into in isolation is the “impulsive” loadings. These impulsive loadings are a fundamental part of the Beddoes model, and apply equally to the process of separation and reattachment. Hence the following investigation was performed:

4.7 Impulsive loadings

A series of tests were performed (Table 3.8) to measure the impulsive loadings on an aerofoil undergoing a short, fast ramp motion. The results from these tests clearly show the ability to isolate these impulsive loads, and that the test facility is capable of producing the very fast ramps required to observe this.

Figure 4.18 shows C_n output for a 0-12 degree arc at a pitch rate of 200 degrees/

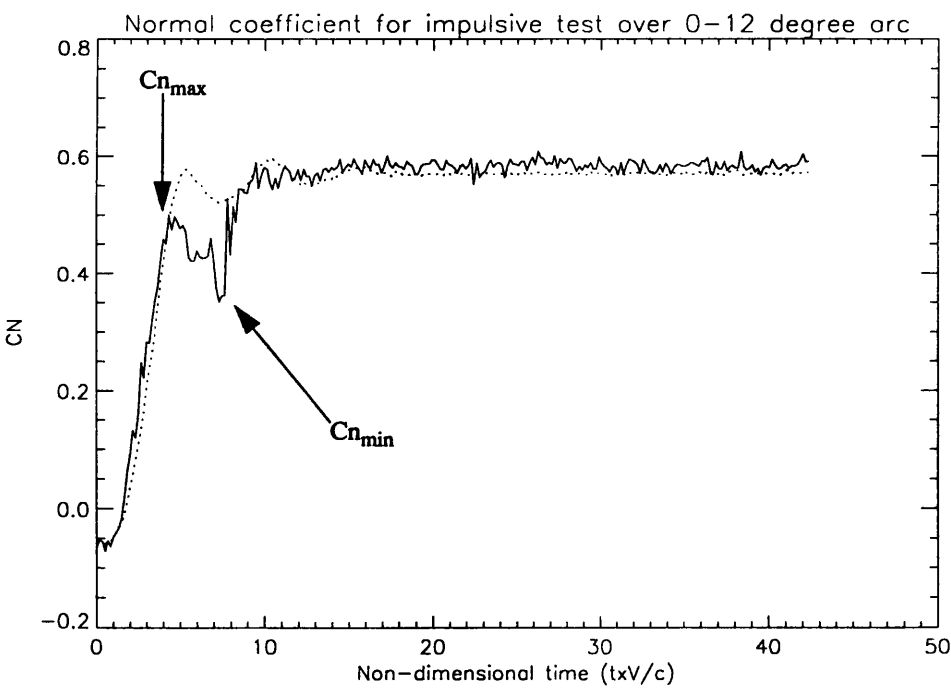


Figure 4.18 - Impulsive loading measurement of C_n

sec. The same test performed over an arc of 0-20 degrees is given in figure 4.19. They

illustrate that, in order to observe the impulsive loadings, you must avoid all the dynamic stall loadings that are several orders of magnitude higher.

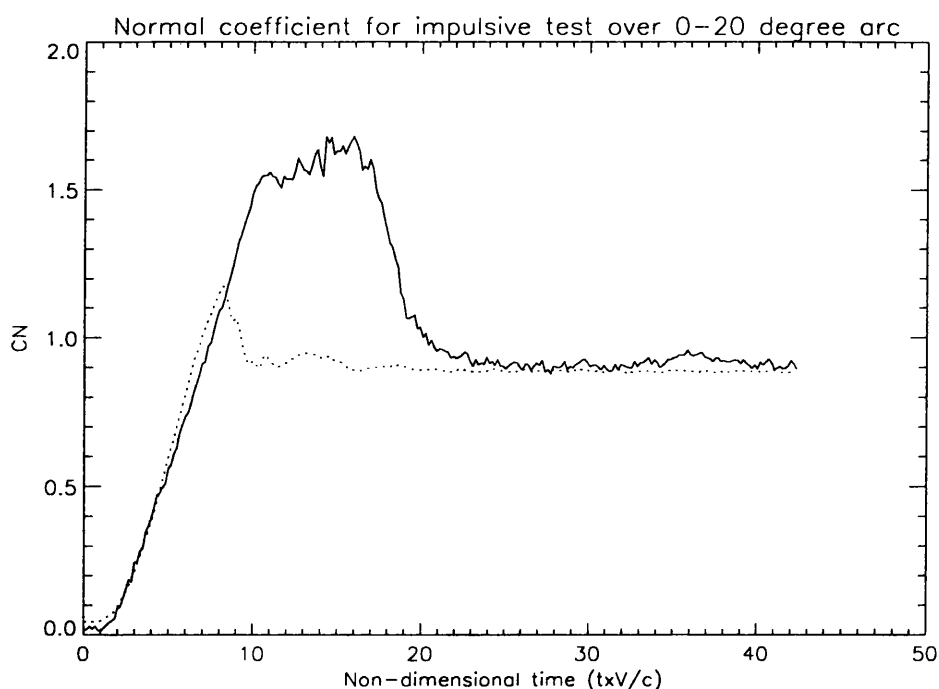


Figure 4.19 - Impulsive loadings being masked by dynamic stall effects

The measurement of $C_{n_{max}}$ and $C_{n_{min}}$ has been carried out over the entire range of impulsive loading tests, and the non-dimensional timing of these events is in broad agreement with the results of Aihara, 1984. However, an additional pressure peak was observed on the fastest ramps, figure 4.20

This additional C_n peak can be attributed to the upper surface trailing two pressure transducers, which show a large suction, see figure 4.21 and 4.22. One possible cause for this could be that they are measuring acceleration forces. However, plots of their output against both normal and tangential accelerations do not give good correlation. Additionally, the sensitivity to acceleration is given by the manufacturer as 0.05%FS per g in the tangential (most sensitive) direction. The maximum order of accelerations is 4g, which in measured pressure terms is only 20% of this observed suction peak.

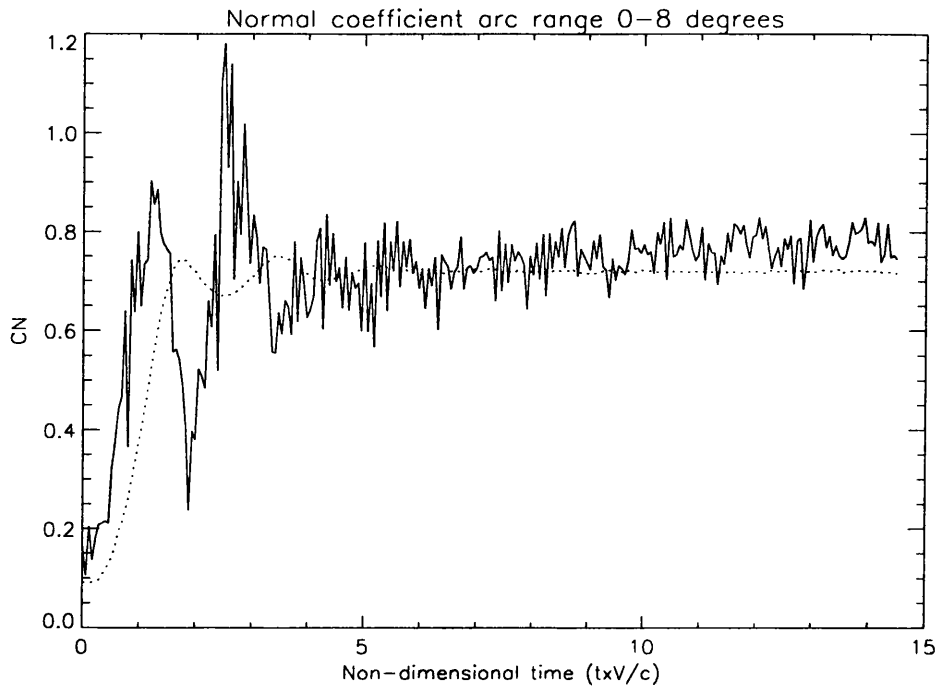


Figure 4.20 - Impulsive loading measurement showing secondary peak

Also, if acceleration was the cause, one would expect to see equal effects on the trailing edge lower surface pressure transducers. Another possible cause could be a wind tunnel interaction, perhaps a reflected pressure wave off the tunnel wall? A simple set of ramp down tests under similar conditions would greatly help in the investigation of this observed phenomena.

Another observed difference with Aihara data was the fact that $C_{n_{max}}$, defined as the first impulsive peak, tended to be less than the equivalent static C_n for a similar incidence. This could infer that the build up in circulatory lift for these tests is somewhat slower than that being measured by Aihara.

A full set of these tests results have been analysed by Tom Beddoes of Westland Helicopters Ltd. His comments are given in appendix C.

4.8 Conclusions

A complete set of dynamic pressure data for an experimental NACA 23012B

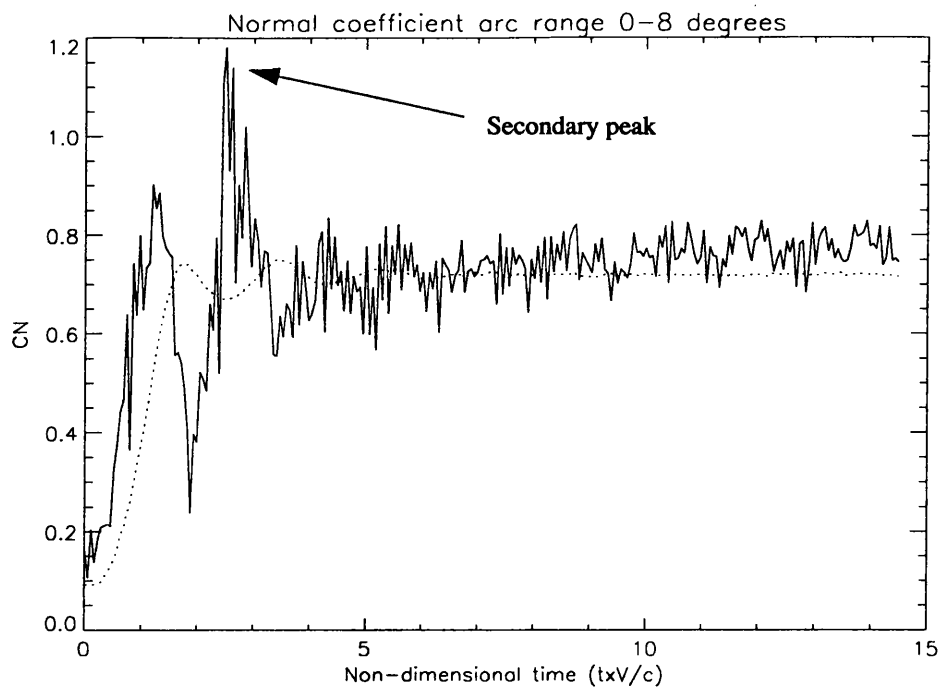
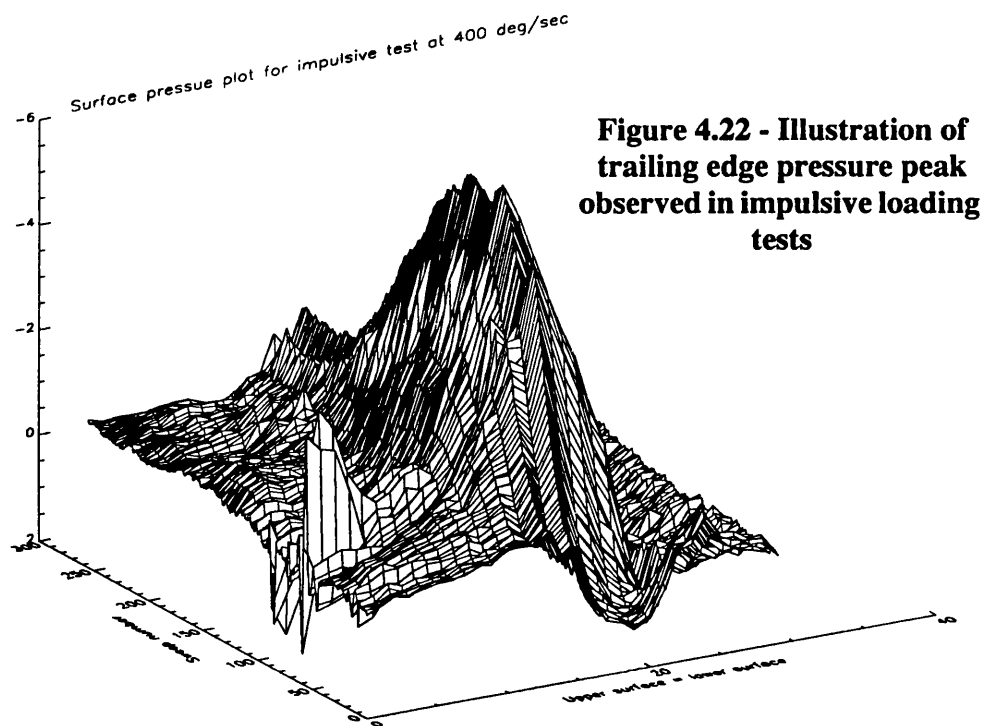


Figure 4.21 - Impulsive Cn loads for fastest ramp (460 degrees/second)



section has been reviewed and found to be of consistent good quality. The data have been made available on the Glasgow University dynamic stall database for future analysis.

A preliminary investigation into impulsive loadings has been made. A more detailed experimental investigation is required before these results can be fully understood. In particular it is recommended that a full set of impulsive tests be carried out with improved transducer layout in the rear section of the model, and that this range of tests include the ramp down motion type.

Chapter 5

Coding the Beddoes dynamic stall model

Nomenclature

C	Chord length of aerofoil
CL_α	Slope of lift curve
C_n	Normal force
C_m	Coefficient of moment about 1/4 chord
C_l	Coefficient of lift
C_{nv}	Coefficient of vortex induced lift
C_{nc}	Circulatory component of Normal force
C_{ni}	Impulsive component of normal force due to step incidence change
C_{nq}	Impulsive component of normal force due to step pitch rate change
n	Subscripts $_n$ and $_{(n-1)}$ are used to denote instantaneous values as the incidence is changed in discrete steps.
f	Separation point ($=x / C$)
V	Freestream velocity
M	Mach number
a	Speed of sound
α	Angle of attack
α_e	Effective angle of attack which incorporates Wagners function.
α_f	Effective angle of attack which models the boundary layer response.
Ed	Exponential decay in impulsive loadings
Ef	Exponential delay in separation point movement
Ev	Exponential decay in vortex induced lift
Ep	Exponential delay in leading edge separation due to pressure lag.
TL	Ratio of chord length to speed of sound (C/a).
KL	Constant used for impulsive loading decay.
K0, K1, K2	Constants to derive coefficient of moment from C_n value
S1, S2, α_l	Constants used to form a function equal to the separation curve derived from static tests.

$X(t)$, $Y(t)$ Functions used to describe the build up in circulatory lift (Wagners function).

T_1 , T_2 Constants used to reproduce Wagners function.

A_1 , A_2 , b_1 , b_2 Constants used to derive a function similar to Wagners function for build up in circulatory lift with time due to a step change in incidence

D_{ai} Impulsive incidence change response

D_{ni} Pressure lag response

D_{qi} Impulsive pitch rate change response

D_{fi} Boundary layer response

Note: This chapter outlines the equations used to define a working model of the Beddoes dynamic stall code. The Reader is encouraged to look at the numerous papers published by Tom Beddoes on this model to gain a fuller understanding into its derivation.

5.1 Introduction.

In static test conditions the streamlined flow around a two-dimensional aerofoil breaks down (stalls) with progressively increasing angle of attack, at a certain point (α_{ss}) called the static stall angle. For an aerofoil undergoing a rapid increase in the angle of incidence, the position is more complicated. The onset of dynamic stall can be delayed to an incidence considerably higher than that for static stall, with flow breakdown more severe and more persistent. The occurrence of an initial surge in the lift force and the strong negative (nose down) pitching moment is followed by a sudden collapse of first the moment and then the lift. The aerodynamic forces show large hysteresis with respect to the angle of attack, and under certain circumstances the hysteresis of the pitching moment can result in a net gain of energy by the aerofoil over the oscillation cycle. Over the years a number of people have developed models for the process of dynamic stall. Dr. Galbraith (1981) discusses the current methods of predicting dynamic stall. One method which uses a predominantly empirical approach is that developed by Tom Beddoes for modeling the in-flight airloads on helicopter rotor blades. The following sections describe Tom Beddoes model for Dynamic Stall.

5.2 Main Features of Dynamic Stall.

For the purposes of modelling, four distinct phases of dynamic stall flow development are given below.

[1] The first and most fundamental of the four phases is that for an appreciable pitch rate which increases the angle of attack, the normal static values of the lift coefficient may be exceeded. The increase in the lift coefficient occurs while the changes in the boundary layer which precede stall are developing. Some flow reversal is observed in the boundary layer but it has little effect on the external flow and thus the lift and moment characteristics appear as a continuation of the fully attached flow regime.

[2] The second phase is the development and shedding of a concentrated vortex from the forward part of the aerofoil or, from behind the recompression shock wave if appropriate. The subsequent motion of the vortex over the aerofoil's surface continues to generate lift, but due to the redistribution of the pressure over the chord the pitching moment is adversely affected and increases rapidly.

[3] When the vortex progresses beyond the trailing edge the lift and consequently the lift induced pitching moment decay rapidly, to the fully separated condition.

[4] If the pitch angle is reduced to an angle below that required for static stall the flow will become reattached from the leading edge.

Beddoes has concluded from experimental data that, to a first order, there is a common time scale for the above events, which is somewhat independent of the aerofoil geometry, intermediate motion and Mach number. He uses the non-dimensionalised time parameter $\tau = t V / C$, which is equivalent to the number of chord lengths travelled. The lift and moment continue to grow after the pitch angle has exceeded that for static stall for approximately two chord lengths, after which the vortex is shed. As the vortex progresses towards the trailing edge the lift continues to grow for a further three to four chord lengths of travel until the vortex passes the trailing edge. With variations in the forcing parameters such as amplitude, mean pitch angle and frequency of motion, the above events move around the cycle and produce significant changes in the lift and moment characteristics. Test results have illustrated the effects of increasing frequency at near constant pitch amplitudes and mean angle of attack. Vortex shedding is delayed as the frequency is increased until it occurs after the maximum angle of attack and lift coefficient have been reached. Finally the frequency is such that it does not allow sufficient time for the processes described above to be completed. This upper limit appears to

be at a reduced frequency of 0.6 and has a time scale of 5 chord lengths of travel. Another reason for which the above processes fail, is when the minimum angle of attack is sufficiently great so as to prevent the reattachment of the flow, in this case depending upon the extent of flow separation, partial re-attachment may occur.

5.3 Linear Dynamic Flow Model.

The classical solution for the time varying aerodynamic loads is that given by Wagner for incompressible flow. Wagners function may be re-formulated for a indicial solution (timewise sampled) and allowing for compressibility as;

$$Cnc(t) = Cl\alpha \times \Phi_c(t) \times \Delta\alpha = Cl\alpha \times \alpha_e(t)$$

$$\alpha_e(t) = [1 - X(t) - Y(t)] \times \Delta\alpha$$

$$X(t) = A1 \times \exp\left(\frac{-t}{T1}\right)$$

$$Y(t) = A2 \times \exp\left(\frac{-t}{T2}\right)$$

$$T1 = \left[b1 \times (1 - M^2) \times \frac{2V}{C} \right]^{-1}$$

$$T2 = \left[b2 \times (1 - M^2) \times \frac{2V}{C} \right]^{-1}$$

where A1=0.165 A2=0.335 b1=0.0455 b2=0.3000 & CL α =0.108

The above formulation may be interpreted as lift deficiencies decaying with time. For general motion, that is a non-uniform downwash across the chord the instantaneous angle of attack is replaced by the value of the downwash at the 75% chord.

5.4 Dynamic Stall.

Beddoes uses a hypothesis of the physical model for his representation of the separated flow regime, which has been developed from the observation of experimental data. His early model depends on the static characteristics of the aerofoil which in turn are dependent upon the aerofoils profile, Reynolds number, Mach number and its sur-

face condition. An important feature of the model is the angle of incidence at which the pitching moment breaks. This angle α_1 , marks the end of the linear region as beyond this point under static conditions the boundary layer can no longer support the adverse pressure gradients generated by the increasing lift and the boundary layer is forced to separate from the surface of the aerofoil. Under dynamic conditions the critical conditions may be delayed so that the boundary layer does not separate and the lift and pitching moment are able to continue growing. The pitching moment continues to grow until the dynamic stall vortex is shed from the region of the leading edge after a delay of approximately two chord lengths of travel. The lift continues to grow until the vortex passes the trailing edge, after a further time delay at which point it falls off rapidly to the fully separated value. The basic feature of the Beddoes model for dynamic stall is the two time delays for the onset of pitching moment and lift divergence. These time delays are modelled as simple exponential functions.

As the angle of attack reduces below the static stall value α_1 the process of re-attachment is initiated. The calculation is re-initialised using the separated value for the lift coefficient as an initial value.

The time delays (T_1 and T_2) do not appear to be sensitive to pitch rate. and have a value of 2.0 for the first and 5.5 for the second (from experimental analysis).

5.5 Types of Aerofoil.

For the purpose of modelling dynamic stall, aerofoils can be divided into two types based on their static stall behaviour, The aerofoil can be described as exhibiting either leading or trailing edge stall characteristics.

[1] Leading edge stall. This type of aerofoil exhibits a fairly abrupt stall resulting either from leading edge stall or the rapid progression of trailing edge separation triggered by leading edge re-separation.

[2] Trailing edge stall. Aerofoils which exhibit a gradual stall resulting from progressive trailing edge separation. Generally thick section aerofoils or ones with a high camber. (NACA0012 is used as an example of a thick section aerofoil.)

5.6 The Point of Flow Separation.

A critical problem in modelling the dynamic stall behaviour of an aerofoil is the determination of the point at which the flow separation process is initiated (the aerofoil 'stalls'). Beddoes' early papers use the break in the static pitching moment as the point for the initialisation of flow separation. This simple criterion will model the dynamic behaviour of aerofoils which exhibit leading edge stall quite satisfactorily, however for aerofoils which exhibit static trailing edge stall the model is inadequate, because the time scale for trailing edge separation is sufficiently long that its inhibiting effect on the circulation is delayed and the apparent delay beyond the static stall is much greater than for an aerofoil which exhibits leading edge stall. To improve the model Beddoes suggests the use of a new criterion for the determination of the initiation of flow separation, which is applicable to all aerofoil sections at low Mach numbers ($Mach < 0.3$). Beddoes new criterion involves the calculation of leading edge velocities under dynamic conditions, as the leading edge has been determined as the critical point for flow separation for an aerofoil when the pitch rate exceeds a small positive value. For practical purposes, a criterion which may be used to denote the onset of leading edge stall is to determine the lift value associated with the critical angle of attack which invokes the leading edge pressure criterion. At Mach 0.3 the critical lift coefficient is 1.45. (See Beddoes, "A generalised model for airfoil unsteady aerodynamic behaviour", 1986, figure 13.) It may be concluded that trailing edge separation which occurs on many aerofoils in the static condition near the stall takes significant time to develop and, when the pitch rate is sufficient, the leading edge region becomes dominant in determining the sequence of dynamic stall.

5.7 Trailing Edge Separation.

Trailing edge separation is involved to some degree in almost all examples of aerofoil stall. Even when the primary source of separation is at the leading edge or at the shock wave the associated boundary layer disturbance is generally sufficient to promote some separation at the trailing edge. The associated loss in circulation introduces a non-linear function in the lift and pitching moment and may delay the onset of the critical conditions for stall elsewhere on the aerofoil, thus delaying the point of flow separation.

Kirchhoff formulated a function for lift by defining the point on the aerofoil at which the flow separates

$$C_n \approx C_l = 0.25 \times C_{l\alpha} \times (1 + \sqrt{f})^2 \times \alpha$$

This may be interpreted as implying that the ratio of the actual lift to the potential value for unseparated flow is equal to $0.25 \times (1 + f^{1/2})^2$ and provides a simple means for determining the lift if the point of flow separation can be determined. To accomplish this the form of the relationship between f and α is generalised, see below. It is comprised of two curves which relates to the fully attached and fully separated conditions from a break point at $f=0.7$ for which the corresponding α is denoted by α_1 .

Beddoes suggests the following functions for the separation point on an NACA0012 aerofoil at a Mach number of 0.3.

when $\alpha > \alpha_1$ then

$$f = 0.04 + 0.66 \times \exp\left(\frac{(\alpha_1 - \alpha)}{S_2}\right)$$

and when $\alpha < \alpha_1$

$$f = 1.0 - 0.3 \times \exp\left(\frac{(\alpha - \alpha_1)}{S_1}\right)$$

where α_1 is 15.25 degrees for a mach number of 0.3. ($S_1 = 3.0$ & $S_2 = 2.3$).

Beddoes also gives the following equations for the pitching moment and drag coefficient of a NACA0012 aerofoil.

$$C_m = C_n \times (K_0 + K_1 \times (1 - f) \times K_2 \times \sin(\pi \times f^2))$$

$$C_d = C_{l\alpha} \times \alpha^2 \times \sqrt{f}$$

where $K_0 = 0.0025$ $K_1 = -0.135$ and $K_2 = 0.04$

The above formulation for the aerofoil's static forces provides a compact structure for the reproduction of their non-linear behaviour. This method also provides a means for extending the model into the unsteady regime, by 'controlling' the point at

which the flow separates from the aerofoil.

5.8 Impulsive Loading.

The impulsive loading comprises the initial loading on the aerofoil in response to an instantaneous change in incidence or pitch rate, and is generated by a compression wave on one surface and a rarefaction wave on the opposite surface. Considering the control point to be at the 3/4 chord, the impulsive loading will be composed of two perturbation modes:

[1] Due to the step change of angle of incidence, $\Delta\alpha$, at the 3/4 chord representing a uniform distribution of normal perturbation velocity.

[2] Due to a step change of pitch rate, $\Delta q = \Delta\theta C / V$, about the 3/4 chord.

The CNi and CNq terms represent these impulsive loadings,

The impulsive normal lift force for a step change in incidence, $\Delta\alpha_n$ is given by;

$$Cni = \left(4.0 \times K1 \times \frac{T1}{M} \right) \times (D\alpha_n - D\alpha_i_n)$$

where $D\alpha_n = \Delta\alpha_n / \Delta t$

$$D\alpha_i_n = D\alpha_i_{(n-1)} Ed + (D\alpha_n - D\alpha_{(n-1)}) \sqrt{Ed}$$

$$Ed = \exp\left(\frac{-\Delta t}{KL \times TL}\right)$$

$KL = 0.75$ and $TL = C / a$ (ratio of chord to sonic velocity).

Similarly, for a step change in pitch rate Δq about the 3/4 chord, the impulsive normal lift force is given by:

$$CNq = \left(-K1 \times \frac{T1}{M} \right) \times (Dq_n - Dq_i_n)$$

where $Dq_n = \Delta q_n / \Delta t$ and,

$$Dqi_n = Dqi_{(n-1)}Ed + (Dq_n - Dq_{(n-1)})\sqrt{Ed}$$

The chordwise force is given by:

$$Cc_n = Cl\alpha \times (\alpha_n - X_n - Y_n)^2$$

5.9 Time Dependent Pressure Response.

From dynamic tests it has been established that under nominally attached flow conditions, there is a phase lag of the aerofoil peak pressures with respect to the instantaneous normal lift force, implying that under dynamic conditions, critical lift conditions may be reached at a higher angle of attack. The pressure phase lag is nominally linear and increases with increasing Mach number (within the range of reduced frequencies and Mach numbers of interest). This behaviour may be modelled using a first order lag with a Mach number dependant time constant T_p . ($T_p = 1.7$ for a Mach number of 0.3) Thus it is possible to relate the peak pressures to the static relationship. This may be accomplished by applying a first order lag to the normal force, thus;

$$CN'(s) = \frac{CN(s)}{(1 + T_p s)}$$

At any instant of time the instantaneous value of lift may be viewed as a steady state value minus an exponentially decaying (deficiency) term. For any sample the total potential normal force is given by;

$$Cn_n = Cni_n + Cnq_n$$

for the additional pressure lag response we have

$$Cn'_n = Cn_n - Dni_n$$

$$Dni_n = Dni_{(n-1)} Ep + (Cn_n - Cn_{(n-1)}) \sqrt{Ep}$$

$$Ep = \exp\left(\frac{-Dt}{Tf} \times \frac{2V}{C}\right)$$

5.10 Time Dependent Boundary Layer.

For the dynamic case, in addition to the temporal effects on the aerofoil pressure distribution, the boundary layer itself is time dependant. The time dependent boundary layer reversal point flags linearly behind the corresponding static variation with increasing pitch rate. The simplest representation of this behaviour is a first order lag;

$$f(s) = \frac{f(s)}{(1 + Tf s)}$$

f(s) represents the response to the pressure distribution and, f'(s) incorporates the additional boundary layer response

This time lag may be incorporated in the computer model as;

$$Dfi_n = Dfi_{(n-1)} Ef + (Cn_n - Cn_{(n-1)}) \sqrt{Ef}$$

$$Ef = \exp\left(\frac{-Dt}{Tf} \times \frac{2V}{C}\right)$$

$$Cnfn = Cn_n - Dfi_n$$

an effective incidence α_f can be defined as

$$\alpha_f = \frac{Cnfn}{Cl\alpha}$$

The effective dynamic point of flow reversal (f') can thus be found from the

curve for the static case. The dynamic values of C_n and hence α_f may be computed from the attached flow algorithm, and hence f' can be found.

5.11 Extension to the non-linear Regime.

To extend the model into the deep stall regime requires the consideration of vortex shedding. As the trailing edge separation progresses local vorticity is shed at the point of flow separation, and is convected downstream towards the trailing edge. These vortices are small and do not affect the pressure distribution significantly, However as the pitch rate increases the effect of the trailing edge separation can be delayed so that the leading edge becomes critical in determining when the aerofoil 'stalls'. If the leading section of the aerofoil becomes critical then a significant vortex will be shed from the region of the leading edge, and will be convected downstream over the aerofoils chord (The dynamic stall vortex). The dynamic stall vortex associated pressure disturbance will induce large changes in the aerofoils lift and associated forces. At low Mach numbers (Mach <0.2) the experimental data shows large non-linear overshoots for the lift and its associated forces, however above this the behaviour seems linear. The vortex lift may be modelled assuming the increment in vortex lift is based on the difference between the instantaneous linear value of the circulatory lift and the corresponding lift as given by the Kirchhoff approximation that is.

$$C_{nv}_n = C_{nc}_n \times (1 - KN_v)$$

$$KN_v = 0.25 \times (1 + \sqrt{f})^2$$

At the same time, the total vortex lift C_{nv} is allowed to decay exponentially with time, but may also be updated by a new increment in lift, that is.

$$C_{nv}_n = C_{nv}_{(n-1)} E_v + (C_{nv}_n - C_{nv}_{(n-1)}) \sqrt{E_v}$$

$$E_v = \exp\left(\frac{-\Delta t}{T_v} \times \frac{2V}{C}\right)$$

When the rate of change in the lift force is low the vortex associated lift will decay as fast as it is generated, thus in the limit as the rate of change tends to zero the aerofoil characteristics will revert to the static behaviour. When conditions at the leading edge become critical and the vortex is shed, abrupt changes will occur in the lift force,

thus accumulating vortex strength. The rate at which the vortex moves downstream has been determined by experiment to be 40% of the freestream velocity, and must be accounted for in the modelling. During the convection of the vortex across the surface of the aerofoil, vortex lift is accumulated via the above equations, but is terminated when the vortex passes the trailing edge. The time taken for the vortex to pass the trailing edge is given in terms of non-dimensional time as 7.0 at a Mach number of 0.3.

During the vortex shedding process, the pressure changes occurring are sufficient to accelerate the forward progression of the separation point. This may be accomplished by halving the time constant associated with the boundary layer response thus; the forward movement of the separation point is accelerated if $f < 0.7$ or during the vortex shedding, that is when the vortex time is less than the vortex time limit. Once the vortex passes the trailing edge the lift associated with it decays more rapidly, and this can be modelled by halving the vortex lift time constant.

5.12 Computer Implementation of the Beddoes Model.

The total linearised unsteady aerodynamic response can be idealised into components of circulatory and impulsive loading, which are computed independently. The non-linear lift characteristic of trailing edge separation is evaluated via the Kirchhoff flow, thus the variation of lift may be obtained using a potential calculation which neglects separation (represented by the zero lift value of the lift curve slope) and an independent representation of the flow separation point. Using timewise lags the additional aerofoil temporal pressure modification and the unsteady boundary layer response is accounted for. The onset of vortex shedding during dynamic stall is denoted by a generalised criterion for the onset of leading edge or shock induced separation, the consequences of which also modify the trailing edge separation calculation.

This model has been reproduced at Glasgow University with the consent and help of Tom Beddoes. It has been coded in Fortran 77 and runs on both a VAX11/780 and Sun SPARCStation. The code comprises roughly 50 subroutines, totalling approximately 5000 lines of code. A typical run takes less than one minute to compute, (for a given motion type).

Chapter 6

ANALYSIS OF REATTACHMENT

This chapter considers the reattachment of the flow over the upper surface of an aerofoil, whilst undergoing a constant negative pitch rate motion, from an incidence well above the static stall value. Experimental data from a variety of aerofoils tested using the University of Glasgow facilities, have been recorded. All data were collected at an effective Mach and Reynolds numbers of 0.11 & 1.5×10^6 respectively. Various improvements for future work are noted, and the predominant features of the reattachment process are discussed. Finally a preliminary consideration of the Beddoes predictive method is presented for reattachment.

[Note: The work presented in this chapter has been published at the European rotor craft forum, and has subsequently been produced in Vertica. The paper is reproduced here in its original form, therefore some of the initial experimental details are in effect summaries of the earlier chapter of this thesis. The computer coding developed in this work now forms part of the dynamic stall predictive code used at Glasgow University.]

Notation

α = Incidence (deg)

C = Aerofoil Chord (m)

f = x/c = Non-dimensional Chord

f_s = Sampling Frequency (Hz)

r = $(\alpha \pi c)/(360U)$ = Reduced Pitch Rate #

n = Sweep Number

U = Freestream Velocity (m/s)

τ = $(\Delta t.U)/c$ = Non-dimensional Time

(Note: both pitch rate and reduced pitch rate are treated as positive values within this chapter.)

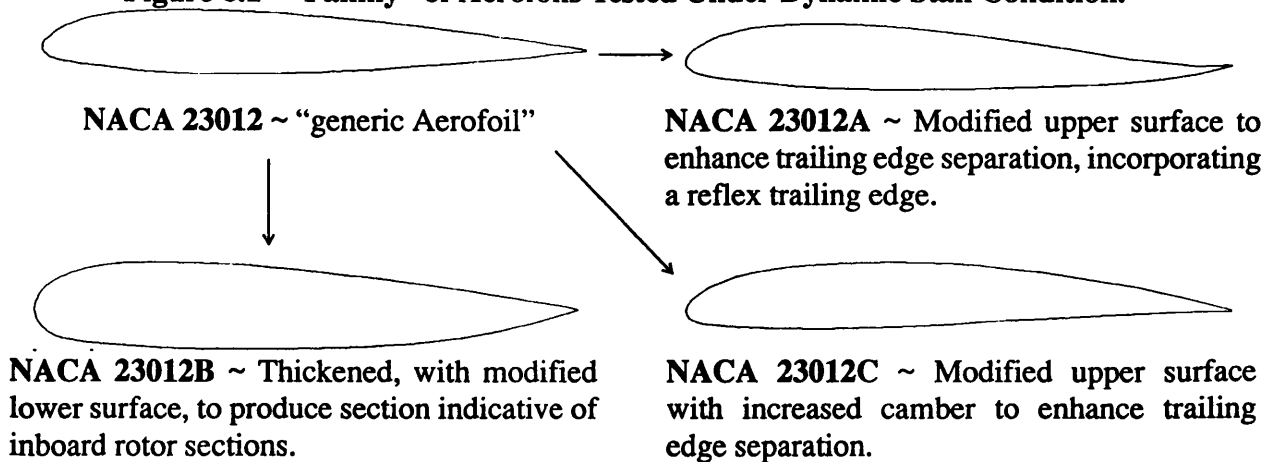
6.1 INTRODUCTION

For particular flight conditions, the retreating blade of a conventional helicopter experiences incidences in excess of the profile's static stall value. These excursions may become so severe that the blade will dynamically stall. Once full dynamic stall is initiated, there follows an inevitable and well known sequence of aerodynamic phenomena (Carr et al, 1977). These events are concluded by the return to the fully attached conditions by a process of reattachment.

Reattachment has received only limited consideration, albeit many dynamic stall models have intuitively proposed mathematical descriptions of it, (Beddoes, 1982, Leishman and Beddoes, 1986, Nash and Scruggs, 1977, Ganwani, 1983, Vezza, 1986, etc.), and they have met with varying degrees of success (Galbraith, 1985, Beddoes, 1980, McCroskey, 1978). This, perhaps, may be associated with both the complex nature of reattachment and the available experimental data which, primarily, is for sinusoidal motions. As can be imagined, such data are both extensive (to cover an appropriate range), and complicated by the non-linear motion. To alleviate the problems of non-linear motions, various investigators (ARA, 1983 Jumper and Shreck, 1986, Seto and Galbraith, 1985, Lorber and Carta, 1987, Ahihara et al, 1985, Robinson and Luttgies, 1983) have considered stall development during constant pitch rate (ramp) displacements. The succinctness of the data, and its clarity of content, have been most useful in aiding our knowledge of the stall process.

It is conceptually easy to perceive that constant negative pitch rate, or ramp down, will yield an equivalent wealth of information about reattachment phenomena. As was discovered during the present investigation, however, the practicalities of imple-


Figure 6.1 - "Family" of Aerofoils Tested Under Dynamic Stall Condition.



menting this concept require more consideration than the straight forward positive pitch rate ramp. In particular, each test starts with an obvious tunnel blockage which reduces to a small value at the low incidence fully attached case. Additionally, at what incidence does one start a given test, and is averaging of the data permissible?

The data considered in the present work have been taken from the current University of Glasgow Database of aerodynamic phenomena. The main portion of the data base relates to dynamic stall data covering four aerofoils. Each of the test programs considered pitching displacements which were not of immediate importance, but would be of future interest. One such motion was contained in a series of ramp-down tests which were a simple inverse of ramp-ups.

Table 6.1 - Summary of Dynamic Stall Database of the NACA 23012 Family.

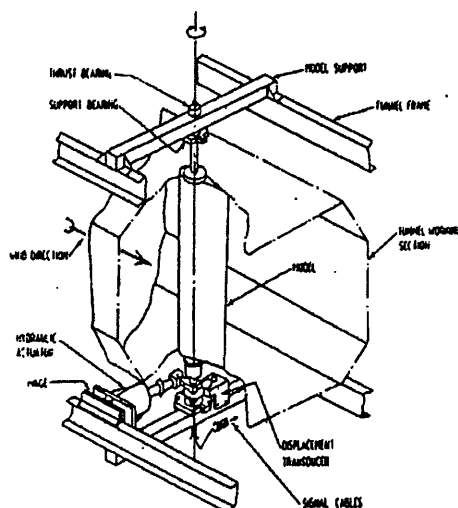
Model	Static	Sine	Ramp Up	Ramp Down	Unsteady Static	Vawt	Other	Total
NACA 23012	47	550	87	37	0	0	0	721
NACA 23012A	1	85	32	13	34	0	0	165
NACA 23012B	56	282	119	45	89	29	45	665
NACA 23012C	23	230	77	32	54	0	0	416
TOTAL	127	1147	315	127	177	29	45	
grand total = 1967								

The aerofoils considered in this chapter form a family of four which has the NACA 23012 as the generic shape, from which three modifications have been considered (Figure 6.1). In total, 1967 different test cases have been considered (Table 6.1), and around one hundred of these were ramp-downs. Data from all the these tests have been averaged and analysed to assess the manner, and rate, of the reattachment process together with an initial attempt to predict the time dependent loadings using the Beddoes model.

The main observations were, that ramp-down experiments are more complicated than ramp-ups; that leading-edge reattachment is always initiated at an incidence close to its static stall counterpart, and the subsequent rate of reattachment is significantly effected by model geometry up until reduced pitch rates of around 0.015, whereafter reattachment is significantly affected by the time scales of the unsteady turbulent boundary-layer response.

6.2 TEST FACILITY

Figure 6.2 - Dynamic Stall Test Rig.



The general arrangement of the aerofoil in the wind tunnel is illustrated in Figure 6.2. The models, of chord length 0.55m and span 1.61m, were constructed of a fibre-glass skin filled with epoxy resin foam and bound to an aluminum spar. Each model was mounted vertically in the University of Glasgow's "Handley Page" wind tunnel which is a low speed (max speed = 57 m/sec) closed - return type with a 1.61 x 2.13m octagonal working section. The model was pivoted about the quarter chord using a linear hydraulic actuator and crank mechanism. The input signal to the actuator controller was provided by a function generator, comprising of a BBC microcomputer and two 12-bit digital to analogue convertors; one to control the shape of the motion, and the other to set the desired voltage governing the amplitude or arc length of the motion. A range of different functions were programmed and tested using this set up (Table 1).

Thirty miniature pressure transducers were installed below the surface of the centre section of each model. These consisted of both KULITE XCS-093-5 PSI G and ENTRAN EPIL-080B-5S transducers. All transducers were temperature compensated and factory calibrated. Whilst these calibrations were accurate, the necessary cabling and signal conditioning of the transducer output may render a slightly different system performance. As a consequence of this, the entire measurement system was calibrated for each model. The method used was to apply a time varying calibrated reference pressure to each of the model's pressure transducers in turn. Both reference and model transducer outputs were simultaneously recorded to yield a well defined calibration.

Instantaneous aerofoil incidence was determined by a linear angular potentiometer geared to the model's tubular support. The dynamic pressure in the wind tunnel working section was obtained from the difference between the static pressure in the

working section, 1.2m upstream of the leading edge, and the static pressure in the settling chamber, as measured by a FURNESS FC012 electronic micromanometer.

For the ramp-down tests, 256 samples per cycle were recorded at a maximum sampling frequency of 550.0 Hz. Five cycles of data were recorded using a DEC MINC 11/23 micro-computer system (Galbraith, 1984). The data were then transferred to a VAX 11/750 for processing, storage and analysis. The subsequent data reduction and presentation is a standard for all such tests, and a typical output is given in figure 6.3.

6.3 EXPERIMENTAL RESULTS

6.3.1 Introduction

The data discussed herein pertain to the NACA 23012 section and its three derivatives. Each ramp-down test was normally initiated from a geometric incidence of around 36 degrees and terminated in the region of -6 degrees. As will be appreciated, pure ramps were not achieved due to start-up and slow-down requirements, but, as will be shown, leading-edge reattachment was always initiated within the linear region of the motion. The aerofoil angular velocity was progressively increased from 0.75 to 400.0 degs/sec, allowing the reduced pitch rate to be varied between 0.001 and 0.05. At the highest reduced pitch rate, the aerofoil completed one ramp-down cycle in 0.1s. The effective freestream velocity was 40.0 m/sec resulting in Reynolds and Mach numbers of 1.5 million and 0.11 respectively.

Figure 6.3 illustrates a standard output, from which a variety of salient features may be observed. For example, at this medium pitch rate (100 degs/sec), there is a marked variation of loading from the equivalent static case, and the detailed time dependent pressure distribution illustrates the causation of this via the evident lag in suction build up. The effect of increasing pitch rate is to further this variation in loadings, and at the faster pitch rates the expected leading-edge pressure build-up became non-existent.

6.3.2 Method of Analysis

Of particular interest is the timing of the reattachment process, and this may be investigated by assuming the following:

- The process develops from the leading to the trailing edge.
- The reattachment location is located at the start of the constant pressure region normally associated with trailing-edge separation. As can be imagined, the location of this point is often difficult to discern, but efforts have been made to define a consis-

DYNAMIC CHARACTERISTICS FOR THE NACA23012B MODEL 03

RUN REFERENCE NUMBER: 32631
 REYNOLDS NUMBER = 1.712E6
 DYNAMIC PRESSURE = 1009.215 N/m²
 NUMBER OF CYCLES = 5
 MOTION TYPE: RAMP DOWN
 START ANGLE = 35.00°
 RAMP ARC = -41.000°
 AVERAGED DATA OF 5 CYCLES

DATE OF TEST: 6/12/87
 MACH NUMBER = 0.118
 AIR TEMPERATURE = 23.3°C
 SAMPLING FREQUENCY = 359.87 Hz.
 REDUCED PITCH RATE = -0.01212
 LINEAR PITCH RATE = -1.07.04°/s

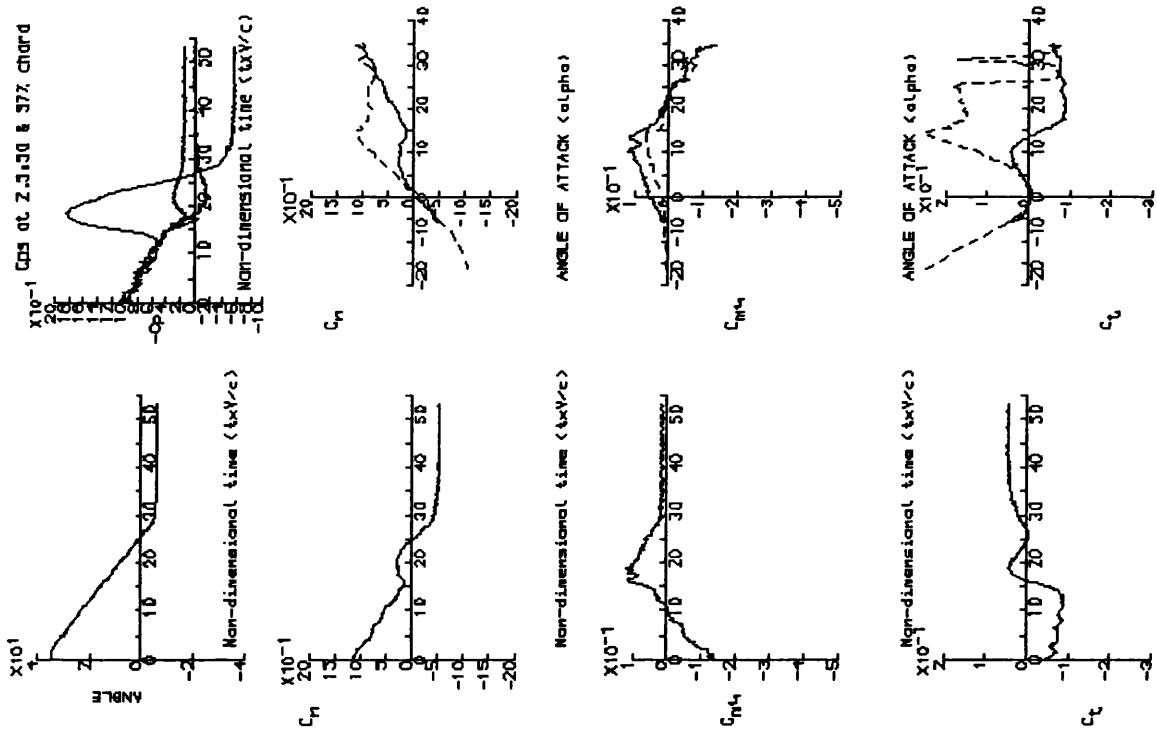
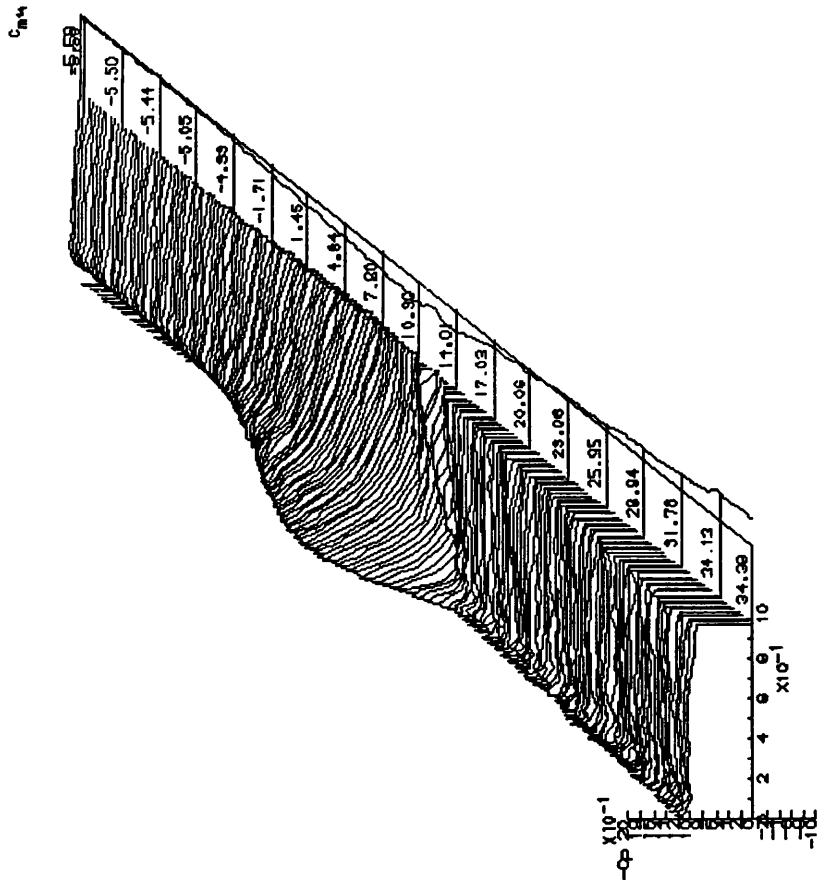
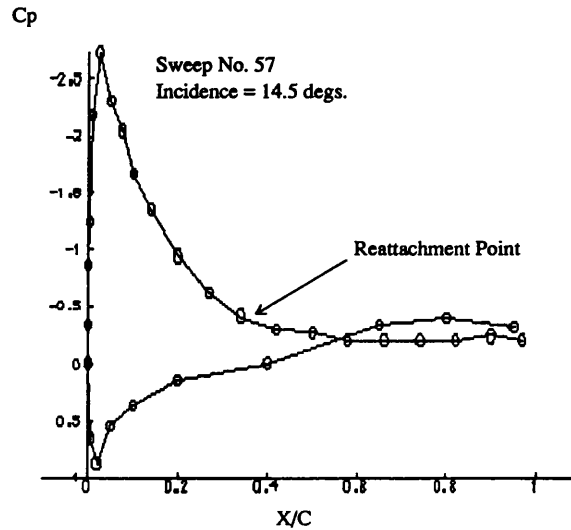


Figure 6.3 - Standard presentation of dynamic stall data

tent approach.

This method is illustrated in Figure 6.4, where the reattachment point is rela-

Figure 6.4 - Typical Chordwise Pressure Distribution.



tively easy to observe, and the constant pressure region is well defined. Obtaining the exact incidence above which fully attached flow cannot be sustained, however, can be difficult, since the trailing-edge pressure gradient may become small at this condition. A complementary method of locating the formation of localised protuberances within the boundary layer, is the inspection of the response of individual pressure-time histories monitored at various chordwise locations. As shown in the top right graph of Figure 6.3, the rate at which a particular pressure-time history diverges can often be used to infer boundary-layer separation and reattachment. Therefore, a heuristic analysis involving both pressure-time histories and discrete chordwise pressure distributions may be used to monitor the translation of the reattachment point across the aerofoil's upper surface. Having established a consistent method of extracting the relevant aerodynamic data, the non-dimensional time delay between two particular events, which occurred during a selected ramp-down test, was calculated from the difference in sweep numbers, associated with each event, (Δn), and the sampling frequency in the following manner:

$$\tau = (\Delta n \cdot U) / (fs \cdot c)$$

6.3.3 Leading-Edge Reattachment

On inspection of selected ramp-down test cases, it was noticed that, at the initial high incidence values, there was a distinctive change in pressure-time history at 2.5%

chord (Figure 6.3) which accompanied the establishment of a small suction peak at the leading edge of the aerofoil. For some test cases a very small suction peak was discernible at 1% chord, but its size and position remained insensitive to incidence variation. It is suggested, that this suction peak was due to the flow curvature over the leading edge, at the initial high incidence values, and therefore its use as the indicator of the onset of reattachment was inappropriate. Only when the suction at 2.5% chord began to rise, did the reattachment process appear to move downstream; this finding was consistent over the entire pitch rate range.

Figure 6.5 - Angle of Reattachment @ 2.5% chord Versus Reduced Pitch Rate.

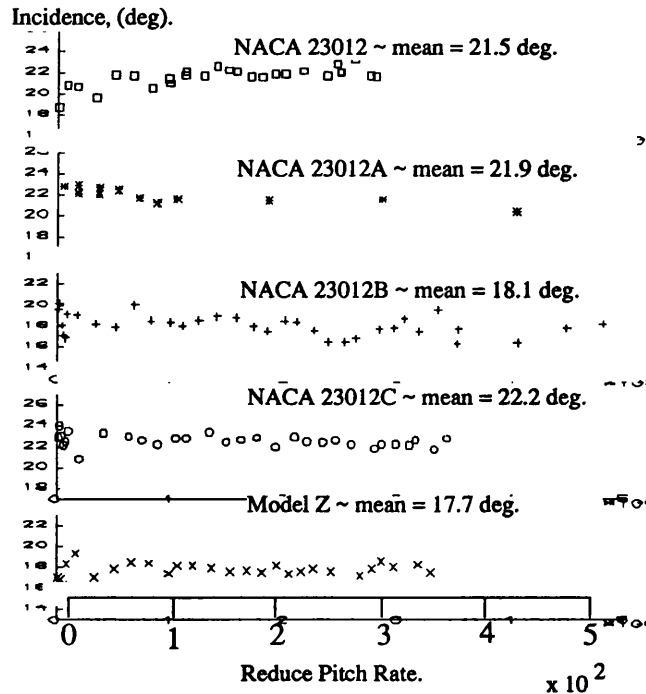
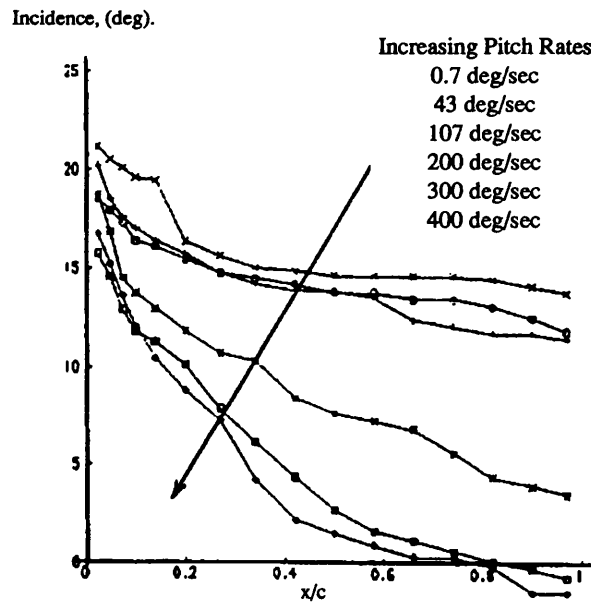


Figure 6.5 presents the variation in leading-edge reattachment incidence with reduced pitch rate for a selection of aerofoils from the Glasgow University Database. It is interesting to note, that the initial reattachment incidence is relatively insensitive to pitch rate. For each aerofoil, the average value of the leading-edge reattachment incidence, obtained from the ramp-down tests, was found to approximately coincide with its steady-state counterpart. Also illustrated is the similarity between initial reattachment incidence for the NACA 23012 and its derivatives 'A' and 'C'. During the development of the 23012A and 23012C profiles, a specified design constraint was, that the leading-edge geometry was not to be significantly altered from that of the NACA 23012. This therefore implies, that the initiation of reattachment depends significantly on the leading-edge geometry, and would explain the differing result obtained for the NACA

**Figure 6. Reattachment point variation
with increasing pitch rates.**



23012B (Figures 6.1 and 6.5).

6.3.4 Speed of Reattachment

Figure 6.6 illustrates the effect of pitch rate on the reattachment characteristics of the NACA 23012B aerofoil. If the aerofoil was within the linear incidence region of the ramp, then, for a particular chordal position, the instantaneous non-dimensional reattachment velocity can be estimated in the following manner:

$$\text{speed of reattachment} = (d\alpha/dt) \times (df/d\alpha)$$

Expressed in this form, the variation in instantaneous reattachment velocity with chordal position can be easily observed from Figure 6.6 since, for a particular pitch rate, its value is inversely proportional to the local gradient of the reattachment curve. If, as was occasionally apparent, the reattachment point moved a large chordal distance within one sample sweep, the instantaneous reattachment velocity, at intermediate points, could not be calculated. This was due to the maximum sampling frequency of 550Hz, used during data acquisition, not being of sufficient magnitude, and therefore, with regard to this specialised area of interest only, was seen to be a limitation of the existing test facility.

6.3.5 Reattachment Time Delays

Figure 6.7 - Reattachment point at 2.5,50 and 97% chord over the range of reduced pitch rates.

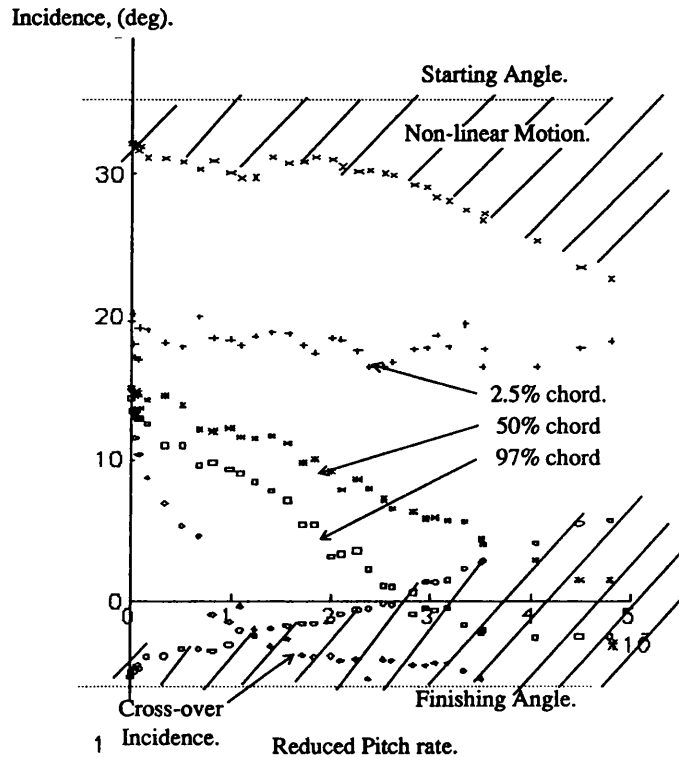
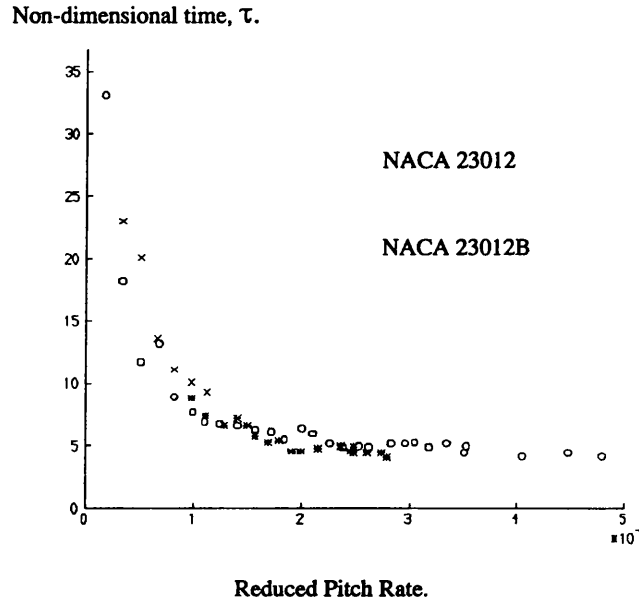


Figure 6.7 illustrates the estimated incidence values for 2.5%, 50% and 97% attached flow as a function of reduced pitch rate. Also marked on this figure are the regions of acceleration and deceleration associated with the range of ramp-down tests, and the cross-over incidence where the dynamic C_n intersects the static C_n curve (Figure 6.7). It may be noticed that, for reduced pitch rates above 0.028, the incidence at which fully attached flow is established lies within the deceleration region. However, as will be shown later, for these values of pitch rate, the reattachment process displays a reduced dependency on the aerofoil motion, and therefore the non-linear incidence variation becomes unimportant.

Having defined the points of leading and trailing edge reattachment, a characteristic time delay associated with the establishment of fully attached flow over the aerofoil's upper surface can be calculated. Figure 6.8 illustrates the full reattachment time delay results associated with the NACA 23012 and 23012B aerofoils. At low pitch rates, a small difference in time delay occurs, and therefore a weak dependence on aerofoil geometry is implied. The apparent convergence in time delay at the higher pitch rates implies that the influence of both aerofoil geometry, and motion, on the reattachment

Figure 6.8. Non-dimensional time for full reattachment to occur once initiated at 2.5% chord.



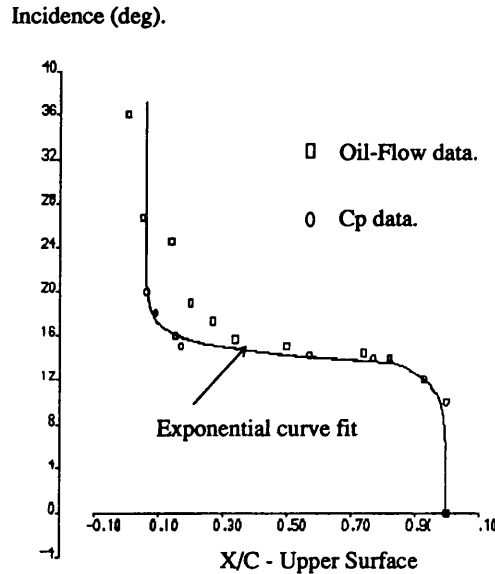
process has now become reduced. Unfortunately, the data available for the NACA 23012 did not cover pitch rates greater than 220 degs/s, and therefore, any differences between the two aerofoils at pitch rates above this value are obscured. What is apparent, though, is that for values of reduced pitch rate above 0.015, the effect of aerofoil geometry is significantly reduced allowing the full reattachment time delay to approach a value of 4, equivalent to 25% of the freestream velocity.

6.3.6 Boundary-Layer Response

Associated with the reattachment process there must be a finite length of time within which the free shear layer develops into an attached boundary layer. Similar to that of boundary-layer detachment, the process of reattachment may be expected to be influenced by the external pressure gradient. At low pitch rates, the downstream advancement of the reattachment point will be influenced by the build-up in upstream pressure distribution and the associated pressure gradients. Therefore, its movement may be expected to be dependent on the aerofoil geometry.

At the high pitch rates, the establishment of a pressure distribution upstream of the reattachment point is retarded by the rapid decrease in incidence, and therefore any effect of aerofoil geometry will be reduced. If this is the case, why does the change of phase from fully separated to fully attached flow not occur within one chord length of

Figure 6.9 - Trailing Edge Separation Movement For Static Tests.

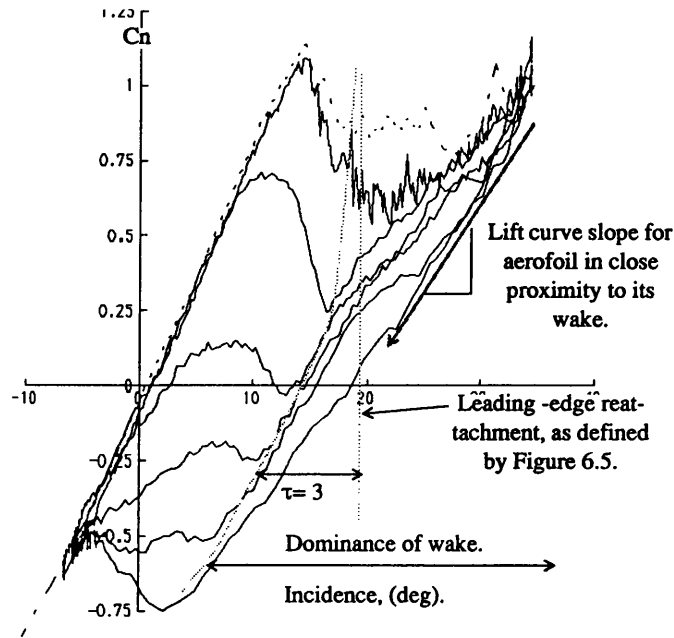


flow i.e., at an average velocity equal to that of the freestream? Kline et al (1981) observed that two-dimensional turbulent flow detachment was not a single event, but a phase change from attached to detached flow. For a turbulent boundary layer, zero wall shear stress is created by the averaging to zero of strong unsteady motions of opposite sign, and therefore full detachment occurs over a zone. The same remarks, concerning zero wall shear, apply qualitatively to reattachment, but Kline noted that the motions at reattachment were even stronger in the turbulent case, owing to larger fluctuations in the free shear layers. It is postulated here, that the reattachment process consists of a damping out of characteristic turbulence structures whose length scale varies from that appropriate to a free shear layer to that of an attached boundary layer. Therefore, there will exist a finite period of time within which the large scale turbulence structures must relax before boundary-layer reattachment and downstream advancement can occur. Once the effect of aerofoil geometry has been suppressed, i.e., at high ramp-down pitch rates, the rate of reattachment is determined by the detailed fluid mechanics of this process.

At present, further data analysis, involving the reattachment characteristics of other aerofoils, available on the Glasgow University Database, is in progress to either substantiate or refute the above postulation.

6.4. MODELLING

Figure 6.10 - C_n versus Incidence for a range of pitch rates.



11-9

The present approach in attempting to model the test data has been to code an existing semi-empirical model (Beddoes, 1982, Leishman and Beddoes, 1986). It is noted that the Beddoes model is only appropriate down to Mach numbers of about 0.15 (Leishman, 1986), below this, additional nonlinear lift and moment overshoots may occur. These limitations are partially due to the restricted number of available low Mach correlations, and it is hoped that the current work will contribute to this area of interest.

The necessary empirical time constants, required for appropriate modelling, have been extrapolated from the static test data, and those defined by Beddoes, 1984; the static separation loci was experimentally determined, and an exponential curve fit applied (Figure 6.9); the angular forcing has been filtered through a five point moving average.

Figure 6.11 illustrates three examples of the predictive code in modelling C_n . At the slowest pitch rate good agreement is observed. As the pitch rate increases, however, the model fails to predict the drop in C_n . This rapid lowering of C_n can be regarded as a following of a lift curve appropriate to an aerofoil within close proximity of its wake; experimentally shown to predominate up until the point of three chord lengths of flow after the initiation of reattachment (Figure 6.10). Modelling this behaviour by using a C_n /relationship representative of "aerofoil plus wake", and allowing a smooth exponential transition back to the Beddoes model radically improves the overall prediction (Fig-

ure 6.12). This method requires further investigation, and correlation with sinusoidal data. It does, however, model a physical flow event which is consistent with the overall concept of the Beddoes model.

6.5. CONCLUSIONS

Figure 6.11 - Correlation of C_n from predictive method and test data.

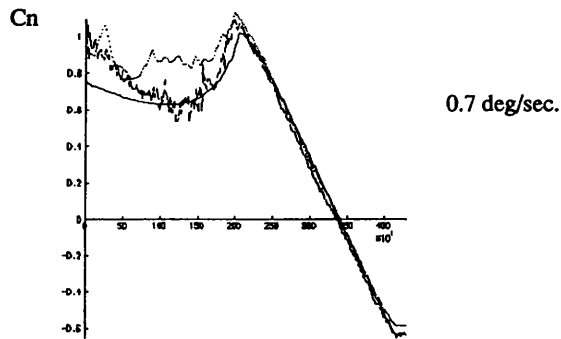
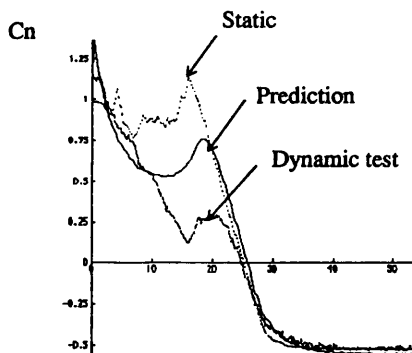
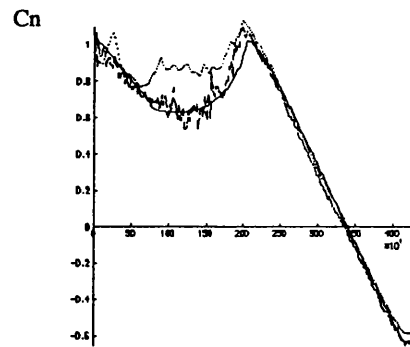
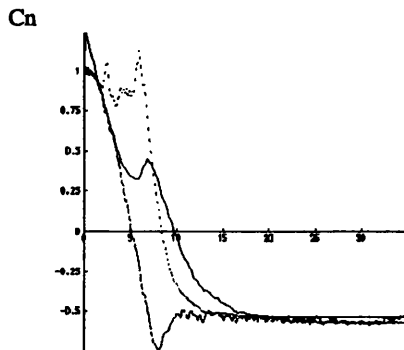
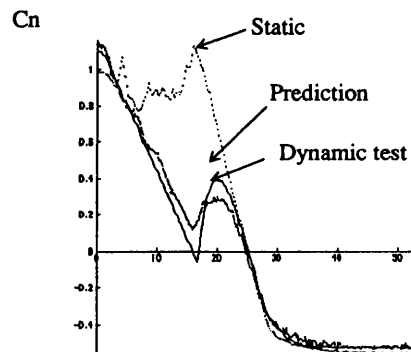


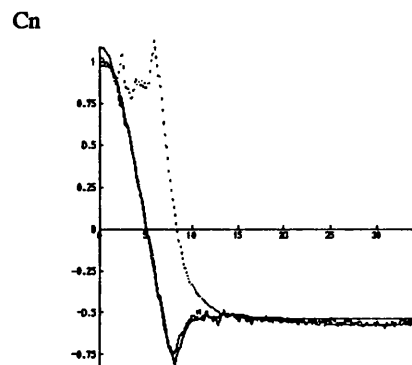
Figure 6.12 - Correlation of C_n from predictive method with wake modelling inclusion and test data.



100 deg/sec.



400 deg/sec.



Non-dimensional Time, τ .

Non-dimensional Time, τ .

The following conclusions have been inferred from the data presented herein:

7. The initiation of reattachment was insensitive to pitch rate, and occurred at an incidence approximately equal to its steady-state counterpart.
8. The non-dimensional time delay associated with the full reattachment was a strong function of reduced pitch rate for low to medium values, whilst the higher rates tended to a constant value of 4.
9. The presence of the wake takes a finite time to diminish, until which it remains a significant component in determining the aerodynamic loads

Chapter 7

Conclusions

- The experimental aerofoil has been designed, built and tested under dynamic stall conditions.
- The process of reattachment has been investigated on three aerofoil sections using the ramp down data. This has yielded the following three conclusions:
- The initiation of reattachment was insensitive to pitch rate, and occurred at an incidence approximately equal to its steady-state counterpart. Note that initiation of reattachment was measured at the 2.5% chord location, however the actual origin of reattachment is somewhat nearer the leading edge. Therefore, as pitch rate increases, the angle at which reattachment is recorded at 2.5% chord will decrease, due to the finite time for the reattachment to propagate to the 2.5% chord location.
- The non-dimensional time delay associated with the full reattachment was a strong function of reduced pitch rate for low to medium values, whilst the higher rates tended to a constant value of 4.
- The presence of the wake takes a finite time to diminish, until which it remains a significant component in determining the aerodynamic loads
- Additionally, an enhancement has been made to the Beddoes dynamic stall model which enables the measured reattachment loads during reattachment to be modelled accurately.

7.1 Recommendations for future research

- Greater utilisation should be made of industry standard visualisation software during data analysis.

- A preliminary study should be carried out on the unsteady static data to see if by recording at high frequencies it may be possible to correlate adjacent pressure transducer outputs in order to infer boundary layer effects.
- The unaveraged data should be made generally available on the dynamic stall database.
- The Handley Page wind tunnel should be instrumented with pressure transducers within the working section walls to enable greater understanding of the blockage effects.
- The Beddoes model should be applied to all the tested motion types to verify it's ability to predict arbitrary motion types.
- A least squares multi-variant optimization should be performed on the Beddoes model across the entire dynamic stall data base to check the physical non-dimensional time constants inferred from the data do give the best correlation within the model.

References

Bibliography in author alphabetical order

A

- Y. Aihara. *Transient aerodynamic characteristics of a two-dimensional airfoil during stepwise incidence variation*. Journal of Aircraft, Vol. 22, No. 8, August 1985.
- J.A. Albertson, T.R. Troutt and W.D. Siuru. *Dynamic stall vortex development and the surface pressure field of a pitching airfoil*. Fluid Dynamics, Plasma Dynamics, and Lasers Conference, AIAA paper 87-1333, Honolulu, U.S.A., June 8-10 1987.
- J.A. Alberston, T.R. Trout and C.R. Christopher. *Unsteady aerodynamic forces at low airfoil pitching rates*. AIAA paper 88-2579, June 1988.
- J.M. Adler and M.W. Luttges. *Three-dimensionality in unsteady flow about a wing*. AIAA Paper No. 85-0132, January 1985.
- J.M. Alder, M.C. Robinson, M.W. Luttges and D.A. Kennedy. *Visualising unsteady separated flows*. Third international symposium on flow visualisation, proceedings Vol. III, pages 806-811, Michigan, September 1983.
- A.J.S. Allaire. *Investigation of potential and viscous flow effects contributing to dynamic stall*. M.S. Thesis, AD-A151696.
- S. Ando and D.-H. Lee. *Effect of hinge gap on aerodynamics of thin airfoils having an oscillating flap*. Journal of Applied Mechanics, Vol. 52, pages 712-717, September 1985.
- J. Ashworth and M.W. Luttges. *Comparisons in three-dimensionality in the unsteady flows elicited by straight and swept wings*. AIAA paper No. 86-2280, August 1986.

B

- W.F. Ballhaus and P.M. Goorjan. *Computation of unsteady transonic flows by the indicial method*. AIAA Journal, February 1978.
- T.S. Beddoes. *A synthesis of unsteady aerodynamic effects including stall hysteresis*. Proceedings of 1st European rotorcraft forum, September 1975.
- T.S. Beddoes. *Representation of airfoil behaviour*. Paper 2, AGARD CP. 337, 1983.
- T.S. Beddoes. *A qualitative discussion of dynamic stall*. paper 3, AGARD Report 679, 1980.
- T.S. Beddoes. *Predicting methods for separated flows*. AGARD report 679, 1979.
- T.S. Beddoes. *Application of indicial aerodynamics in rotor calculations*.
- T.S. Beddoes. *Onset of leading edge separation effects under dynamic conditions and low mach number*. 34th Annual Forum of AHS, 1978.
- T.S. Beddoes. *Practical computation of unsteady lift*. Proceedings of 7th European rotorcraft forum, September 1982.
- T.S. Beddoes. *Unsteady flows associated with helicopter rotors*. Paper 7, AGARD Report 679, 1980.
- T.S. Beddoes. *An analytical model for trailing edge stall*. Westland research paper R.P. 637, 1981.
- T.S. Beddoes. *A qualitative discussion of dynamic stall*. AGARD special course on unsteady aerodynamics. AGARD Report 679, 1979.

- T.S. Beddoes. *Onset of leading edge separation effects under dynamic conditions and low Mach Number*.
- R.G. Benson. *Influence of airfoils on stall flutter boundaries of articulated helicopter rotors*.
- R.L. Bielewa. *Synthesised unsteady airfoil data with applications to stall flutter calculations*. AHS Annual Forum, Reprint 935, 1975.
- L. Bernstein. *The measurement of unsteady pressure, force and acceleration*.
- D.F. Billings. *The unsteady boundary layer on an elliptic cylinder following the impulsive onset of translational and rotational motion*. Ph.D. Thesis.
- W.G. Bousman and W.R. Mantay. *A review of research in rotor loads*. NASA/Army Rotorcraft technology. Vol. 1: Aerodynamics, and dynamics, and aeroelasticity.
- P. Bradshaw, J.T. Stuart and J. Watson. *Flow stability in the presence of finite initial disturbances*.
- M. Brendel and T.J. Mueller. *Boundary layer measurements on an airfoil at a low Reynolds number in an oscillating freestream*. AIAA paper 87-1332.
- G. Brochier, P. Fraunie, C. Beguier and I. Parashivoiu. *Experimental study of dynamic stall on Darrieus wind turbine blades*. Intersociety energy conversion engineering conference, 20th, Miami beach, August 18-23 1985.
- G.M. Byham, and T.S. Beddoes. *The importance of unsteady aerodynamics in rotor calculations*. AGARD-Cp-227, 1977.

C

- J.L. Cardona. *Flow curvature and dynamic stall simulated with an aerodynamic free-vortex model for VAWT*. Wind Engineering, Vol. 8, No. 3, pages 135-143, 1984.
- R.G. Carlson, R.H. Blackwell, G.L. Commerford and P.H. Morick. *Dynamic stall modelling and correlation with experimental data on airfoils and rotors*. AHS/NASA Ames specialist meeting on rotorcraft dynamics, 1974.
- L.W. Carr, K.W. McAlister and W.J. McCroskey. *The effect of a leading edge slat on the dynamic stall of an oscillating airfoil*. AIAA paper No. 83-2533, October 1983.
- L.W. Carr and T. Cebeci. *Boundary layers on oscillating airfoils*. Symposium on Numerical and Physical Aspects of Aerodynamic Flows, 3rd, Long Beach, CA, January 21-24 1985.
- L.W. Carr. *Dynamic stall progress in analysis and prediction*. AIAA paper 85-1769.
- L.W. Carr and W. Lawrence. *Progress in analysis and prediction of dynamic stall*. Journal of Aircraft, Vol. 25, January 1988.
- L.W. Carr. *A directionally sensitive hot-wire probe for detection of flow reversal in highly unsteady flow*.
- L.W. Carr, K.W. McAlister and W.J. McCroskey. *Analysis of the development of dynamic stall based on oscillating airfoil experiments*. NASA TN-D 8382, 1977
- F.O. Carta and P.F. Lorber. *Dynamic stall penetration experiments on a swept wing*. August 1986.
- F.O. Carta. *Dynamic stall of swept and unswept oscillating wings*. AGARD Unsteady Aerodynamics-Fundamentals and applications to aircraft dynamics.
- F.O. Carta, G.L. Commerford and R.G. Carlson. *Determination of airfoil and rotor blade dynamic stall response*. Journal of AHS, Vol. 18, 1973.
- F.O. Carta. *Analysis of oscillatory pressure data including dynamic stall effects*. NASA CR-2394, 1974.
- F.O. Carta. *Unsteady normal force on an airfoil in a periodically stalled inlet flow*. Journal of Aircraft, Vol. 4, no. 5, 1967.
- F.O. Carta. *Effect of unsteady pressure gradient reduction on dynamic stall delay*. Engineering note, Journal of Aircraft, 1971
- F.O. Carta. *A comparison of the pitching and plunging response of an oscillating airfoil*. 1979.
- F.O. Carta. *Experimental investigation of the unsteady aerodynamic characteristics of a NACA 0012 airfoil*. Research report M-1283-1, United aircraft corporation, July 1960.
- F.O. Carta. *Investigation of airfoil dynamic stall and its influence on helicopter control loads*. USAAM-RNL Technical report 72-51, September 1972.

- T. Cebeci, A.A. Khattab and S.M. Schimke. *Some important problems in unsteady boundary layers including separation. 1: Nature of singularity on oscillating airfoils*. Annual report.
- T. Cebeci, A.H. Kattad and S.M. Schimke. *Can the singularity be removed in time-dependent flows*.
- T. Cebeci and L.W. Carr. *Calculation of boundary layers of oscillating airfoils*. NASA-TM-85943.
- T. Cebeci, A.A. Khattab, A.A. Khattab and S.M. Schimke. *Separation and reattachment near the leading edge of a thin oscillating airfoil*. October 1986.
- W.G. Chapin. *Dynamic pressure measurements using an electronically scanned pressure module*.
- L.Y. Chow and C.-S. Chin. *Unsteady aerodynamic loading of an airfoil due to vortices released intermittently from its upper surface*.
- C.S. Chiu. *Vortical flows about oscillating airfoil with surface suction*. Ph.D Thesis.
- D.R. Clark and R.T. Leitner. *Application of an aerodynamic configuration modelling technique to the design and analysis of X-wing aircraft configurations*.
- P. Crimi. *Analysis of stall flutter of a helicopter rotor blade*. 1975
- P. Crimi. *Analysis of helicopter rotor blade torsional oscillations due to stall*.
- P. Crimi, B.L. Reeves. *A method for analysing dynamic stall of helicopter rotor blades*. NASA CR-2009, 1972.
- P. Crimi. *Investigation of nonlinear inviscid and viscous effects in the analysis of dynamic stall*. NASA CR-2335, 1974.
- J.D. Crouch and W.S. Saric. *Oscillating hot-wire measurements above an FX63-137 airfoil*.

D

- D.C. Daley and E.J. Jumper. *Experimental investigation of dynamic stall for a pitching airfoil*. Journal of Aircraft, Vol. 21, October 1984.
- Leo Dadone. *Rotor airfoil optimization: An understanding of the physical limits*. AHS pre-print 78-4, 34th Annual forum of AHS, 1978.
- L.U. Dadone. *Two-dimension wind tunnel test of an oscillating rotor airfoil. Volume 2*. NASA CR 2914, 1977.
- F.J. Davenport and J.V. Front. *Airfoil sections for rotor blades - a reconsideration*. 22nd Annual National Forum, AHS, 1966.
- S.S. Davis. *Experimental unsteady aerodynamics of conventional and supercritical airfoils*. NASA TM 81221, 1980.
- S.S. Davis and G.N. Malcolm. *Experimental aerodynamics of conventional and supercritical airfoils*. NASA TM-81221, 1980.
- J. Deruyck and C. Hirsch. *Velocity and turbulence measurements in dynamically stalled boundary layers on an oscillating airfoil*. AGARD Unsteady Aerodynamics-Fundamentals and applications to aircraft dynamics.
- F. Dietze. *The airforces of the harmonically vibrating wing at subsonic velocity (plane problem)*. Parts I and II, U.S. Air Force translations F-TS-506-RE and F-TS-948-RE, 1947.
- R.L. Dimmick. *Pitch-location effects on dynamic stall*. M.S. Thesis.

E

- J. W. Elliott and F. T. Smith. *Dynamic stall due to unsteady marginal separation*. Journal of Fluid Mechanics, Vol. 179, pages 489-512, June 1987.
- L.E. Ericsson and J.P. Reding. *Shock-induced dynamic stall*. AIAA paper 83-0547.
- L.E. Ericsson. *Comment on unsteady airfoil stall*. Journal of Aircraft. Vol. 4, No. 5, October 1967.
- L.E. Ericsson. *Dynamic stall of helicopter blades*.
- L.E. Ericsson. *Effects of Karman vortex shedding on dynamic stall*. AIAA paper 84-2077.
- L.E. Ericsson and J.P. Reding. *Ground interference effects on subsonic dynamic stall in pitch and plunge*. Journal of Aircraft, Vol. 22, pages 109-116, February 1985.

- L.E. Ericsson and J.P. Reding. *Dynamic overshoot of the static stall angle*. Journal of Aircraft, Vol. 22, pages 637-638, July 1985.
- L.E. Ericsson and J.P. Reding. *Dynamic stall overshoot of static airfoil characteristics*. AIAA paper 85-1773.
- L.E. Ericsson and J.P. Reding. *Unsteady flow concepts for dynamic stall analysis*. AIAA paper 82-1324.
- L.E. Ericsson and J.P. Reding. *Quasi-steady and transient dynamic stall characteristics*. AGARD CP-204, paper No. 24, 1976.
- L.E. Ericsson and J.P. Reding. *Fluid mechanics of dynamic stall. I - Unsteady flow concepts*. Journal of fluids and structures, Vol. 2, January 1988.
- L.E. Ericsson and J.P. Reding. *Fluid mechanics of dynamic stall. II - Prediction of full scale characteristics*. Journal of fluids and structures, Vol. 2, March 1988.

F

- D. Favier, C. Maresca, C. Barbi and A. Castex. *Vortex influence on oscillating airfoil at high angle of attack*. Applied Aerodynamics Conference, 4th, AIAA Paper 86-1837, San Diego, U.S.A., June 9-11 1986.
- D. Favier, C. Maresca, C. Barbi and A. Castex. *Vortex influence on oscillating airfoils at high angle of attack*. Journal of Aircraft, Vol. 24, pages 424-432, July 1987.
- D. Favier, A. Agnes, C. Barbi and C. Maresca. *A new simulation of airfoil dynamic stall due to velocity and incidence fluctuations*. Fluid Dynamics, Plasma Dynamics, and Lasers Conference, AIAA paper 87-1242, Honolulu, U.S.A., June 8-10 1987.
- D. Favier, C. Maresca and J. Rebont. *Modelling of an airfoil empirical flow field below and through dynamic stall*. Journal de Mecanique et Appliquee, Vol. 3, No. 1, pages 15-39, 1984.
- D. Favier, C. Maresca and J. Rebont. *Dynamic stall due to fluctuations of velocity and incidence*. AIAA Journal, Vol. 20, No. 7, 1982.
- A.A. Fejer. *Studies of the dynamic stall of airfoil profiles for helicopter rotors*.
- M.S. Francis and J.E. Keesee. *Airfoil dynamic stall performance with large-amplitude motions*. AIAA Journal, Vol. 23, pages 1653-1659, November 1985.
- M.S. Francis, J.E. Keesee and J.P. Retell. *An investigation of airfoil dynamic stall with large amplitude motions*. FJSRL-TR-63-0010, October 1983.
- P. Fraunie, C. Beguier and I. Paraschivoiu. *The Importance of dynamic stall in the modelling of the Darrieus rotor*. Journal de Mecanique Theorique et Appliquee, Vol. 4, No. 6, pages 785-804, 1985.
- P. Fraunie, C. Beguier, I. Paraschivoiu and G. Brochier. *Water channel experiments of dynamic stall on Darrieus wind turbine blades*. Intersociety Energy Conversion Engineering Conference, 20th, Vol. 3, papers 3.663-3.639, Miami Beach, U.S.A., August 18-23 1985.
- P. Freymuth, M. Palmer and W. Bank. *Visualisation of accelerating flow around an airfoil at angles of attack*. Eight biannual symposium on turbulence, University of Missouri, September 1983.
- P. Freymuth, M. Palmer and W. Bank. *Further experimental evidence of vortex splitting*. Journal of Fluid Mechanics, Vol. 157, pages 289-299, 1984.
- P. Freymuth. *The vortex patterns of dynamic separation: A parametric and comparative study*. Progress in aerospace sciences, Vol. 22, pages 161-209, 1985.
- P. Freymuth, P. Finaish and W. Bank. *Visualisation of wing tip vortices in unsteady and steady wind*. AIAA paper No. 86-1036, May 1986.
- K.Y. Fung and L.W. Carr. *The effects of compressibility on dynamic stall*. AIAA paper No. 88-3541, 1988.

G

- M. Gad-el-Hak and C. Ho. *Unsteady vortical flow around three-dimensional lifting surfaces*. AIAA Journal, Vol. 24, No. 5, May 1986.
- R.A. McD. Galbraith. *Proposal to carry out a study into the effect on the dynamic stall characteristics of a NACA 23023 due to thickening on the lower surface profile*.

- R.A.McD. Galbraith, J. Barrowman and J.G. Leishman. *Description of the sample and hold circuits for the Glasgow University dynamic stall facility*. Glasgow University, internal report 8208, 1982.
- R.A.McD. Galbraith and J.G. Leishman. *A micro-computer based test facility for the investigation of dynamic stall*. International conference on the use of micros in fluid engineering, 1983.
- R.A.McD. Galbraith. *A data acquisition system for the investigation of dynamic stall*. Proceedings of Second International conference on computational methods and experimental measurement, Mechanics Centre publication, Southampton, England, 1984.
- R.A.McD. Galbraith. *Comments on the prediction of dynamic stall*. Glasgow University, Aeronautics report No. 8501.
- R.A.McD. Galbraith, A.J. Niven and L.Y. Seto. *On the duration of low speed dynamic stall*. ICAS conference, 15th, London, England, September 7-12 1986.
- S.T. Gangwani. *Synthesized airfoil data method for prediction of dynamic stall and unsteady airloads*. American helicopter society annual forum, 39th, St. Louis, MO, May 9-11 1983.
- M.S. Garelick. *Non-steady airloads on dynamically stalling two-dimensional wings*. M.S. thesis, MIT, 1967.
- I.E. Garrick. *On some reciprocal relations in the theory of non-stationary flows*. NACA report 629, 1938.
- D.E. Gault. *Correlation of low speed airfoil sections stall characteristics with Reynolds number and airfoil geometry*. NACA TN3963. March 1957.
- W. Geisser, L. W. Carr and T. Cebeci. *Unsteady separation characteristics of airfoils operating under dynamic stall conditions*. Twelfth European Rotorcraft Forum, Garmisch-Partenkirchen, West Germany, September 22-25 1986.
- W. Geissler. *Unsteady boundary-layer separation on airfoils performing large-amplitude oscillations: Dynamic Stall*. AGARD Unsteady Aerodynamics-Fundamentals and applications to aircraft dynamics.
- W. Geissler. *Unsteady laminar boundary-layer calculations on oscillating configurations including backflow. Part 2: Airfoil in high-amplitude pitching motion. Dynamic stall*. NASA-TM-84319-PT-2.
- P. Gillant, P. Sagnes and JP. Ollier. *Calculation of cascade behavior in a dynamic stall regime*. AGARD Engine Response to Distorted Inflow Conditions.
- R.E. Gormont. *A mathematical model of unsteady aerodynamics and radial flow for application to helicopter rotors*. USAAMRDL Technical report 72-67, 1973.
- Mark Gracey and R.A.McD. Galbraith. *An account of the design procedure for the NACA 23012C airfoil*. Glasgow University, internal report 8608, 14 January 1987.
- G.M. Graham and J.H. Strickland. *The effect of moderate to high pitching rates on the aerodynamic performance of a NACA 0015 airfoil at a Reynolds number of 1×10^5* . Report for Southeastern center for electrical engineering education, contract No. F49620-82-0-0035, 1985.
- G.M. Graham and J.H. Strickland. *An experimental investigation of an airfoil pitching at moderate to high rates to large angles of attack*. AIAA paper No. 86-0008, January 1986.
- L. Gray. *Wind tunnel investigation of airfoils oscillating near stall*.
- J.M. Greenberg. *Airfoil in sinusoidal motion in pulsating stream*. NACA TN 1326, 1977.
- L. Grey, J. Liiva and F.J. Davenport. *Wind tunnel tests of thin airfoils oscillating near stall. Volume 1: Summary and evaluation of results*. USAAVLABS TR-68-89A, 1969.

H

- N.D. Ham. *Aerodynamic loading on a two-dimensional airfoil during dynamic stall*. AIAA Journal, Vol. 6, No. 10, 1968.
- N.D. Ham. *Some recent MIT research on dynamic stall*. Journal of Aircraft, Vol. 9, No. 5, 1972.
- N.D. Ham. *Aerodynamic loading on a helicopter blade during pitching motion in the presence of stall*. Sc.D. Thesis, MIT, 1968.
- N.D. Ham and M.S. Garelick. *Dynamic stall considerations in helicopter rotors*. Journal of AHS, Vol. 13, No. 2, 1968.

G.J. Hancock and J.S.Y. Lam. *On the application of axiomatic aerodynamic modelling to aircraft dynamics. IV - Two dimensional dynamic stall*. Aeronautical Journal, Vol. 91, pages 2-88, February 1987.

P.M. Harper and R.E. Flanigen. *Investigation of the variation of maximum lift for a pitching airplane model and comparison with flight results*. NACA TN-1734, October 1948.

F.D. Harris and R.R. Pruyn. *Blade stall - Half fact half fiction*. Journal of the American Helicopter Society, Vol. 17, No. 1, January 1972.

M.A. Heaslet and J.R. Spreiter. *Reciprocity relations in aerodynamics*. NACA report 1119, 1953.

H.E. Helin, M.C. Robinson and M.W. Luttges. *Visualization of dynamic stall controlled by large amplitude interrupted pitching motions*. AIAA paper 86-2281.

H.E. Helin and J.M. Walker. *Interrelated effects of pitch rate and pivot point on airfoil dynamic stall*. AIAA paper 85-0130, January 1985.

H.E. Helin, M.C. Robinson and M.W. Luttges

H.E. Helin. *Experimental studies on the dynamic development and control of unsteady separated flows*. Air Force inst. of tech. Wright-Patterson AFB OH.

D.G.F. Herring, A.J. Niven, and R.A. McD. Galbraith. *Analysis of reattachment during ramp down tests*. Fourteenth European Rotorcraft Forum, Milan, Italy, 20-23 September 1988.

B.D. Hibbs. *HAWT performance with dynamic stall*.

J.G. Hicks and J.F. Nash. *The calculation of three-dimensional turbulent boundary layers on helicopter rotors*. NASA CR-1845, 1971.

C.-M. Ho and H.K. Cheng. *Aerodynamic research on flow separation and dynamic stall. Some recent advances*. Aerospace simulation II, Proceedings of the Second conference, San Diego, January 23-25 1986.

S.A. Huyer and M.W. Luttges. *Unsteady flow interactions between the wake of an oscillating airfoil and a stationary trailing airfoil*. AIAA paper 88-2581, June 1988.

I

A. Ichikawa. *Improved numerical method for lifting airfoils with oscillating control surfaces in subsonic flow*. Japan society for Aeronautical and Space Sciences Journal, Vol. 33, No.383, pages 697-703, 1985.

S. Ishii, H. Tanaka and I. Fujimoto. *Unsteady aerodynamic characteristics of abrupt stall type airfoil in pitching oscillation near stall angle of attack. 1 - On dynamic characteristics of flow separation and regions corresponding to separation patterns*. JSME Bulletin, Vol. 29, pages 67-76, January 1986.

J

E.C. James. *Leading edge separation criterion for an oscillating airfoil*. Proceedings of the workshop on separate flow, pages 177-183, (N85-17937 09-01).

W. Johnson. *On the mechanism of dynamic stall*.

W. Johnson. *Recent developments in rotary wing aerodynamic theory*.

W. Johnson. *The effect of dynamic stall on the response and airloading of helicopter rotor blades*. Journal of AHS, Vol. 14(2), 1969.

W. Johnson and N.P. Ham. *On the mechanism of dynamic stall*. J. AHS, Vol. 17, 1972.

W. Johnson. *Comparison of three methods for calculation of helicopter rotor blade loading and stresses due to stall*. NASA TN D-7833.

W.P. Jones. *Oscillating wings in compressible subsonic flow*.

J.P. Jones. *Unsteady aerodynamics of helicopter rotors*. AGARD-R-595, 1972.

E.J. Jumper. *A summary overview of work on dynamic stall*. Mini-Symposium on Aerospace Science and Technology, 10th, March 20th 1984.

E.J. Jumper and J.E. Hitchcock. *Theoretical investigation of dynamic stall using a momentum integral method*. Proceedings of the workshop on separate flow, pages 148-151, (N85-17937 09-01).

E. J. Jumper, R. L. Dimmick and A. J. S. Allaire. *The effect of pitch location on dynamic stall*. American society of Mechanical Engineers. Vol.201-208, New York, U.S.A., 1987.

E.J. Jumper, J.E. Hitchcock, R.G. Docken and T.S. Lawrence. *Investigating dynamic stall using a modified momentum-integral method*. Aerospace Sciences Meeting, 25th, AIAA Paper 87-0431, Reno, U.S.A., January 12-15 1987.

E.J. Jumper, S.J. Shreck and R.L. Dimmick. *Lift-curve characteristics for an airfoil pitching at constant rate*. AIAA paper No. 86-0117, 1986.

E.J. Jumper, W.J. Dardis and E.J. Stephen. *Toward an unsteady-flow airplane*. AIAA paper 88-0752, January 1988.

K

H.C. Kao. *Some aspects of airfoil stall in low speed flow*. Journal of aircraft, Vol 11, No. 3, 1974.

S.J. Kline, J. Bardina and R. Strawn. *Correlation and computation of detachment and reattachment of turbulent boundary layers on two-dimensional flared surfaces*. AIAA paper 81-1220, 1981.

M.M. Koochesfahani. *Vortical patterns in the wake of an oscillating airfoil*. Aerospace Sciences Meeting, 25th, AIAA Paper 87-0111, Reno, U.S.A., January 12-15 1987.

S.B.R. Kottapalli. *Unsteady aerodynamics of oscillating airfoils with inplane motions*. American helicopter society Journal, Vol. 30, pages 62-63, January 1985.

M. Krama. *Increase in the maximum lift of an aerofoil due to a sudden increase in its effective angle of attack resulting from a gust*. NACA Technical Memorandum 678, 1932.

D.L. Kunz. *The effect of varying freestream velocity on airfoil dynamic stall characteristics*.

L

N.C. Lambourne. *Experimental techniques in unsteady aerodynamics*. AGARD R-679, 1980.

A. Laneville, P. Vittecoq and J. Cote. *Experimental study of the effect of turbulence on dynamic stalling*. AGARD Unsteady Aerodynamics-Fundamentals and applications to aircraft dynamics.

A. Laneville and P. Vittecoq. *Dynamic stall - The case of the vertical axis wind turbine*. Journal of Solar Energy Engineering, Vol. 108, pages 140-145, May 1986.

R.H. Landon. *A description of the ARA 2-D pitch and heave rig and some results from the NACA 0012 wing*. ARA Memo 199, 1977.

G. Lee, D.A. Buell, J.P. Licursi and J.E. Craig. *Laser holographic interferometry for an unsteady airfoil undergoing dynamic stall*. AIAA paper 83-0388.

J.G. Leishman. *Contributions to the experimental investigation and analysis of aerofoil dynamic stall*. Ph.D. thesis, University of Glasgow, March 1984.

J.G. Leishman and T.S. Beddoes. *A generalised model for airfoil unsteady aerodynamic behaviour and dynamic stall using the indicial method*. Washinton D.C., U.S.A, Annual forum of the American Helicopter Society, June 1986.

J.G. Leishman. *Modelling of trailing edge separation on arbitrary two-dimensional aerofoils in incompressible flow using an inviscid flow algorithm*.

J.G. Leishman, L.Y. Seto and R.A. McD. Galbraith. *Collected data for sinusoidal tests on a NACA 23012 aerofoil*. Glasgow University, internal report 8600, March 1986.

J.G. Leishman. *A semi-empirical model for dynamic stall*. UM-AERO-87-24, July 1987.

J.G. Leishman. *Practical modelling of unsteady airfoil behaviour in nominally attached two-dimensional compressible flow*. UM-AERO-87-6, April 1987.

J.G. Leishman. *A review of the calculation of non-circulatory aerodynamic loads in incompressible and compressible flow*. UM-AERO-87-27, August 1987.

J.G. Leishman. *Validation of approximate indicial functions for two-dimensional subsonic compressible flow*. UN-AERO-87-2, february 1987.

J.G. Leishman. *A comparison of a second generation model for unsteady aerodynamic behaviour and dynamic stall with 2-D test data for a NACA 0012 airfoil*. Research paper 710, Westland Helicopters Ltd, June 1986.

- E. Leitch and R.A.McD. Galbraith. *Guide to Glasgow University's aerofoil database - Version 1*. Glasgow University, internal report 8700, February 1987.
- J. Liiva. *Two-dimensional tests of airfoils oscillating near stall. Vol. 1: Summary and evaluation of results*. USAAVLABS Technical Report 68-13A, 1968.
- J. Liiva. *Unsteady aerodynamic and stall effects on helicopter rotor blade airfoil sections*. Journal of Aircraft, Vol. 6, No. 1, 1969.
- J. Liiva and F.J. Davenport. *Dynamic stall of airfoil sections for high-speed rotors*. Journal of AHS, Vol. 14, No. 2, pages 26-33, April 1969.
- R.G. Loewy. *A two-dimensional approximation of unsteady aerodynamics of rotary wings*. Journal of the Aeronautical Sciences, Vol. 24, No. 2, February 1957.
- H. Lomax, M.A. Heaslet, F.B. Fuller and L. Sluder. *Two and three dimensional unsteady lift problems in high speed flight*. NACA Report 1077, 1952.
- R.H. London. *Some sources of error with Kulite pressure transducers in the A.R.A pitch/heave rig*. Peter F. Lorber and Franklin O. Carta. *Airfoil dynamic stall at constant pitch rate and high Reynolds number*. Fluid Dynamics, Plasma Dynamics, and Lasers Conference, AIAA paper 87-1329, Honolulu, U.S.A., June 8-10 1987.
- M.W. Luttges, C. Somps, M. Kliss and M.C. Robinson. *Unsteady separated flows: Generation and use by insects*. Workshop on unsteady separated flow, University of Colorado, August 1983.
- M.W. Luttges, M.C. Robinson and D.A. Kennedy. *Control of unsteady separated flow structures on airfoils*. AIAA paper No. 85-0531, March 1985.
- K.H. Ly. *Results of recent measurements on an oscillating aerofoil*.

M

- R.J. Magnus. *Calculations of some unsteady transonic flows about the NACA 64A006 and 64A010 airfoils*. AFFDL-TR-77-46, 1977.
- Laure Mane, Henri Werle and Ta Phuoc Loc. *Dynamic stall around an airfoil at high Reynolds numbers-A comparison between numerical results and experimental visualization*. Sciences de la Terre, Vol. 305 No. 4, pages 229-232, June 28 1987.
- C.A. Maresca. *Unsteady aerodynamics of an aerofoil at high angle of incidence performing various linear oscillations in a uniform flow*.
- J.M. Martin, R.W. Empey, W.J. McCroskey and F.X. Caradona. *An experimental analysis of dynamic stall on an oscillating airfoil*. Journal of AHS, Vol. 19, No. 1, 1974.
- J.M. Martin. *A detailed experimental analysis of dynamic stall on an unsteady two-dimensional airfoil*.
- B. Maskew and F.A. Dvorak. *Prediction of dynamic stall characteristics using advanced nonlinear panel methods*. Proceedings of the workshop on separate flow, pages 58-72, (N85-17937 09-01).
- B. Maskew and F.A. Dvorak. *Prediction of dynamic stall characteristics using advanced non-linear panel methods*. Final Report, November 1982 - April 1984.
- B. Maskew. *The prediction of C_{lmax} using a separated flow model*.
- B. Maskew. *Investigation of separation models for the prediction of C_{lmax}* .
- C. Masson. *Dynamic and viscous effects on the vertical-axis wind turbine*. AIAA paper 88-0087, January 1988.
- B. Mazelsky. *Numerical determination of indicial lift and moment of a two-dimensional sinking airfoil at subsonic mach numbers from oscillatory lift coefficients with calculations for mach number 0.7*. NACA TN 2562, 1951.
- B. Mazelsky and J.A. Drischler. *Numerical determination of indicial lift and moment functions of a two-dimensional sinking and pitching airfoil at mach numbers 0.5 and 0.6*. NACA TN 2739, 1952.
- U.B. Mehta. *Dynamic stall of an oscillating airfoil*. AGARD CP-227, 1972.
- A.N. Menendez. *Measurement of skin friction in boundary layers using a flush mounted hot-film gauge*.
- K.W. McAlister, O. Lambert and D. Petot. *Application of the ONERA model of dynamic stall*. NASA-TP-2399.

- K.W. McAlister. *Water-tunnel experiments on an oscillating airfoil at Re No. = 21,000*. NASA TM-78446, 1977.
- K.W. McAlister. *Water tunnel visualizations of dynamic stall*. ASME Journal of Fluids Engineering, Vol. 101, September 1979.
- K.W. McAlister, L.W. Carr and W.J. McCroskey. *Dynamic stall experiments on the NACA 0012 airfoil*. NASA TP 1100, 1978.
- W.J. McCroskey and R.K.Jr Fisher. *Detailed aerodynamic measurements on a model rotor in the blade stall regime*. Journal of the American Helicopter Society, Vol. 17, No. 1, January 1972.
- W.J. McCroskey. *Recent developments in rotor blade stall*. AGARD conference proceedings, No. 111, Aerodynamics of rotary wings, Marseilles, France, September 1972.
- W.J. McCroskey. *Recent developments in dynamic stall*. Symposium on unsteady aerodynamics, Kinney R.B. ed, Tuscon, Arizona, 1975.
- W.J. McCroskey. *Unsteady aerofoils*. Annual review of Fluid Mechanics, 1982.
- W.J. McCroskey, L.W. Carr and K.W. McAlister. *Dynamic stall experiments on oscillating airfoils*. AIAA paper 75-125, 1975.
- W.J. McCroskey and J.J. Philippe. *Unsteady viscous flows on oscillating airfoils*. AIAA Journal, Vol. 13, 1975.
- W.J. McCroskey, K.W. McAlister, L.W. Carr, S.L. Pucci, O. Lambert and R.F. Indergrand. *Dynamic stall on advanced airfoil sections*. AHS Pre-print 80-01, 1980.
- W.J. McCroskey. *Inviscid flowfield of an unsteady airfoil*. AIAA Journal, Vol. 11, No. 8, 1973.
- W.J. McCroskey. *Some current research in unsteady fluid dynamics*. Journal of Fluids Engineering, Vol. 99, No. 1, 1977.
- W.J. McCroskey. *Prediction of unsteady separated flows on oscillating airfoils*. AGARD LS-94, 1978.
- W.J. McCroskey. *Unsteady airloads and aeroelastic problems in separated and transonic flow*.
- W.J. McCroskey. *An experimental study of dynamic stall on advanced airfoil sections. Vol. 1: Summary of the experiment*. NASA TM 84245, 1982.
- W.J. McCroskey. *Measurements of boundary layer transition, separation and streamline direction on rotating blades*. NASA TN D-6321, 1971.
- W.J. McCroskey. *Flow angle and shear stress measurements using heated films and wires*.
- W.J. McCroskey, W.J. McAlister and K.W. Carr. *Dynamic stall experiments on oscillating airfoils*. AIAA Journal, Vol. 14, No. 1, 1976.
- W.J. McCroskey. *Dynamic stall of airfoils and helicopter rotors*. AGARD-R-595, 1972.
- W.J. McCroskey and R.K. Fisher. *Detailed aerodynamic measurements on a model rotor in the black stall regime*. Journal of AHS, Vol. 17, No. 1, 1972.
- W.J. McCroskey and S.L. Pucci. *Viscous-inviscid interaction on oscillating airfoils*. AIAA paper 81-0051, 1981.
- G.F. Moss. *Two-dimensional low-speed tunnel tests on the NACA 0012 section, including measurements made during pitching oscillations at the stall*. ARC CP 1145, 1968.
- E Murray Smith and R.A.McD. Galbraith. *User manual for the Glasgow University unsteady aerodynamic facility software*. Glasgow University, internal report 8800, 1988.

N

- J.F. Nash, L.W. Carr and R.E. Singleton. *Unsteady turbulent boundary layers in two dimensional incompressible flow*. AIAA paper No. 73-650, 1973.
- J.F. Nash. *Further studies of unsteady boundary layers with flow reversal*. NASA-CR-2767, 1976.
- J.F. Nash and R.M. Scruggs. *Unsteady boundary layers with reversal and separation*. AGARD CP-227, 1977.
- A. J. Niven and A. McD. Galbraith. *The effect of pitch rate on the dynamic stall of a modified NACA 23012 aerofoil and comparison with the unmodified case*. Twelfth European Rotorcraft Forum, Garmisch-Partenkirchen, West Germany, September 22-25 1986.

A.J. Niven and R.A.McD. Galbraith. *An investigation into the three-dimensional stall developments on a modified NACA 23012 aerofoil*. Glasgow University, internal report 8414, November 1984.

A.J. Niven. *Flow visualisation of an oscillating airfoil*.

A.J. Niven. *A design procedure to modify the trailing edge upper surface pressure gradient of a given aerofoil*.

A.J. Niven, R.A.McD Galbraith and David G. F. Herring *Analysis of reattachment during ramp down tests*. Vertica Vol 13, No2, pp 187-196 1989.

Q

K. Ono. *Numerical study on the dynamic stall process of a NACA 0012 airfoil*. AIAA paper 85-0128.

F.K. Owen. *Laser velocimeter measurements of dynamic stall*. NASA-CR-166603.

F.K. Owen. *Measurements of unsteady vortex flow fields*.

P

M. Palmer. *Analysis of vortex development from visualization of accelerating flow around an airfoil, starting from rest*.

I. Paraschivoiu and J.-M. Parrouffe. *Unsteady potential flow for oscillating airfoils*. Canadian Aeronautics and Space Journal, Vol. 31, pages 142-158, June 1985.

I. Paraschivoiu and Azeddine Allet. *Aerodynamic analysis of the Darrieus wind turbine including dynamic-stall effects*. Proceedings of the Twenty-second Intersociety Energy Conversion Engineering Conference, Vol. 2, Philadelphia, U.S.A., August 10-14 1987.

I. Paraschivoiu. *Double-multiple streamtube model for studying vertical-axis wind turbines*. Journal of Propulsion and power, Vol. 4, July-August 1988.

I. Paraschivoiu, P. Desy and C. Masson. *Blade tip, finite aspect ratio, and dynamic stall effects on the Darrieus rotor*. Journal of propulsion and power, Vol. 4, January-February 1988.

S. O. Park and J. S. Kim. *Wake measurements of an oscillating airfoil*. Turbulence measurements and flow modelling; Proceedings of the International Symposium, Iowa City, U.S.A., September 16-18 1985.

A.G. Parker and J. Bicknell. *Some measurements on dynamic stall*. Journal of Aircraft, Vol. 11, No. 7, 1974.

A.G. Parker. *Force and pressure measurements on an airfoil oscillating through stall, part 2*. Final report.

S.A. Patay. *Leading edge separation on an airfoil during dynamic stall*.

H.H. Pearcey, P.G. Wilby, M.J. Reiley and P. Brotherhood. *The derivation and verification of a new rotor profile on the basis of flow phenomena*. paper 16, AGARD CP-111, 1972.

A. Pendleton. *A high speed data acquisition system for oscillatory aerodynamic studies*.

D.A. Peters. *Effect of dynamic stall and elastic parameters on the fundamental mechanisms of helicopter vibrations*. Final Report, September 1983 - August 1985.

David A. Peters. *Effect of dynamic stall and elastic parameters on the fundamental mechanisms of helicopter vibrations*. September 1986.

D.A. Peters and M. Chouchane. *Effect of dynamic stall on helicopter trim and flap-lag response*. Journal of Fluids and Structures, Vol. 1, pages 299-318, July 1987.

D. Petot. *Dynamic stall modelling of the NACA 0012 profile*. La recherche Aerospatiale, Bimonthly bulletin, no. 1984-6, November/December 1984.

J.J. Philippe. *Aerodynamic research work on helicopters*.

J.J. Philippe. *Dynamic stall: An example of strong interaction between viscous and inviscid flows*. Paper 21, AGARD CP 227, 1977.

J.J. Philippe. *A survey of recent development in helicopter aerodynamics*.

G.A. Pierce. *The effect of varying freestream velocity on dynamic stall characteristics*.

Q

R

- B.M. Rao and B. Maskew. *Theoretical prediction of dynamic stall on oscillating airfoils*. ASH Annual forum pre-print 78-62, 1978.
- H.C. Razavi and R.K. Mehra. *Bifurcation techniques for nonlinear dynamic analysis of compressor stall phenomena*. American Control Conference, 4th, Boston, June 19-21 1985.
- T.S.R. Reddy and K.R.V. Kaza. *A comparative study of some dynamic stall models*. Toledo University Ohio, U.S.A.
- J. Renaud. *Effects of the airfoil choice on rotor aerodynamic behaviour in forward flight*.
- M.C. Robinson and M.W. Luttges. *Unsteady separated flow: Forced and common vorticity about oscillating airfoils*. Proceedings of the workshop on separate flow, pages 117-126, (N85-17937 09-01).
- M.C. Robinson and M.W. Luttges. *Unsteady flow separation and attachment induced by pitching airfoils*. AIAA paper 83-0131, January 1983.
- M.C. Robinson, H.E. Helin and M.W. Luttges. *Control of wake structure behind an oscillating airfoil*. AIAA paper 86-2282, August 1986.
- M.C. Robinson and M.W. Luttges. *Vortices produced by air pulse injection from the surface of an oscillating airfoil*. AIAA paper 86-0118.
- M.C. Robinson and M.W. Luttges. *Vortex generation induced by oscillating airfoils: Maximizing flow attachment*. 8th Biennial symposium on turbulence rolls, September 1983.
- M.C. Robinson, H. Helin, F. Gilliam, J. Russell and J. Walker. *Visualization of three-dimensional forced unsteady separated flow*. AIAA paper 86-1066, May 1986.
- M.C. Robinson and J.B. Wissler. *Pitch rate and Reynolds number effects on a pitching rectangular wing*. AIAA paper 88-2577, June 1988.
- J.P. Rogers. *Application of an analytic stall model to dynamic analysis of rotor blades*. European Rotorcraft forum, 8th, paper 26, August 31-September 3 1982.
- A.P. Rothmayer and R.T. Davis. *Massive separation and dynamic stall on a cusped trailing-edge airfoil*. Symposium on Numerical and Physical Aspects of Aerodynamic Flows, 3rd, Long Beach, CA, January 21-24 1985.
- J.D. Ruyck and C. Hirsch. *Turbulence structure in the boundary layers of an oscillating airfoil*. Final Technical report, January - December 1983.
- J. De Ruyck and C. Hirsch. *Instantaneous flow field measurements of stalled regions on an oscillating airfoil*. AIAA paper 84-1565.

S

- W.S. Saric and J.D. Crouch. *Oscillating hot-wire measurements above an FX63-137 airfoil*. AIAA paper 86-0012.
- N.L. Sankar and W. Tung. *Numerical solution of unsteady viscous flow past rotor sections*. AIAA paper 85-0129, 1985.
- R.M. Scruggs. *Analysis of dynamic stall using boundary layer theory*.
- R.M. Scruggs, R.M. Nash and R.E. Singleton. *Analysis of dynamic stall using unsteady boundary layer theory*. NASA CR-2462, 1974.
- R.M. Scruggs, R.M. Nash and R.E. Singleton. *Analysis of flow-reversal delay for a pitching foil*. AIAA paper 78-183, 1974.
- R.M. Scruggs. *An investigation of near wake in airfoil dynamic stall*. G.I.T.A.E.R. Report No. 71-1, 1971.
- W.R. Sears. *Potential flow around a rotating cylindrical blade*.
- W.R. Sears. *Unsteady motion of aerofoils with boundary-layer separation*.
- W.R. Sears and D.P. Telionis. *Boundary layer separation in unsteady flow*. SIAM Journal Applied Mathematics, Vol. 28, No. 1, 1975.
- W.R. Sears. *Operational methods in the theory of airfoils in nonuniform motion*. Journal of the Franklin Institute, Vol. 230, July 1940.

- W. Send. *Oscillating airfoils and their wake*. DFVLR-Nachrichten, Vol. 42, pages 13-18, June 1984.
- W. Send. *Oscillating airfoils and their wake*. NASA-TM-77831.
- L.Y. Seto, J.G. Leishman and R.A.McD. Galbraith. *An investigation of the three-dimensional stall developments on a NACA 23012 and NACA 0012 aerofoils*. Glasgow University, internal report 8300, January 1983.
- L.Y. Seto and R.A.McD. Galbraith. *The collected data for ramp function tests on a NACA 23012 aerofoil. I: Description and pressure data*. Glasgow University, internal report 8413, November 1984.
- Lup Seto and A. McD. Galbraith. *The effect of pitch rate on the dynamic stall of a NACA 23012 airfoil*. Eleventh European Rotorcraft Forum, London, England, September 10-13 1985.
- L.Y. Seto. *An investigation of three-dimensional stall developments on a NACA 23012 and NACA 0012 aerofoils*.
- S.J. Shamroth. *A Navier-Stokes calculation of the airfoil dynamic stall process*. Proceedings of the workshop on separate flow, pages 82-89, (N85-17937 09-01).
- S.J. Shamroth. *A weak interaction study of the viscous flow about oscillating airfoils*. NASA CR-132425, 1974.
- Y. Shida, H. Takami, K. Kuwahara and K. Ono. *Computation of dynamic stall of NACA 0012 airfoil by block pentadiagonal matrix scheme*. AIAA paper 86-0116.
- Yoshifumi Shida, Kunio Kuwahara, Hideo Takami and Kiyoaki Ono. *Computation of dynamic stall of a NACA-0012 airfoil*. AIAA Journal, Vol. 25, pages 408-413, March 1987.
- R.J. Silcox. *Wind tunnel dynamic analysis of an oscillating airfoil*.
- R.E. Singleton, J.F. Nash, L.W. Carr and V.C. Patel. *Unsteady turbulent boundary layer analysis*. NASA TM X-62, 242, 1973.
- J.J. Smolderen. *Introduction to the theory of unsteady flow*.
- M.R. Soltani, M.B. Bragg and J.M. Brandon. *Experimental measurements on an oscillating 70-degree delta wing in subsonic flow*. AIAA paper 88-2576, June 1988.
- A.O. St Hilaire. *The influence of sweep on the aerodynamic loading of an oscillating NACA 0012 airfoil*. paper 79-4 AHS 35th national forum, 1979.
- E.J. Stephen, J.M. Walker, M.C. Robinson, R.Llobet and B. La Charite. *Forced internal unsteady aerodynamics*. AIAA paper 88-0324, January 1988.
- C.D. Sticht. *Development of drive mechanism for an oscillating airfoil*. The 22nd aerospace Mechanisms symposium, pages 189-197.
- J.H. Strickland and G.M. Graham. *Dynamic stall inception correlation for airfoils undergoing constant pitch rate motions*. AIAA Journal, Vol. 24, pages 678-680, April 1986.

T

- D.P. Telionis. *Unsteady boundary layers, separated and attached*. AGARD CP-227, paper No. 16, 1977.
- D.P. Telionis. *Calculations of time-dependant boundary layers*. Unsteady Aerodynamics, symposium proceedings at the university of Arizona, Vol. 1, pages 155-190, 1975.
- T. Theodorsen. *General theory of aerodynamic instability and mechanism of flutter*.
- J.J. Thibert. *Design and test of a helicopter blade with evolutive profile*.
- J.J. Thibert. *Advanced research on helicopter blade airfoils*.
- H.H.B.M. Thomas. *On the problems of flight over an extended angle of attack range*.
- C.T. Tran and D. Petot. *Semi-empirical model for the dynamic stall of airfoils in view of the application to the calculation of responses of a helicopter blade in forward flight*. Paper 48, 6th European rotorcraft and powered lift forum, 1980.

U V

- James E. Valdes. *Dynamic stall calculations using a Navier-Stokes solver*. M.S. Thesis

H.R. Velkoff and R.L. Ghai. *Hot-wire measurements of stall and separation on helicopter rotor blades*. Vertica, Vol. 3, 1979.

M. Vezza. *A method for predicting unsteady potential flow about an aerofoil*.

M. Vezza. *An inviscid model of unsteady aerofoil flow with fixed upper surface separation*.

M. Vezza. *An algorithm for the prediction of unsteady potential flow about an arbitrary aerofoil*.

M. Vezza. *Modelling of unsteady incompressible separation on an aerofoil using an inviscid flow algorithm*.

M.R. Visbal. *Effect of compressibility on dynamic stall of a pitching airfoil*. AIAA paper 88-0132, January 1988.

Th. Von Karman and W.R. Sears. *Airfoil theory for non-uniform motion*. Journal of the Aeronautical Sciences, Vol. 5, No. 10, 1938.

W

John M. Walker. *Dynamic stall wake interaction with a trailing airfoil*. Aerospace Sciences Meeting, 25th, Reno, U.S.A., January 12-15 1987.

J.M. Walker, H.e. Helin and J.H. Strickland. *An experimental investigation of an airfoil undergoing large amplitude pitching motions*. AIAA paper 85-0039, January 1985.

J.M. Walker, H.E. Helin and D. Chou. *Unsteady surface pressure measurements on a pitching airfoil*. AIAA paper 85-0532, March 1985.

J.M. Walker and M.C. Robinson. *Impingement of orthogonal unsteady vortex structures on trailing aerodynamic surfaces*. AIAA paper 88-2580, June 1988.

C.M. Wang, J.C. Wu and L.N. Sankar. *Unsteady aerodynamics of airfoils oscillating in and out of dynamic stall*. AIAA paper 85-4078.

R.H. Wickens. *Wind tunnel investigation of dynamic stall of an NACA 0018 airfoil oscillating in pitch*. NAE-AN-27.

R.H. Wickens. *Wind tunnel investigation of dynamic stall of an NACA 0018 airfoil oscillating in pitch*.

R.H. Wickens. *Aerodynamic characteristics of an oscillating airfoil (for vertical axis wind turbine)*. Canadian Aeronautics and Space Journal, Vol. 32, pages 34-49, March 1986.

P.G. Wilby. *An experimental investigation of the influence of a range of aerofoil design features on dynamic stall onset*. European Rotorcraft Forum, 10th, The Hague, Netherlands, August 28-31, 1984.

P.G. Wilby. *The aerodynamic characteristics of some new RAE blade sections, and their potential influence on rotor performance*.

P.G. Wilby. *The aerodynamic characteristics of some new RAE blade sections and their potential influence on rotor performance*. 5th European rotorcraft and powered lift aircraft forum, 1979.

M.E. Wood *Results of oscillatory pitch and ramp tests on the NACA 0012 blade section*. ARA memo 220, 1979.

J.C. Wu, C.M. Wang, J.-C. Wu and L.N. Sankar. *Dynamic stall of oscillating airfoils*. American Helicopter Society, Annual Forum, 42nd, Washington DC, U.S.A., June 2-4 1986.

X Y

W.H. Young (Jr). *Fluid mechanic mechanisms in the stall process for helicopters*. NASA TM 81956, 1981.

Z

Appendix A - Memo on update of Data Analysis facility for Dynamic Stall Data at Glasgow University

DEPARTMENT OF AEROSPACE ENGINEERING

Mechan Professor
BRYAN E. RICHARDS
B.Sc.(Eng).,D.I.C.,Ph.D.
C.Eng.,A.F.A.I.A.A.,F.R.Ae.S.

THE UNIVERSITY
GLASGOW G12 8QQ
TELEX: 777070 UNIGLA
TEL: DIRECT DIAL 041-330 4304
ENQUIRES: DIRECT DIAL 041-330 5560
FAX: 041-330 4808

Memo: To all Dynamic Stall research team.

21st November 1988

Computer Programming

Proposal

Update all DSPLay software on VAX to capability of displaying unaveraged data and comparison of different data files.

Reasons

- The analysis of unaveraged data is at present very restricted due to lack of available display software.
- The unaveraged data would have a recognized "home" on the main VAX computer even if storage there is periodic.
- Will give impetus to change over all the raw data files to VAX formatted unaveraged files.
- The analysis of unaveraged data will allow a further answer to the question of whether the averaged/unaveraged data should be used with regard to different areas of research.
- Comparison of files is frequently required and yet no general programs exist to do this.

Timing

This could be achieved with one week of dedicated work, however the changing over all the raw files to VAX unaveraged will take longer, but could be ran as a background job.

Proposal

Give all the display programs on the VAX a single command file from which any DSPLay program can be run.

Reasons

- Simplifies all running, remembering of program names.

Reasons against

- What is the point of this when a software manual would tell potential users far more? The effort to achieve this would be minimal, and also the advantages. All the programs are dealing with large quantities of data, not sure how this could be passed around within a command file without using disc storage, slowing the running considerably. Also who is running this software, and for what purpose?

Proposal

Write a completely new data display facility on the sun microcomputer. This facility would include real time simulation display; ability to "cross-hair" extract values from graphs; have a totally mouse menu driving option; allow for multiple graphs to be displayed simultaneously and hence multiple files; would be written with colour options in; have security password for execution, thus allowing whole network access whilst restricting users; allow reading in files automatically from VAX disc and also use of personnel data bases of files on tape (4000 files per tape); would run a database management system (available within C language) to extract and display possible files of interest; allow for visual imaging of pressure distributions in an application environment (i.e.

VAWT's or within Wind Tunnel); could be written with regard to display of blade vortex interaction data and also formats of future dynamic stall data (e.g. display of hot film data).

Reasons

- Sun cluster - take advantage of.
- Assuming much more data analysis will be done on the ds database and much of this analysis involves the inspection of graphical display specific points, cross-hair will greatly speed up. Also multiple display of graphs at once will speed up analysis.
- Excellent quality output via the laser printer when required, but also less hard copy output will be required as the analysis will be more easily achieved at the terminal with multiple windows.
- Graphical display of extracted data immediately as data is extracted.
- Output can go straight into FRAME for production of reports, as both work with Postscript.
- With the ever increasing amounts of data the problem of data analysis becomes more difficult by the sheer numbers of files that must be considered, the speed, selection and multiple display with help greatly reduce this, and secondly the problem of physical storage that maintains easy access for use could be overcome by having many mini databases on sun archival tapes that are far easier to deal with than VAX tapes. (However the optical disc may alter this once again, but if it's on the network... the network is the computer).

Future Analysis of Dynamic Stall Data

Beddoes Model

"An optimisation of an existing empirical dynamic stall model for low Mach/Reynolds number test case."

Take the existing Beddoes code on the VAX, use NAG routines to optimise the time constants for the comparison with our test data for each model, motion type and Reynolds number. Also validate addition of wake modelling as used in reattachment paper, perhaps use the f ratio test (null hypothesis, that a given parameter is zero within the model) to validate all the many variable constants used within the model at various times.

Dynamic stall testing

"A comparison of the dynamic stalling of a family of modified NACA 23012 aerofoils."

Quantify all the aerodynamic constants for the properties of each section under both static and dynamic stall conditions (separation point movement, Wilby constants etc.). Directly compare identical motion runs for each profile, perhaps some motion runs will differ more than others, quantify this difference and plot against the variation of motion type (mean angle, amplitude, frequency...), examine and quantify the differences between the sections in geometric terms look at the work of McCroskey on the eight sections.

VAWT's

"An optimal symmetrical section for the VAWT at Carnarthen bay."

Based upon 4 digit section tests, discuss the advantages of stall regulation; maximum C_t generation; lessening of cyclic C_n loading; structural advantages of thicker sections. Plot these as functions of the thickness, hence by giving each of the variables a weighting an optimal thickness in the NACA 4 digit sections can be extrapolated. Perhaps discuss the possible benefits of cambered sections in conclusion.

Other possible internal reports

Data Acquisition

"An enhanced data acquisition system for the analysis of unsteady aerodynamics."

Discuss previous system. Limitations discovered hence specification for new system. Hardware solution and software solution. Hot wire implementation, cost, etc.

Data Presentation

"An advanced experimental data display facility on the Sun microcomputer."

"A software manual for the VAX based dynamic stall presentation programs."

David Herring.

(Research Assistant).

Appendix B - Letter confirming Shock Stall testing had been successfully completed at RAE Farnborough



Procurement Executive Ministry of Defence

Royal Aircraft Establishment

Farnborough Hants GU14 6TD

Telex 858134

Telephone 0252 (Aldershot) 24461 ext 5126

Materials & Structures Department, X32 Building

Dr R A McD Galbraith
Dept of Aeronautics & Fluid Mechanics
The University
GLASGOW
G12 8QQ

Your reference

Our reference

Date

24 October 1986

Dear Roddy,

Reference David Herring's letter of 2 September 1986, I have now completed some check calculations using our Viscous Garabedian & Korn program for steady flow. Results are included for inviscid flow on the aerofoils denoted 211T and 211T Mod 2 by David Herring, at a Mach Number of 0.6 and zero incidences. Further results are given for 211T Mod 2 in inviscid flow at a Mach number of 0.3 and incidences of 4° , 6° , 8° . Finally a viscous calculation is made for a Reynolds Number of 1.5×10^6 at a Mach Number of 0.3 and incidence 8° .

Basically the calculations show that the lower surface peak has been controlled so that shock waves are unlikely to arise at 0.6 Mach Number for zero incidences and low C_p . Also that up to 8° and 0.3 Mach number, there is no indication of premature body layer separation, if the assumption of transition at $0.05c$ is correct.

The inviscid calculations indicate that some further smoothing of the ordinates is desirable around the "join" at $x/c = 0.25$ and also around the leading edge. The former should be quite straightforward, but the latter may require some care.

On the question of the vortex interaction studies, I have followed this up and an extension for 12 months should be going through the normal contracts procedures.

Best wishes.

Alfred Jones

A JONES

Appendix C - Letter discussing the impulsive load tests

Westland

Westland Helicopters Limited

Yeovil, Somerset, England, BA20 2YB
Telephone Yeovil (Code 0935) 75222 Telex 46277 WHLYEO G

HA D HERRING,
DEPT OF AERONAUTICS
GLASGOW UNIVERSITY.

12 May 1988

Dear David,

Thanks for the package of data you sent on the 14th of April. You are to be congratulated on the results you have obtained. I am sure there has been a lot of work to resolve the limitations of the hardware, not to mention the bugs which always appear. The results will prove most valuable in substantiating the theoretical/empirical model of the impulsive lift component. Together with Tassus' BVI experiment the data will provide an increased level of confidence for our predictive rotor loads capability.

With regard to your queries:

Concerning the spikes in the TE pressures, Roddy presumably has passed on my suggestion that they may be related to interference with the starting vortex. This could turn into a topic in its own right and you should take Roddy's advice as to what extent you should pursue it within the context of your Degree. My feeling is that it is a secondary issue and may be strongly influenced by:

1. Reynolds Number and Mach Number.
2. The phasing of the cessation of motion or time scale of the ramp.
3. The natural frequency of the apparatus.

In addition it seems that the phenomenon is suppressed by the dynamic stall LE vortex under appropriate conditions; i.e. the high angle cases.

Another possibility involves excitation of the chordwise bending mode, in which case the timescale is unique.

All of these reservations are open to question and may be put to the test. There is, no doubt, a natural time scale for the TE vortex formation which is related to the Strouhal frequency. In the AHS publication co-authored with Gordon Leishman we showed a simulation of secondary vortex shedding which may be related. I enclose a paper which may be of interest and refer you to a paper in the Dec 87 issue of the Journal of Aircraft by Ericsson, although I find it difficult to form a coherent picture of his work.

With regard to presentation etc. I have examined most of the data only superficially due to lack of time. The following items, however, are apparent. In the catalogue of tests the airfoils are identified by number but there does not seem to be a means of relating to the airfoil description. The summary of the piston theory tests is very useful but the timescale presentation makes it difficult to compare features of different runs. I suggest you use a scale of $t.V/c$ and a maximum of 20, 40, 60 or whatever, depending on the rate, for a constant overall length of scale. Compared with the individual plots of C_n , the plots in the summary appear to incorporate some zero drift; likewise the moment data seems to have some zero shift. On the subject of moment data I would appreciate having some better plots of C_m vs $t.V/c$ like the C_n ones. The data you sent is preliminary so no doubt you would have sorted out these problems anyway.

I enclose the results of some comparisons with theory, the model used incorporates the subroutine for the BVI evaluations and the rotor loads acoustic program and does not include dynamic

stall which is only of secondary interest in this aspect of the problem. You may, however, find it worthwhile to compare the dynamic stall behaviour with that obtained at higher RN. In the absence of the static data I have assumed a lift curve slope of 2π , zero C_m , and an aerodynamic centre at the quarter chord. Runs 24861, 71 and 81 have been concentrated on as most appropriate to demonstrate the piston theory terms, a velocity of 35.8 ft/sec and a chord of 1.76 ft were deduced from the parameters included in the data.

Studying the time histories, it appeared possible to simulate the drive system using two first order lags and a spring mass damper combination. The advantage of this approach is that both the displacement and rate are smooth functions. After some effort the first two runs were simulated fairly successfully but the third proved impossible without further complication. The alternative was to digitise the forcing time history and tolerate the somewhat noisy derivative, which may not be unrepresentative anyway. The differences in the resulting C_n and C_m are of interest too. Figs 1 and 2 show the theoretical results for run 861 using the system equations, 3 and 4 relate to 871 and 5 and 6 to run 881. For the latter, a spurious perturbation is apparent in the lift and moment, whereas the error in the forcing does not appear very great but is obviously quite significant.


Using the digitised forcing, the comparisons are repeated in figs. 7 to 12 and finally compared with the test values of C_n in figs 13 to 15. The breakdown of the impulsive and circulatory components is shown in fig. 16. It is apparent that, apart from the influence of the starting vortex or whatever, the tests substantiate the theoretical model very well and even subtle differences in the forcing time history for the first two runs show up in the comparison. Allowing for the apparent drift in the experimental moment data the C_m 's also appear well modelled which is important because the moment is particularly sensitive to the impulsive loading.

It would certainly be of interest to establish whether, for the full scale rotor application, we would be justified in ignoring the additional perturbation demonstrated by your test. Some indication might be obtained by shaping the termination of the ramp and repeating at higher RN with duplicated non dimensional forcing. It would also be interesting to see whether the phenomenon can be induced during harmonic forcing by suitable choice of amplitude and reduced frequency.

In answer to your query about the lift behaviour during run 24451 I have included a simulation of this case (figs. 17, 18 and 19). It is apparent that the behaviour is explainable in terms of the forcing time history. In fig. 18 the asymptotic value of lift is too high, not surprising in view of the test RN, so the consequence of a 20% reduction in C_l is shown in fig. 19 which duplicates the zero offset of the forcing time history.

In conclusion, I would like to reiterate my appreciation of your efforts and offer my encouragement for the completion of your research project.

Yours sincerely,

 T.S. Beddoes

**Appendix D - Complete set of tables for experimental tests performed on the
NACA 23012B**

Flow visualisation test tests at 1.5 million Reynolds Number.,				
Upper Surface Photographed Angles of Attack				
-10.0	-8.3	-8.0	-5.8	-3.5
-2.6	-1.6	0.6	2.3	2.7
4.8	6.5	9.9	11.2	11.7
13.3	13.8	14.9	16.0	16.8
17.0	17.8	18.0	20.4	21.8
23.9	25.9	277.7	29.6	31.8
34.1	36.6	39.9		
Upper surface with trip wire - Angles of attack				
-2.0	2.3	3.0	7.4	11.7
12.6				
Lower surface - Angle of attack				
-9.2	-4.9	0.9	5.5	10.1
14.4	19.4	24.2		

Static tests

Run No.	Start Angle (deg).	End angle (deg).	Reynolds No.
801	-5	24	1.56
811	-5	25	1.51
821	-5	25	1.53
921	-5	30	1.49
931	-5	24	1.50
932	-5	20	1.49
1181	-5	30	1.49
1411	-5	25	0.81
1421	-5	25	1.01
1431	-5	25	1.51
1801	-5	25	1.47
1811	-5	25	1.49
2911	-5	25	1.52
2921	-5	24	1.93

Static tests

Run No.	Start Angle (deg).	End angle (deg).	Reynolds No.
3341	-5	30	1.49
3351	-5	34	1.48
3363	-5	34	1.49
3371	-10	29	1.48
3381	26	-4	1.49
3391	10	20	1.48
3743	-5	34	1.48
3991	-5	34	1.51
4271	-5	34	1.47
4281	-5	34	1.70
4291	-5	34	1.93
4301	-10	34	1.50
4302	-5	34	1.51
5211	-5	34	1.45
5221	-5	34	1.45
5231	5	-14	1.43
5241	5	17	1.46
5251	5	-16	1.46
5261	-17	34	1.47
5271	0	-16	1.47
5281	-5	34	1.89
5282	-5	34	1.86
5361	-5	34	1.45
5371	25	28	1.46
7001	-20	17	1.42
7011	18	-19	1.42
7021	-20	17	1.41
105381	-5	34	1.45
105391	25	28	1.44
105421	-5	34	1.44
105431	-5	34	1.46
105441	-5	34	1.45
105451	22	32	1.45
105461	5	-16	1.44
105791	-5	34	1.46
105801	5	-16	1.46
105811	-5	34	1.46
105821	5	-16	1.45
105831	-5	34	1.49
105841	5	-16	1.48
105941	0	40	1.50
105951	5	-16	1.51

Oscillatory tests

Run No.	Mean Angle	Amplitude	Reduced Frequency	Reynolds No.
10831	4	10	0.010	1.48
10841	6	10	0.010	1.47
10851	8	10	0.010	1.47
10861	10	10	0.010	1.47
10871	10	10	0.010	1.47
10872	10	10	0.010	1.49
10881	4	10	0.025	1.48
10891	6	10	0.025	1.48
10901	8	10	0.025	1.47
10911	10	10	0.025	1.47
10912	10	10	0.024	1.49
10941	4	10	0.052	1.47
10951	6	10	0.052	1.46
10961	8	10	0.052	1.46
10971	10	10	0.052	1.46
10972	10	10	0.051	1.48
10981	4	10	0.076	1.50
10991	6	10	0.076	1.50
11001	8	10	0.076	1.50
11011	10	10	0.075	1.50
11012	10	10	0.076	1.50
11021	4	10	0.101	1.49
11031	6	10	0.101	1.49
11041	8	10	0.101	1.49
11051	10	10	0.101	1.49
11052	10	10	0.101	1.49
11061	4	10	0.126	1.50
11071	6	10	0.126	1.49
11081	8	10	0.126	1.49
11091	10	10	0.126	1.49
11092	10	10	0.132	1.68
11101	4	10	0.151	1.50
11111	6	10	0.151	1.50
11121	8	10	0.151	1.50
11131	10	10	0.151	1.50
11132	10	10	0.152	1.49
11141	4	10	0.177	1.50
11151	6	10	0.177	1.49
11161	8	10	0.177	1.49
11171	10	10	0.177	1.49
11172	10	10	0.177	1.50
11191	4	10	0.203	1.50
11201	6	10	0.203	1.49
11211	8	10	0.202	1.49
11221	10	10	0.202	1.49

Oscillatory tests

Run No.	Mean Angle	Amplitude	Reduced Frequency	Reynolds No.
11222	10	10	0.202	1.50
11231	15	10	0.010	1.49
11241	20	10	0.010	1.49
11251	15	10	0.024	1.48
11261	20	10	0.024	1.48
11271	15	10	0.051	1.47
11281	20	10	0.051	1.47
11291	15	10	0.076	1.49
11301	20	10	0.076	1.49
11311	15	10	0.101	1.49
11321	20	10	0.101	1.49
11331	15	10	0.126	1.50
11341	20	10	0.126	1.49
11351	15	10	0.152	1.49
11361	20	10	0.152	1.49
11361	20	10	0.152	1.49
11381	20	10	0.177	1.50
11391	15	10	0.202	1.50
11392	15	10	0.203	1.45
11401	20	10	0.202	1.49
11402	20	10	0.203	1.45
11441	10	4	0.010	1.49
11451	10	6	0.010	1.48
11461	10	8	0.010	1.48
11471	10	12	0.010	1.48
11481	10	4	0.025	1.50
11491	10	6	0.025	1.49
11501	10	8	0.025	1.49
11511	10	12	0.025	1.49
11521	10	4	0.051	1.49
11531	10	6	0.050	1.48
11541	10	8	0.050	1.48
11551	10	12	0.050	1.48
11561	10	4	0.076	1.49
11571	10	6	0.076	1.48
11581	10	8	0.076	1.48
11591	10	12	0.076	1.48
11601	10	4	0.101	1.49
11611	10	6	0.101	1.48
11621	10	8	0.101	1.48
11631	10	12	0.101	1.48
11641	10	4	0.126	1.50
11651	10	6	0.126	1.49
11661	10	8	0.126	1.49
11671	10	12	0.126	1.49

Oscillatory tests

Run No.	Mean Angle	Amplitude	Reduced Frequency	Reynolds No.
11681	10	4	0.152	1.49
11691	10	6	0.151	1.49
11701	10	8	0.151	1.49
11711	10	12	0.151	1.49
11721	10	4	0.177	1.49
11731	10	6	0.177	1.49
11741	10	8	0.177	1.49
11751	10	12	0.177	1.49
11761	10	4	0.203	1.49
11762	10	4	0.205	1.44
11771	10	6	0.203	1.49
11772	10	6	0.205	1.44
11781	10	8	0.203	1.49
11782	10	8	0.205	1.44
11791	10	12	0.203	1.49
11792	10	12	0.205	1.44
11821	5	8	0.010	1.48
11831	6	8	0.010	1.47
11841	7	8	0.010	1.47
11851	8	8	0.010	1.47
11861	9	8	0.010	1.46
11871	10	8	0.010	1.46
11881	11	8	0.010	1.46
11891	12	8	0.010	1.46
11901	13	8	0.010	1.45
11911	14	8	0.010	1.45
11921	15	8	0.010	1.45
11931	16	8	0.010	1.45
11941	5	8	0.025	1.48
11951	6	8	0.025	1.48
11961	7	8	0.025	1.47
11971	8	8	0.025	1.47
11981	9	8	0.025	1.47
11991	10	8	0.025	1.47
12001	11	8	0.025	1.47
12011	12	8	0.025	1.47
12021	13	8	0.025	1.47
12031	14	8	0.025	1.47
12041	15	8	0.025	1.47
12051	16	8	0.025	1.47
12061	5	8	0.051	1.47
12071	6	8	0.051	1.47
12081	7	8	0.051	1.47
12091	8	8	0.051	1.47
12101	9	8	0.051	1.47

Oscillatory tests

Run No.	Mean Angle	Amplitude	Reduced Frequency	Reynolds No.
12111	10	8	0.051	1.47
12121	11	8	0.051	1.47
12131	12	8	0.051	1.47
12141	13	8	0.051	1.47
12151	14	8	0.051	1.47
12161	15	8	0.051	1.47
12171	16	8	0.051	1.47
12181	5	8	0.076	1.48
12191	6	8	0.076	1.48
12201	7	8	0.076	1.48
12211	8	8	0.076	1.48
12221	9	8	0.076	1.48
12223	10	10	0.203	1.45
12231	10	8	0.076	1.48
12241	11	8	0.076	1.48
12251	12	8	0.076	1.47
12261	13	8	0.076	1.47
12271	14	8	0.076	1.47
12281	15	8	0.076	1.47
12291	16	8	0.076	1.47
12301	5	8	0.102	1.47
12311	6	8	0.102	1.47
12321	7	8	0.102	1.47
12331	8	8	0.102	1.47
12341	9	8	0.102	1.47
12351	10	8	0.102	1.47
12361	11	8	0.102	1.47
12371	12	8	0.102	1.47
12381	13	8	0.102	1.47
12391	14	8	0.102	1.47
12401	15	8	0.102	1.47
12411	16	8	0.102	1.47
12431	6	8	0.127	1.48
12441	7	8	0.127	1.48
12451	8	8	0.127	1.48
12461	9	8	0.127	1.48
12471	10	8	0.127	1.48
12481	11	8	0.128	1.48
12491	12	8	0.128	1.48
12501	13	8	0.128	1.48
12511	14	8	0.128	1.48
12521	15	8	0.128	1.47
12531	16	8	0.128	1.47
12541	5	8	0.153	1.49
12551	6	8	0.152	1.48

Oscillatory tests

Run No.	Mean Angle	Amplitude	Reduced Frequency	Reynolds No.
12561	7	8	0.152	1.48
12571	8	8	0.152	1.48
12581	9	8	0.152	1.48
12591	10	8	0.152	1.48
12601	11	8	0.153	1.49
12611	12	8	0.152	1.48
12621	13	8	0.152	1.48
12631	14	8	0.152	1.48
12641	15	8	0.152	1.48
12651	16	8	0.152	1.48
12661	5	8	0.178	1.49
12671	6	8	0.178	1.48
12681	7	8	0.178	1.48
12691	8	8	0.178	1.48
12701	9	8	0.178	1.48
12711	10	8	0.178	1.48
12721	11	8	0.178	1.49
12731	12	8	0.178	1.48
12741	13	8	0.178	1.48
12751	14	8	0.178	1.48
12761	15	8	0.178	1.48
12771	16	8	0.178	1.48
12782	5	8	0.202	1.46
12792	6	8	0.202	1.46
12801	7	8	0.204	1.48
12802	7	8	0.202	1.46
12812	8	8	0.202	1.46
12822	9	8	0.202	1.46
12832	10	8	0.202	1.46
12842	11	8	0.202	1.46
12852	12	8	0.202	1.46
12862	13	8	0.202	1.46
12872	14	8	0.202	1.46
12882	15	8	0.202	1.46
12891	15	8	0.203	1.49
12892	16	8	0.202	1.46
13751	0	2	0.042	1.50
13752	0	2	0.041	1.50
13761	4	2	0.042	1.49
13762	4	2	0.041	1.49
13771	4	4	0.042	1.49
13772	4	4	0.041	1.49
13781	0	4	0.042	1.49
13782	0	4	0.041	1.49
13791	0	2	0.105	1.49

Oscillatory tests

Run No.	Mean Angle	Amplitude	Reduced Frequency	Reynolds No.
13792	0	2	0.104	1.49
13801	4	2	0.104	1.48
13802	4	2	0.104	1.48
13811	4	4	0.104	1.48
13812	4	4	0.104	1.48
13821	0	4	0.104	1.48
13822	0	4	0.104	1.48
13831	0	2	0.210	1.47
13832	0	2	0.208	1.49
13841	4	2	0.210	1.47
13842	4	2	0.208	1.49
13851	4	4	0.210	1.47
13852	4	4	0.208	1.49
13861	0	4	0.210	1.47
13862	0	4	0.208	1.49
13871	0	2	0.313	1.49
13872	0	2	0.317	1.46
13881	4	2	0.312	1.48
13882	4	2	0.317	1.46
13891	4	4	0.312	1.48
13892	4	4	0.317	1.46
13901	0	4	0.312	1.48
13902	0	4	0.317	1.46
13911	0	2	0.414	1.49
13912	0	2	0.413	1.50
13921	4	2	0.414	1.49
13922	4	2	0.412	1.50
13931	4	4	0.414	1.49
13932	4	4	0.412	1.50
13941	0	4	0.414	1.49
13942	0	4	0.412	1.49
13951	0	2	0.517	1.50
13952	0	2	0.927	1.50
13961	4	2	0.516	1.49
13962	4	2	0.926	1.50
13971	4	4	0.516	1.49
13972	4	4	0.926	1.50
13981	0	4	0.516	1.49
13982	0	4	0.926	1.50
14001	0	8	0.010	1.49
14011	20	8	0.010	1.49
14021	25	8	0.010	1.49
14031	0	8	0.026	1.46
14041	20	8	0.025	1.46
14051	25	8	0.025	1.45

Oscillatory tests

Run No.	Mean Angle	Amplitude	Reduced Frequency	Reynolds No.
14061	0	8	0.051	1.46
14071	20	8	0.051	1.46
14081	25	8	0.051	1.46
14091	0	8	0.076	1.46
14101	20	8	0.076	1.46
14111	25	8	0.076	1.46
14121	0	8	0.102	1.46
14131	20	8	0.102	1.45
14141	25	8	0.102	1.45
14151	0	8	0.127	1.46
14161	20	8	0.127	1.46
14171	25	8	0.127	1.46
14181	0	8	0.153	1.45
14191	20	8	0.153	1.45
14201	25	8	0.153	1.45
14211	0	8	0.178	1.46
14221	20	8	0.178	1.45
14231	25	8	0.178	1.45
14241	0	8	0.203	1.46
14251	20	8	0.203	1.46
14261	25	8	0.203	1.46
15961	5	8	0.150	0.99
15971	6	8	0.150	0.99
15981	7	8	0.150	0.99
15991	8	8	0.150	0.99
16001	9	8	0.150	0.99
16011	10	8	0.150	0.99
16031	12	8	0.149	1.00
16041	13	8	0.149	1.00
16051	14	8	0.149	1.00
16061	15	8	0.149	1.00
16071	16	8	0.149	1.00
115571	5	8	0.104	1.44
115581	6	8	0.103	1.43
115591	7	8	0.103	1.43
115601	8	8	0.103	1.43
115611	9	8	0.103	1.43
115621	10	8	0.104	1.43
115631	11	8	0.104	1.43
115641	12	8	0.104	1.43
115651	13	8	0.104	1.43
115661	14	8	0.104	1.43
115671	15	8	0.104	1.43
115681	16	8	0.104	1.43

Ramp Up tests

Run No.	Arc (deg).	Pitch rate (deg/sec).	Reduced pitch rate	Reynolds No.
23001	41	0.7	0.0001	1.50
23011	41	1.5	0.0002	1.49
23021	41	3.0	0.0003	1.49
23031	41	4.4	0.0005	1.49
23041	41	6.0	0.0007	1.47
23051	41	7.5	0.0009	1.47
23061	41	14.8	0.0017	1.46
23071	41	29.2	0.0034	1.46
23081	41	44.7	0.0053	1.46
23091	41	58.7	0.0069	1.46
23101	41	74.3	0.0087	1.46
23111	41	91.5	0.0107	1.46
23121	41	100.6	0.0117	1.48
23131	41	114.3	0.0133	1.47
23141	41	127.8	0.0149	1.47
23151	41	143.8	0.0166	1.50
23161	41	157.7	0.0181	1.49
23171	41	173.1	0.0199	1.49
23181	41	185.9	0.0215	1.49
23191	41	197.6	0.0229	1.48
23201	41	211.8	0.0245	1.48
23211	41	223.9	0.0259	1.48
23221	41	240.2	0.0276	1.50
23231	41	253.1	0.0291	1.50
23241	41	263.5	0.0303	1.50
23251	41	280.7	0.0322	1.50
23261	41	286.5	0.0332	1.49
23271	41	299.4	0.0347	1.49
23281	41	317.6	0.0368	1.49
23291	41	328.1	0.0380	1.48
23301	41	333.0	0.0385	1.50
23311	41	366.5	0.0423	1.49
23321	41	397.7	0.0459	1.49
23331	41	423.5	0.0489	1.49
24311	4	58.1	0.0067	1.49
24321	4	112.6	0.0130	1.49
24331	4	145.2	0.0167	1.49
24411	8	47.8	0.0055	1.45
24421	8	108.2	0.0125	1.44
24431	8	193.8	0.0224	1.44
24441	8	210.2	0.0243	1.44
24451	8	212.9	0.0246	1.44
24511	12	51.8	0.0060	1.46

Ramp Up tests

Run No.	Arc (deg).	Pitch rate (deg/sec).	Reduced pitch rate	Reynolds No.
24521	12	94.0	0.0108	1.45
24531	12	195.8	0.0226	1.45
24541	12	259.6	0.0299	1.45
24551	12	271.5	0.0313	1.45
24561	12	276.0	0.0319	1.45
24571	12	274.5	0.0317	1.45
24581	12	292.5	0.0338	1.45
24591	12	299.0	0.0345	1.45
24601	12	304.4	0.0351	1.45
24611	20	49.4	0.0057	1.48
24621	20	97.9	0.0113	1.48
24631	20	219.8	0.0253	1.48
24641	20	301.6	0.0346	1.48
24651	20	327.0	0.0375	1.48
24661	20	344.9	0.0398	1.47
24671	20	350.5	0.0405	1.47
24681	20	374.0	0.0431	1.47
24691	20	364.0	0.0420	1.47
24701	20	372.9	0.0430	1.47
24711	30	49.5	0.0057	1.47
24721	30	100.2	0.0115	1.47
24731	30	200.4	0.0229	1.46
24741	30	325.3	0.0372	1.46
24751	30	375.9	0.0430	1.46
24761	30	395.6	0.0458	1.45
24771	30	422.5	0.0489	1.45
24781	30	430.6	0.0498	1.45
24791	30	443.6	0.0513	1.45
24801	30	455.5	0.0527	1.44
24861	12	286.5	0.1232	0.40
24871	20	361.7	0.1556	0.40
24881	30	447.5	0.1925	0.40
24891	4	147.4	0.0635	0.40
24901	8	237.9	0.1024	0.40
24911	4	154.1	0.0430	0.62
24921	8	241.5	0.0675	0.62
24931	12	290.1	0.0810	0.62
24941	20	377.6	0.1055	0.62
24951	30	442.2	0.1235	0.62
24961	4	158.6	0.0396	0.69
24971	8	232.6	0.0580	0.69
24981	12	281.1	0.0701	0.69
24991	20	357.2	0.0891	0.69
25001	30	438.6	0.1094	0.69
25011	4	120.6	0.0245	0.85

Ramp Up tests

Run No.	Arc (deg).	Pitch rate (deg/sec).	Reduced pitch rate	Reynolds No.
25021	8	245.1	0.0498	0.85
25031	12	288.3	0.0586	0.85
25041	20	368.6	0.0749	0.85
25051	30	439.6	0.0894	0.85
25061	4	131.8	0.0237	0.96
25071	8	254.1	0.0458	0.96
25081	12	291.9	0.0526	0.96
25091	20	364.8	0.0657	0.96
25101	30	448.5	0.0808	0.96
25111	4	107.2	0.0156	1.19
25121	8	246.0	0.0358	1.19
25131	12	290.1	0.0422	1.19
25141	20	370.7	0.0540	1.19
25151	30	452.5	0.0659	1.19
25161	4	137.6	0.0180	1.32
25171	8	232.6	0.0304	1.32
25181	12	293.6	0.0384	1.31
25191	20	371.2	0.0486	1.31
25201	30	452.5	0.0592	1.31
26081	41	49.5	0.0086	0.98
26091	41	98.9	0.0172	0.98
26101	41	198.3	0.0345	0.98
26111	41	287.5	0.0501	0.98
26121	41	366.5	0.0638	0.98
26131	41	427.0	0.0743	0.98
125691	41	49.6	0.0057	1.45
125701	41	98.9	0.0112	1.44
125711	41	198.6	0.0226	1.44
125721	41	291.4	0.0331	1.44
125731	41	367.1	0.0417	1.44

Ramp down tests

Run No.	Arc (deg).	Pitch rate (deg/sec).	Reduced pitch rate	Reynolds No.
33401	-41	-0.7	-0.0001	1.49
33411	-41	-1.5	-0.0002	1.50
33421	-41	-2.9	-0.0003	1.47
33431	-41	-4.4	-0.0005	1.48
33441	-41	-6.0	-0.0007	1.48
33451	-41	-7.2	-0.0008	1.48
33461	-41	-15.0	-0.0017	1.48
33471	-41	-29.1	-0.0034	1.48
33481	-41	-43.9	-0.0051	1.48
33491	-41	-58.4	-0.0068	1.48

Ramp down tests

Run No.	Arc (deg).	Pitch rate (deg/sec).	Reduced pitch rate	Reynolds No.
33501	-41	-71.0	-.0082	1.47
33511	-41	-85.8	-.0099	1.47
33521	-41	-94.7	-.0110	1.47
33531	-41	-107.0	-.0124	1.47
33541	-41	-120.7	-.0140	1.47
33551	-41	-135.6	-.0157	1.47
33561	-41	-148.7	-.0172	1.47
33571	-41	-159.5	-.0184	1.47
33581	-41	-172.4	-.0200	1.47
33591	-41	-181.5	-.0210	1.47
33601	-41	-195.2	-.0226	1.47
33611	-41	-205.7	-.0238	1.47
33621	-41	-217.7	-.0253	1.46
33631	-41	-226.1	-.0262	1.46
33641	-41	-243.8	-.0283	1.46
33651	-41	-255.3	-.0296	1.46
33661	-41	-262.7	-.0305	1.46
33671	-41	-273.8	-.0318	1.46
33681	-41	-288.1	-.0334	1.46
33691	-41	-302.7	-.0351	1.46
33701	-41	-302.7	-.0353	1.46
33711	-41	-347.7	-.0405	1.45
33721	-41	-384.7	-.0448	1.45
33731	-41	-412.1	-.0479	1.45
36141	-41	-48.2	-.0083	1.00
36151	-41	-95.4	-.0164	1.00
36161	-41	-182.8	-.0314	1.00
36171	-41	-263.9	-.0453	1.00
36181	-41	-357.7	-.0614	1.00
36191	-41	-415.8	-.0714	1.00
135741	41	-48.4	-.0055	1.45
135751	41	-94.7	-.0107	1.45
135761	41	-179.4	-.0202	1.45
135771	41	-265.8	-.0300	1.45
135781	41	-351.1	-.0396	1.45

Unsteady static tests

Run No.	Angle	Sampling Frequency.	Reynolds No. (10-6)
40011	-10	250.0	1.49
40021	-8	250.0	1.49
40031	-8	250.0	1.49

Unsteady static tests

Run No.	Angle	Sampling Frequency.	Reynolds No. (10-6)
40041	-5	250.0	1.48
40051	-3	250.0	1.48
40061	-2	250.0	1.48
40071	-2	250.0	1.48
40081	-1	250.0	1.48
40091	0	250.0	1.48
40101	2	250.0	1.48
40111	2	250.0	1.48
40121	3	250.0	1.48
40131	4	250.0	1.48
40141	6	250.0	1.48
40151	7	250.0	1.48
40161	9	250.0	1.48
40171	11	250.0	1.49
40181	11	250.0	1.49
40191	12	250.0	1.49
40201	13	250.0	1.49
40211	13	250.0	1.49
40221	14	250.0	1.48
40231	16	250.0	1.48
40241	16	250.0	1.48
40251	17	250.0	1.48
40261	17	250.0	1.48
40271	18	250.0	1.48
40281	20	250.0	1.48
40291	21	250.0	1.48
40301	23	250.0	1.48
40311	25	250.0	1.48
40321	27	250.0	1.48
40331	29	250.0	1.48
40341	31	250.0	1.48
40351	34	250.0	1.48
40361	36	250.0	1.48
40371	38	250.0	1.49
40501	0	100.0	1.48
40511	2	100.0	1.47
40521	4	100.0	1.47
40531	6	100.0	1.47
40541	8	100.0	1.47
40551	10	100.0	1.47
40561	12	100.0	1.47
40571	13	100.0	1.47
40581	14	100.0	1.46
40591	15	100.0	1.46
40601	16	100.0	1.46

Unsteady static tests

Run No.	Angle	Sampling Frequency.	Reynolds No. (10-6)
40611	18	100.0	1.46
40621	20	100.0	1.46
40631	24	100.0	1.46
40641	30	100.0	1.46
40651	0	500.0	1.49
40671	4	500.0	1.49
40681	6	500.0	1.49
40691	8	500.0	1.48
40701	10	500.0	1.48
40711	12	500.0	1.48
40721	13	500.0	1.48
40731	14	500.0	1.48
40741	15	500.0	1.48
40751	16	500.0	1.48
40761	18	500.0	1.48
40771	20	500.0	1.48
40781	24	500.0	1.48
40791	30	500.0	1.48
45341	26	50.0	1.45
45351	26	50.0	1.45
145401	26	50.0	1.44
145411	26	50.0	1.44
145471	-5	500.0	1.46
145481	0	500.0	1.45
145491	5	500.0	1.45
145501	10	500.0	1.45
145511	15	500.0	1.45
145521	19	500.0	1.42
145531	25	500.0	1.42
145541	28	500.0	1.42
145551	30	500.0	1.42
145561	35	500.0	1.42
145851	-5	500.0	1.48
145861	0	500.0	1.47
145871	5	500.0	1.47
145881	10	500.0	1.48
145891	14	500.0	1.47
145901	20	500.0	1.47
145911	25	500.0	1.47
145921	30	500.0	1.47
145931	35	500.0	1.47

VAWT tests

Run No.	Mean angle (deg).	Amplitude (deg).	Reduced pitch rate	Reynolds No.
56701	0	5	0.051	1.44
56711	0	9	0.051	1.43
56721	0	12	0.051	1.43
56731	0	13	0.051	1.43
56741	0	17	0.051	1.43
56751	0	22	0.051	1.43
56761	0	5	0.040	1.44
56771	0	9	0.040	1.44
56781	0	12	0.040	1.44
56791	0	13	0.040	1.44
56801	0	17	0.040	1.43
56811	0	22	0.040	1.43
56821	0	5	0.061	1.43
56831	0	9	0.061	1.43
56841	0	12	0.061	1.43
56851	0	13	0.061	1.43
56861	0	17	0.061	1.43
56881	0	5	0.051	1.49
56891	0	9	0.051	1.48
56901	0	12	0.050	1.48
56911	0	13	0.050	1.48
56921	0	17	0.050	1.48
56931	0	22	0.050	1.48
56941	-6	13	0.051	1.49
56951	-4	13	0.051	1.49
56961	-2	13	0.051	1.49
56971	2	13	0.051	1.49
56981	4	13	0.051	1.49
56991	6	13	0.051	1.49

Ramp wave

Run No.	Mean angle (deg).	Reduced frequency	Reynolds No.
65291	15	0.037	1.47
65301	15	0.037	1.47
65311	15	0.037	1.47
65321	15	0.037	1.47
65331	15	0.037	1.47
66261	15	0.069	1.45
66271	15	0.052	1.44
66281	15	0.026	1.44
66291	15	0.020	1.44

Ramp wave

Run No.	Mean angle (deg).	Reduced frequency	Reynolds No.
66301	15	0.016	1.44
66311	10	0.089	1.44
66321	10	0.069	1.44
66331	10	0.030	1.44
66341	10	0.022	1.44
66351	10	0.017	1.44
66361	5	0.150	1.44
66371	5	0.096	1.44
66381	5	0.034	1.44
66391	5	0.024	1.44
66401	5	0.019	1.44
66411	20	0.052	1.44
66421	20	0.041	1.43
66431	20	0.023	1.43
66441	20	0.018	1.43
66451	20	0.015	1.43
66461	15	0.006	1.44
66471	15	0.024	1.44
66481	0	0.052	1.43
66491	15	0.061	1.43
66501	15	0.067	1.43
66511	10	0.009	1.45
66521	10	0.032	1.44
66531	10	0.062	1.64
66541	10	0.067	1.44
66551	10	0.071	1.44
66561	5	0.103	1.44
66571	5	0.037	1.43
66581	5	0.025	1.43
66591	5	0.023	1.43
66601	5	0.022	1.43
66611	20	0.353	1.43
66621	20	0.087	1.42
66631	20	0.037	1.42
66641	20	0.030	1.42
66651	20	0.027	1.42

Random incidence variation

Run No.	Reynolds No.
76201	1.46
76211	1.45
76221	1.45
76231	1.45

Random incidence variation

Run No.	Reynolds No.
76241	1.45
76251	1.45